CELLULAR ORGANISATION OF PERIPHERAL NERVE AND THE NEUROMUSCULAR JUNCTION

Felipe A. Court

Ph.D.
University of Edinburgh

Centre for Neuroscience Research
2004

DECLARATION

I declare that this thesis and the work described in it is my own except where indicated and has not been submitted for any other degree.

Felipe A. Court
September 2004

ACKNOWLEDGEMENTS

I will always be thankful to my father and mother for encourage in my projects and give me the possibility to explore a broad range of subjects in addition to their support at all times. I am also grateful to all the people from diverse disciplines that in different ways have influenced my way of thinking.

I am particularly thankful to my undergraduate adviser Jaime Alvarez. By long and stimulating discussions together with hard lab work, I learned from Jaime my first steps in scientific reasoning and rigour in the experimental activity.

I would like to acknowledge my PhD supervisors, Peter J. Brophy and Richard R. Ribchester for their excellent supervision and valuable advice throughout my PhD.

I am also grateful to all members of PJB and RRR group for assistance during my work. For their expert help I want to thanks Diane Sherman, Derek Thomson, Adrian Thomson, David Cotrell, Linda Ferguson, Heather Anderson, Billy Smith, Christine Forrest and Mary David.

I would also like to acknowledge Graham Pettigrew and Peter Kind for their advice and the Wellcome Trust and the ORS organisation for funding my PhD.

I am infinitely thankful to my wife Karin for her continuous support during this time in the University and to my daughter Mila for the meaning she has given to my life.

CONTENTS

LIST OF FIGURES

ABBREVIATIONS

3D	Three-dimensional
Ach	Acetylcholine
AchR	Acetylcholine receptor
bHLH	Basic helix-loop-helix
BrdU	Bromodeoxyuridine
BSA	Bovine serum albumin
BTX	α-Bungarotoxin
c_m	Membrane capacitance
CMT	Charcot-Marie-Tooth
CMTX	Connexin-32 knock-out mice
CNS	Central nervous system
DEPC	Diethyl pyrocarbonate
DeSyn	Delayed Synapsing
DG	Dystroglycan
DGC	Dystrophin glycoprotein complex
DL	Deep lumbrical
DRP2	Dytroglycan-related protein 2
E	Embryonic day
ECL	Enhanced chemiluminescence
EDL	Extensor digitorium longus
EDTA	Ethylene diaminetetra-acetic acid
EM	Electron microscopy
EPP	End-plate potential
ES	Embryonic stem
ExS^{2166+}	Extrasynaptic 2166 positive cells
FACS	Fluorescent-activated cell sorting
FAK	Focal adhesion kinase
FaSyn	Fast Synapsing
FDB	Flexor digitorum brevis
FGF2	Fibroblast growth factor 2
FITC	Fluorescein isothiocyanate
GGF II	Glial growth factor II
h	Hour
HRP	Horseradish peroxidase
Hz	Hertz
Ig	Immunoglobulin
IL	Internodal length
ISH	*in situ* hybridization
kDa	KiloDalton

KLH	Keyhole limpet hemocyanin
KO	Knock-out
LMC	Lateral motor column
MBP	Myelin basic protein
MEPP	Miniature end-plate potential
min	Minutes
mm	Millimetre
μm	Micron
MMC	Medial motor column
mRNA	Messenger RNA
ms	Milliseconds
MuSK	Muscle-specific receptor tyrosine kinase
NDF	Neu differentiation factor
NF	Neurofilament
NFC	Neurofascin
NGF	Neural growth factor
NMJ	Neuromuscular junction
NMJ^{2166+}	Neuromuscular junction-associated 2166 positive cells
P0	Myelin protein zero
PBS	Phosphate buffer solution
PDZ	PSD95/disc large/zona occludens
PLP	Protolipid protein
PNS	Peripheral nervous system
rpm	Revolutions per minute
r_i	Internal resistance
r_m	Membrane resistance
ROCK	Rho kinase
rPH	Rat prolyl-4-hydroxylase
s	Second
SDS	Sodium dodecyl sulfate
Shh	Sonic hedgehog
SP	Side population
TRITC	Tetramethylrhodamine isothiocyanate
TS	Transversal sterni
tSC	Terminal Schwann cell
WT	Wild-type

ABSTRACT

The organisation of cells in the peripheral nervous system is crucial for its proper function. Action potential generation, conduction and synaptic transmission to the muscle fibres are dependent not only on cells directly implicated in these functions (i.e. neurons and muscle fibers) but also on accessory cells with important modulatory roles. These cells are also essential for adaptive responses by the peripheral nervous system during development, injury and pathological conditions. Schwann cells represent one of the principal cellular components regulating nerve function. In peripheral nerves, myelin-forming Schwann cells specify distinct domains in the axon, allowing fast and efficient propagation of the action potential. At the neuromuscular junction, terminal Schwann cells are necessary for stability of motor nerve terminals and motor endplates and they are involved in plastic responses of the neuromuscular system to injury and in disease.

This thesis is a study of how the cellular organisation of the peripheral nerve and neuromuscular junction determines their morphological and electrophysiological characteristics as well as their functional role in plastic responses following destabilizing stimuli. The mechanism by which Schwann cells regulate the length of the myelinated segment over the axon is addressed and this parameter, *i.e.* the internodal length, is shown experimentally for the first time as a key determinant of nerve conduction velocity (Court et al., 2004). At the neuromuscular junction, immunostaining with a panel of antibodies revealed a novel cell type, distinct from Schwann cells and possibly related to fibroblasts. These cells lie outside the synaptic basal lamina, but in adults they are highly restricted to the neuromuscular junction. Studies of the development of the novel cells, and their reaction to nerve injury and paralysis, suggest they play a crucial role in the maintenance and disposition of motor nerve terminals and terminal Schwann cells. Finally, studies of periaxin null mutant mice, which show a demyelinating neuropathy, yielded new insights into the relationships between axons and Schwann cells at the neuromuscular junction. Defects observed in morphology and electrophysiology of junctions in these mice may contribute to their behavioural phenotype (i.e. trembling, weakness), suggesting

that disruption of nerve terminal-Schwann cell relationships may also contribute to disability in demyelinating diseases.

1- INTRODUCTION

1.1- OVERVIEW

Perception and reaction to the external environment is accomplished by the nervous system by means of bidirectional information movement in the form of electrical impulses between the central nervous system (CNS) and the sensory and motor systems. The CNS is composed of the brain, the principal integrative area of the nervous system and the spinal cord that serves as a conduit for nervous pathways to and from the brain and also acts as an integrative area for coordinating many subconscious nervous activities. The peripheral nervous system (PNS) comprises all neural tissue that transmit information between the spinal cord and the sensory inputs and motor outputs.

The proper electrophysiological function of the peripheral nervous system not only requires cells directly involved in this process, i.e neurons, muscle fibres and sensory endings but also a variety of cells that modulate their function. This fact is underscored by the complex relationships exhibited by cellular components of the peripheral nervous system. One of the most striking examples of this cell-cell relation is found in the myelinated nerve fibre, which comprises the peripheral extension of the neuron -the axon- and its associated glial component, the Schwann cell. Both axon and Schwann cell phenotypes are mutually dependent during development and maintenance of the nerve fibre. The extent and significance of glial to axon communication is dramatically revealed in several inherited diseases product of mutations in glial cell genes in which impairment in axonal structure and function are ultimately responsible for motor function defects.

Schwann cells regulate the function of the axon not only by forming a specialised structure, the myelin sheath, but also by imposing regional specialization along the axonal membrane. The subcellular compartmentalisation of the Schwann cell and its effects on the heterogeneity of the axonal membrane have been a focus of intensive studies in recent years, and a common finding has been the presence of macromolecular complexes between axons and Schwann cells involved in the formation and maintenance of their structural organization. Functionally, the characteristics of the axon-Schwann cell relationship allow the fast conduction of the

nerve impulse by restricting the regeneration of action potentials to specific region of the axonal membrane devoid of the insulating myelin sheath and endowed with the molecular components involved in transmembrane ion movement. Although the parameters regulating this type of nerve conduction, known as "saltatory", has been extensively studied, some of them still remain theoretical, awaiting experimental examination.

The synapse between the motor axon and the muscle fibre represents another example of complex cellular interaction, responsible for the chemical relay of the action potential. In this region, a functional unit is formed by axon terminals, muscle fibres and a glial cell component that differs from Schwann cells located in more proximal regions. The analysis of the neuromuscular synapse has been centered almost exclusively in these three cell types and the roles of the glial component in the formation, development, stabilisation and repair of the neuromuscular connection has received considerable attention at the expense of the characterisation of other cell types that may be crucial components of the neuromuscular apparatus.

This thesis addresses the role of cellular relationships in the function, maintenance and repair of the peripheral nervous system. This following section presents the necessary background information to appreciate the results. In three main parts, I review the formation, structure and function of the myelinated fibre and the neuromuscular junction with particular attention paid to the role played by the glial cell component.

1.2- DEVELOPMENT OF THE PERIPHERAL NERVOUS SYSTEM

1.2.1- Origin of principal cells forming the PNS

The formation of the peripheral nervous system requires the coordinated interaction of several cell types that originate in different regions of the embryo. Three of these cell types, motor neurons, Schwann cells and muscle fibres organise themselves into a functional unit specialised for transmission of information required for muscle contraction. The origin of these cells in vertebrates and the mechanisms involved in their final location will be addressed in the following section.

Motor neurons

Neuronal cell-types develop in the neural tube at specific locations in the dorsoventral and rostrocaudal axes. In the ventral region, uncommitted, mitotically active progenitors give rise to motor neuron progenitors.

This differentiation process is induced by the ventral to dorsal gradient of the transcription factor Sonic hedgehog (Shh), secreted from the underlying notochord and floor plate, creating multiple motor neuron progenitor domains that give rise to distinct neuronal classes (Jacob et al., 2001).

Once the motor neuron progenitor domains are established, a cell-autonomous, transcription factor-mediated program of differentiation follows, characterised by the combinatorial expression of the four LIM-homeodomains proteins Islet1, Islet2, Lim1 and Lim3 (Lhx3) by distinct motor neuron subtypes (Kania et al., 2000), distinguished by their peripheral axon projections and location within medial or lateral subdivisions of the two longitudinal columns of the ventral spinal cord (Jacob et al., 2001; Thaler et al., 2004).

Motor neurons innervating axial muscles are located in the medial motor column (MMC) along all segmental levels of the spinal cord. Motor neurons innervating limb muscles are located in the lateral motor column (LMC), but only at the levels of the neural tube that lie in register with the limb fields (Kania et al., 2000).

After specification of motor neuron subtypes, the correct innervation of their target structures is controlled by the action of axon guidance cues, which are present in discrete locations along the pathway to the target zone (Jacob et al., 2001). As there

are multiple guidance cues that axons should recognize, the growth cone is endowed with all components of the protein synthesis machine that allows it to change their responsiveness to intermediate targets by regulating the local expression of specific receptor (Brittis et al., 2002).

Initially, motor axons are repelled by the floor plate by chemorepulsive factors (Guthrie and Pini, 1995) and penetrate the neuroepithelium at specific exit points. In these locations, diffusible and contact-mediated guidance molecules, as well as localised cellular components, are responsible for segregation of motor axons along dorsal and ventral routes (Guthrie and Lumsden, 1992). In the limb region, motor axons grow along common routes demarcated by repulsive effects of semaphorin proteins, which interact with plexin receptors located in growth cones (Nakamura et al., 2000). In addition, diffusible molecules generated by the target zones appear to act as guidance and survival factors for motor axons (Ebens et al., 1996).

Once in the vicinity of the muscle, motor neurons generate a precise topographic map with their targets (Laskowski and Sanes, 1987). The mapping of motor pools onto muscles results from the differential muscle expression of ephrins and the expression of at least three Eph receptors by subsets of motor axons (Feng et al., 2000).

Schwann cells

The mature population of Schwann cells develops from neural crest cells following a process that involves two intermediate states, Schwann cell precursors and immature Schwann cells. Therefore, three main transition events are necessary to reach the adult Schwann cell phenotype (Fig. 1).

The signals driving the transition from neural crest (neural crest cells give rise to other lineages, including neurones and melanocytes) to Schwann cell precursors are still unclear, but some evidence shows that β-neuregulin might act instructively on the neural crest population, promoting glial lineage differentiation (Shah et al., 1994).

Schwann cell precursors, present in mouse peripheral nerves at E12 and E13 (rat E14 and E15) are highly motile, flattened and with extensive cell-cell contacts. One of the most singular characteristics of the precursor cells is their dependence on axonal trophic signals since they undergo apoptotic cell death when they are removed from

contact with axons (Jessen and Mirsky, 1999; Syroid et al., 1996). Several *in vitro* and *in vivo* studies have shown that the neuronal trophic support for the survival of precursors Schwann cells is β-neuregulin and the signalling cascade involves the binding of neuregulin to the ErbB3 receptor in glial cells (Syroid et al., 1996).

In an abrupt transition, nearly all precursor cells become immature Schwann cells (E17 and E15 in rat and mouse, respectively). Studies show that NDF (neu differentiation factor) is probably the neuron-glia signalling molecule that regulates the transition from precursors to immature Schwann cells (Dong et al., 1995). At this stage, immature Schwann cells have the capacity to support their own survival by establishing an autocrine survival loop (Meier and Wallace, 1998). Schwann cells follow motor axons until they reach the muscle. Schwann cells located in pre-terminal regions acquire a myelinating phenotype, whereas those located above nerve terminals differentiate into a distinct phenotype in terms of structure and gene expression (Balice-Gordon, 1996; Son et al., 1996).

Muscle fibres

From the three germ layers present in the early embryo, the paraxial mesoderm forms the somites, which contain a population of committed, yet actively-dividing muscle precursor cells, termed myoblasts. The somite is subdivided into the dorsomedial epaxial domain, which generates the back muscles and the ventrolateral hypaxial, which gives rise to abdominal, intercostal and limb musculature (Sharma and Belmonte, 2001).

In muscle cell precursors, inductive signals from the neural tube and ectoderm, lead to the activation of the family of basic helix-loop-helix (bHLH) transcription factors, which are expressed in temporally and spatially specific ways reflecting the origin of muscle precursors cells (Brand-Saberi and Christ, 1999).

Myoblasts from the hypaxial region of the somite, express the surface receptor c-met, required for migration to the limb region (Bladt et al., 1995). After this process, proliferating myoblasts intermingle into dorsal and ventral premuscle masses, which will correspond to the future flexor and extensor compartments. Proliferating myoblasts, express members of the MyoD family of muscle-specific transcription factors (Williams and Ordahl, 1997), withdraw from the cell cycle, fuse and form

multinucleated primary myofibers, thus activating genes encoding proteins involved in muscle contraction (Crow and Stockdale, 1986). In addition to this early migrating population of myoblasts, a secondary population arrives and form secondary myofibers in parallel to the primary ones (Duxson et al., 1989; Harris et al., 1989). This late population will constitute the predominant multinucleated myofibers in late stages of embryogenesis and postnatal skeletal muscle.

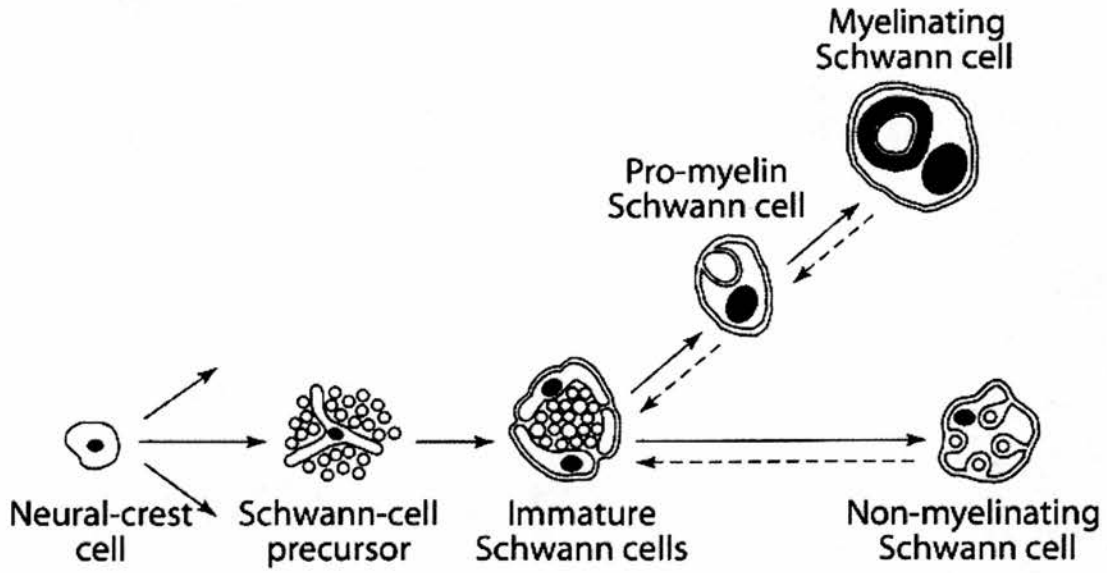

Figure 1. Stages involved in Schwann cell development.
As despicted in the diagram, the development of mature Schwann cells from neural crest cells involves two intermediate states, Schwann cell precursors and immature Schwann cells and three main transition events (after Mirsky et al., 2001).

1.2.2- Formation of the myelinated nerve fibre

In the peripheral nervous system, large caliber axons are myelinated by Schwann cells. The highly specialised relationship between axons and Schwann cells is achieved through a series of processes regulated by axons, Schwann cells and the extracellular matrix. During embryonic and early postnatal development, Schwann cells surround bundles of axons, sorting individual ones by extending sheet-like processes until a 1:1 relationship with the axon is accomplished in a process referred to as radial sorting (Martin and Webster, 1973) (Fig. 2). Schwann cells that segregate individual axons become committed to a myelinating phenotype. Other axons remain in groups ensheathed by non-myelinating Schwann cells (Fig. 2).

The two key processes involved in the formation of the myelinated nerve fibre, i.e. axonal sorting and Schwann cell myelination, are finely regulated ensuring that each nerve fibre will exhibit optimal morphological characteristics for the conduction of the action potential. In the following section, the processes of axonal sorting and myelination will be reviewed, to finish with a discussion on the possible mechanisms responsible for the regulation of two morphological parameters of Schwann cells that are crucial for the function of the myelinated nerve fibre, viz. Schwann cell length and myelin thickness.

Axonal Sorting

The diameter of an axon determines whether a Schwann cell will segregate it (Voyvodic, 1989). The sorting of individual axons by Schwann cells occurs only if the axonal diameter is greater than about 1 μm (Fraher, 1978; Nilsson and Berthold, 1988). This process starts at around E15.5 and is concluded during the first few days of postnatal development. However, the increase in axonal diameter is not synchronous, with axons that become the largest growing first (Nilsson and Berthold, 1988). This process has important consequences for the morphological parameters of the nerve fibre that will be detailed at the end of the section (see page 24-25).

The axonally-derived signal responsible for axonal sorting by Schwann cells has not yet been identified. A second requirement for sorting is the deposition of basal lamina, or at least laminin, by Schwann cells, a process promoted by axons (Bunge et al., 1986). Several studies have shown that laminins are the key basal lamina

components implicated in sorting and myelination. In cell-culture, Schwann cells myelinate axons upon addition of purified laminin (Eldridge et al., 1989) and Schwann cell specific deletion of the γ1-laminin chain gene leads to axonal sorting defects (Chen and Strickland, 2003). Schwann cells express several laminin receptors which are developmentally regulated. During axonal sorting, Schwann cells express the laminin receptor β1 integrin, whereas during myelination they express β4 integrin and dystroglycan (Previtali et al., 2003). The implication of β1 integrin in Schwann cell sorting of axons has been revealed by conditional deletion of the β1 integrin gene in immature Schwann cells (Feltri et al., 2002). In these mice, Schwann cells fail to segregate axons, resulting in a phenotype similar to the γ1-laminin conditional knock-out.

Upon binding to basal lamina ligands, integrins cluster and recruit signalling and structural proteins in specific regions of the plasma membrane, termed focal adhesions (Jockusch et al., 1995). Focal adhesions are both structural link and convergence points for proteins tyrosine kinases that can activate multiple signalling pathways (Juliano, 2002). In Schwann cells cocultured with neurons, basal lamina formation leads to the association of β1 integrin with focal adhesion kinase (FAK) and the actin cytoskeleton-linked protein paxillin, and to their phosphorylation (Chen et al., 2000). The formation and activation of this complex, that has been associated with the regulation of the actin cytoskeleton (Juliano, 2002; Turner, 2000) could be involved in the intracellular events leading to axonal sorting.

Myelination

The process of axonal sorting results in axons separated from the main bundle and with individual Schwann cells associated along their lengths; at this stage two main domains of the nerve fibre can be distinguished; the internode, which corresponds to the region of the axon concealed by the Schwann cell and the node of Ranvier, where two adjacent Schwann cells encounter each other. After axonal sorting, Schwann cells become committed to a myelin-forming phenotype and their genetic expression program is modified to allow the synthesis of myelin constituents. Although the axonal-derived signal that induces myelination is unknown, some studies suggest that axonally-expressed neural growth factor (NGF) might induce Schwann cell

myelination (Chan et al., 2004). In addition, significant information has been reported in the intracellular signals and transcription factors activated during myelination. Two main transcription factors are known to be involved in the regulation of myelination, Oct6/Scip/Tst-1 and Krox20/Egr2. In Oct6 null mice, myelination is delayed (Bermingham et al., 1996; Jaegle et al., 1996) and in Krox20 null mice myelination is completely arrested (Topilko et al., 1994). Studies directed to reveal the signalling cascades downstream Krox-20 have shown that two phenotypic changes involved in myelination are under the control of Krox-20, i.e. escape from the cell cycle and protection of Schwann cells from death triggered by growth factor deprivation (Parkinson et al., 2004).

The myelin sheath is produced in the internodal region by the extension of the inner (axon-related) Schwann cell process around the axon (Bunge et al., 1989). Recent studies have shown that the coordinated spiraling of the internodal Schwann cell membrane around the axon is dependent on the activation of Rho proteins and its downstream effector Rho kinase (ROCK) (Melendez-Vasquez et al., 2004). After 3 to 4 turns of the Schwann cell process, the exclusion of cytoplasm and the association of adjacent extracellular membrane surfaces lead to the formation of a compact myelin sheath (Geren, 1954). Apposition of the cytoplasmic faces of the membranes is dependent in myelin basic protein (MBP) (Rosenbluth, 1980) and the cytoplasmic tail of the integral membrane protein P0, the major protein of the peripheral myelin; whereas the association of extracellular faces of the membrane is achieved by the homophilic association of the extracellular domains of the protein P0 (D'Urso et al., 1990; Martini et al., 1995).

During myelination several domains are created in the Schwann cell that remodel axons into highly polarised structures. The myelin in turn can be divided into two distinct domains, compacted myelin and non-compacted myelin (Fig. 3). Interdispersed through the myelin sheath, non-compacted regions of the Schwann cell plasma membrane containing cytoplasm, known as Schmidt-Lanterman incisures, radially traverse the compact myelin, providing a conduit between the Schwann cell cytoplasm outside the myelin sheath (abaxonal compartment) and the cytoplasm adjacent to the axonal plasma membrane (adaxonal compartment).

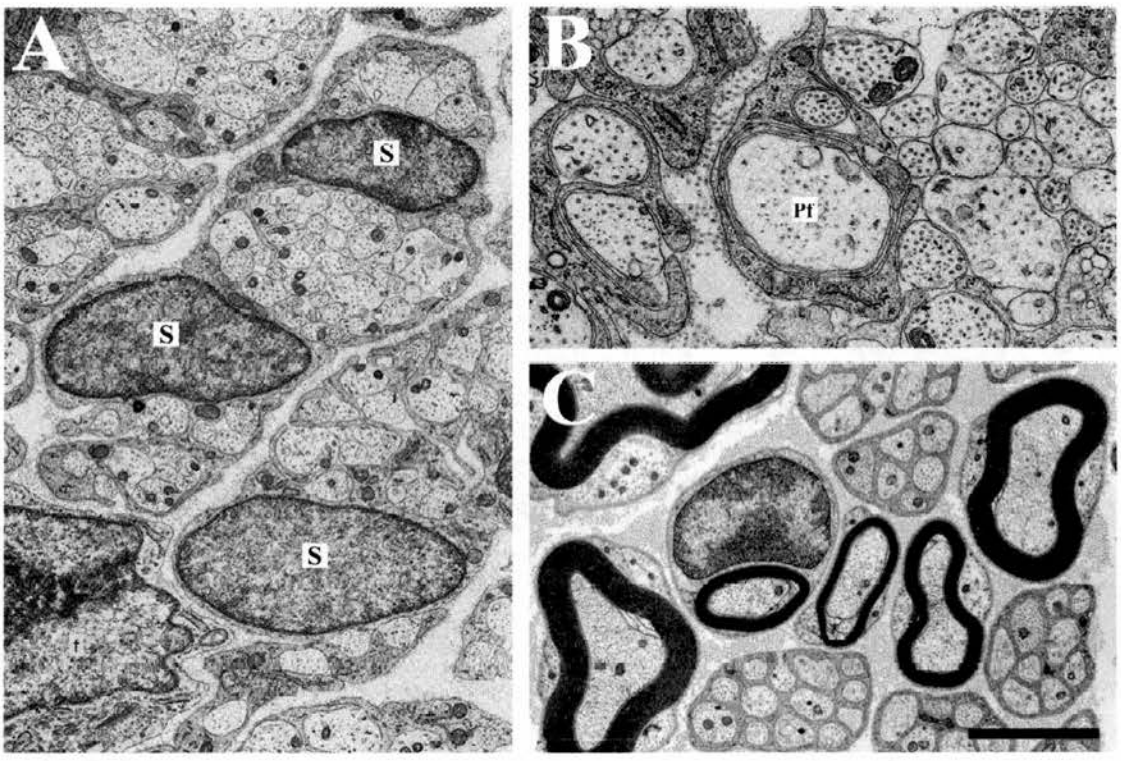

Figure 2. Structure of the peripheral nervous system.
(A) Electron micrograph of a transverse section through a peripheral nerve during embryonic development, showing axons organised in bundles within extensions of Schwann cell cytoplasm; S, Schwann cell nuclei. **(B)** Transverse section through a peripheral nerve during the process of axonal sorting, showing a large diameter axon segregated by a Schwann cell; Pf, promyelin fibre. **(C)** In the adult peripheral nerve two populations of nerve fibers can be distinguish, non-myelinated and myelinated, according to the structural relationship between the axon and the Schwann cell. Scale bar; A, 2 μm; B, 1 μm; C, 2 μm. (Panels **A** and **B** from Landon, 1975).

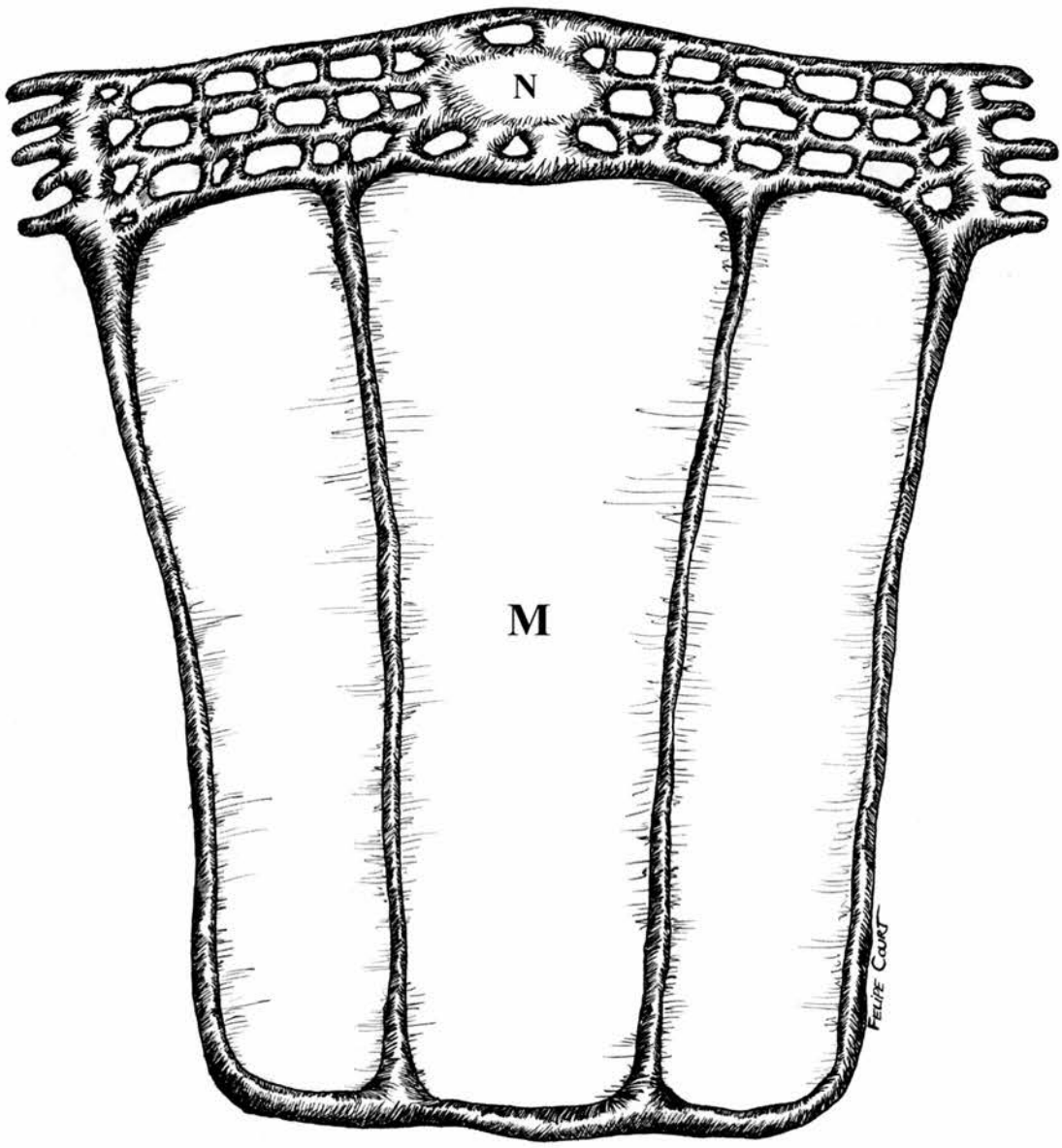

Figure 3. Domain structure of the myelin forming Schwann cell.
Diagram showing an unrolled Schwann cell to expose the organization of its distinct domains. The perinuclear region is connected to the whole extension of the Schwann cell by longitudinal and transverse cytoplasmic channels; N, nuclei; M, myelin sheath.

Internodal length of the Schwann cell and myelin thickness control

The myelin sheath allows rapid and efficient conduction of the action potential. Many morphological parameters of the axon and the Schwann cell are finely regulated in order to accomplish this function and will be reviewed in detail in a following section (1.4- Electrophysiology of the peripheral nervous system). Two of these parameters that arise during development are the control of the myelin sheath thickness and the longitudinal size of the Schwann cell (internodal length).

Very early studies showed that myelin sheath thickness and internodal length were positively related to axonal diameter (Hiscoe, 1947). Axonal size controls the timing of sorting and subsequent myelination by Schwann cells (Voyvodic, 1989). Axons destined to be large in the nerve are sorted first and start to be myelinated before smaller axons (Nilsson and Berthold, 1988). Therefore, the myelin thickness-axon diameter correlation can originate simply by the above described differential initiation of myelination related to axonal size and a general "stop" signal of myelination that applies to the whole population of myelinated fibres (Fraher and Dockery, 1998). As an alternative mechanisms, Schwann cells could "sense" via molecular receptors a size-related signal secreted by the axon. A recent report proposes that the axonal protein neuregulin-1 could act as this axonal signal through ErbB receptors in Schwann cells. The authors showed that downregulation of neuregulin-1 in axons results in thinner myelin sheaths and upregulation of this protein increases myelin thickness (Michailov et al., 2004). Nevertheless, both results can be explained by delay in Schwann cell maturation and continuous myelination due to downregulation or upregulation of neuregulin-1, respectively. Leaving unresolved the mechanisms responsible for the axonal diameter-myelin thickness relation. After submission of this thesis, it was shown that the thinner myelin sheaths of axons with decreased neuregulin-1 expression was a consequence of myelination delay by Schwann cells (Schwab et al., 2004), confirming the alternative explanation exposed above.

Ranvier (1872) was the first to notice that internodal lengths (IL) were greater in larger than in smaller animal species, leading him to propose that elongation of the nerve was controlling the longitudinal size of Schwann cells. In addition, internodal lengths are positively correlated with axonal diameter. The origin of this relation can

be explained by the differential association of Schwann cells to axons of different diameters (as described above). Thus, axons that will become the largest in the nerve are sorted and associate first with individual Schwann cells. As the animal grows Schwann cells also extend longitudinally; those Schwann cells associated first with an axon will have a growth advantage over the smaller axons with Schwann cells associated later in development. This model suggests that the final internodal length is dependent on two parameters, the time of association of Schwann cells to an individual axon and the subsequent growth of the nerve fibre that determines the growth rate of the associated Schwann cell. Although several studies support this mechanism (Hiscoe, 1947), there are other studies showing that the growth rate of IL is higher than the growth rate of nerve fibres (Hildebrand et al., 1996; Nilsson and Berthold, 1988) implying the elimination of Schwann cells from the nerve fibre during development to compensate for this mismatch in growth rates.

1.2.3- Formation of the neuromuscular junction

The high fidelity of electro-chemical transmission displayed by the neuromuscular synapse is based on the formation of a complex and precise topography by discrete domains of several cells. Motor axon bundles reach the muscle and form extensive collaterals often confined to a central band across the muscle surface. At this stage, two types of muscles can be recognised in terms of the differentiation degree of their muscle fibres as the growth cone approach them (Pun et al., 2002). In the first class of muscles, termed "Delayed Synapsing" (DeSyn), the growth cone is responsible for the differentiation of muscle fibres in the contacted region. In "Fast Synapsing" (FaSyn) muscles, by contrast, growth cones encounter muscle fibres that have previously acquired nerve-independent differentiated features (henceforth referred to as primary specialisation), revealed by clustering of acetylcholine receptors. Subsequently, contact-dependent signals refine the preformed postsynaptic specialisation, and presynaptic differentiation develops.

In the following section, I briefly overview the cellular steps involved in synaptogenesis, followed by a description of molecules and mechanisms involved in hallmarks events of synaptogenesis.

Primary postsynaptic specialisation in FaSyn muscles: AchR clustering in absence of innervation

When myoblasts fuse to form myotubes, they begin to transcribe AchR subunit genes (α, β, γ and δ). For several years, AchR expression and other differentiation landmarks of muscle fibres were thought to be induced by motor neuron derived signals secreted when they approach the developing muscle (Burden, 1998; Sanes and Lichtman, 1999). Nevertheless, studies in aneural muscles generated by surgical procedures (Fallon and Gelfman, 1989) and in transgenic mice lacking motor neurons (Lin et al., 2001; Yang et al., 2001) have shown that transcription of AchR and the clusters of this protein localize to the midline of the muscle, which reveals a primary stage of differentiation in the absence of motor neurons and their axons (Pun et al., 2002). This process requires postsynaptic components involved in the neurally-induced AchR clustering (see below). The muscle-specific receptor tyrosine kinase (MuSK) is required for this localised AchR transcription in the absence of motor axons. As this role is not dependent on neurally derived agrin, a known activator of this receptor, an alternative pathway must be present. MuSK can be activated independently of agrin by its overexpression or by coexpression with rapsyn, an intracellular protein that clusters MuSK (Apel et al., 1997); therefore, it is possible that a high level of expression of MuSK in the central band of the developing muscle activates MuSK, which results in the cluster of AchR. Alternatively, other cellular components present in the developing muscle may be responsible for the patterning of AchR in the muscle fibre. In this regard, connective tissue cells located in the muscle tissue are known to be involved in shaping individual muscles from embryonic muscle cell masses (Harris, 1981). Also in *Drosophila*, specialized "founder cells" are responsible for the patterning of immature muscle and are thought to regulate the targeting of motor axons (Landgraf et al., 1999).

Clearly, the "neurocentric" view of synaptic formation does not account for early differentiation processes in a subset of developing muscles. An interesting possibility is that this primary muscle fibre differentiation regulates axonal pathfinding, restricting innervation to the muscle midline and perhaps stimulating nerve terminal differentiation (Ferns and Carbonetto, 2001).

Presynaptic differentiation

In contrast to the vast knowledge that is available about the mechanisms and molecules responsible for neurally-induced postsynaptic differentiation (see below), the factors and processes that stimulate presynaptic differentiation remain to be unveiled.

Newly-formed nerve terminals contain few synaptic vesicles and no recognizable active zones. Subsequently, nerve terminal specialisations are produced at sites of contact with the muscle fibre. Proteins present in the basal lamina, have been proposed as candidates for presynaptic differentiation; fibroblast growth factor 2 (FGF2) and the protein agrin, stimulate clustering of synaptic vesicles (Campagna et al., 1995; Dai and Peng, 1995). In addition, laminin isoforms exclusively present in synaptic basal lamina, inhibit axonal growth and stimulate the accumulation of synaptic vesicles (Porter et al., 1995). Nevertheless, *in vivo* evidence has not yet been provided to support the essential role of these factors in the initial stages of presynaptic differentiation.

Recently, proteins that initiate and promote presynaptic differentiation have been identified in the central nervous system, which could shed light onto motor axon differentiation at peripheral synapses. The first one, WNT7a a member of the family of secreted WNT proteins that is involved in cell fate decision and patterning events, acts as target-derived, secreted synaptogenic signal (Hall et al., 2000). In addition, the neuroligin-neurexin complex has been demonstrated to act as a contact-dependent signalling event that induces synapse formation (Scheiffele et al., 2000).

Arrival of the growth cone: Agrin signalling in postsynaptic specialisation

The results described above indicate that muscle fibres from FaSyn muscle types can generate a postsynaptic specialisation aneurally. Following this primary specialisation, signals derived from the motor axon are required to refine the previously-formed, muscle autonomous pattern (Yang et al., 2001). In addition, DeSyn muscle fibers are more dependent in the arrival of the growth cone for their end plate differentiation. In both cases, differentiation is characterised by AchR clustering and specialisation of a basal lamina component.

The fine tuning of AchR clusters is ensured by two main mechanisms: the redistribution of AchR and local gene transcription in subsynaptic muscle nuclei. These events are thought to be stimulated by the nerve-derived proteins agrin and neuregulin, respectively.

Agrin was first identified by its capability to induce AchR aggregation (Nitkin et al., 1987) and several subsequent studies have provided support to the hypothesis that agrin is the principal nerve-derived postsynaptic differentiation signal (Gautam et al., 1996). Although diverse proteins present in the myotube surface bind agrin, the muscle-specific tyrosine kinase (MuSK) has been proposed as the main postsynaptic signal-transducing factor that mediates AchR clustering (Hoch, 1999). The binding of agrin to a yet unidentified muscle receptor, leads to the phosphorylation of MuSK, and a yet unresolved signal transduction cascade triggers the aggregation of the protein rapsyn, required for AchR aggregation (Sanes and Lichtman, 1999).

The selective transcription of AchR genes by synaptic nuclei has been shown to be stimulated by the nerve-derived protein ARIA. This neuregulin-1 isoform, expressed by motor neurons and secreted into the synaptic cleft, activates AchR gene expression by a cascade of events downstream of the phosphorylation of the family of transmembrane tyrosine kinases receptors ErbBs (Fischbach and Rosen, 1997), which are concentrated in the postsynaptic membrane at the NMJ (Jo et al., 1995). As neuregulin-ErbB signalling is also essential for proliferation, migration and survival of Schwann cells (Garratt et al., 2000), the interpretation of the neuromuscular phenotypes of mice lacking this protein is complex, because Schwann cells develop poorly or not at all in its absence.

Synaptic maturation

During the first 1-3 postnatal weeks, neuromuscular junctions experience profound structural and functional changes. Synapse formation during foetal development results in muscles fibres being innervated by several motor neurons. Postnatally, this polyneuronal innervation pattern is transformed to a mononeural innervation state by a process normally referred to as "synapse elimination", which is driven by competitive and activity-dependent mechanisms but is also influenced by non-

competitive and activity-independent processes (Gates and Ridge, 1992; Thompson, 1983); (Buffelli et al., 2003; Costanzo et al., 2000; Goda and Davis, 2003).

As synapse elimination proceeds, the uniform plaque of AchR starts to exhibit low density areas of AchR, acquiring a pretzel-like configuration. The spatial register between pre- and postsynaptic structures becomes more precise, suggesting an increasing interdependence as developmental proceeds (Sanes and Lichtman, 1999). Topographically, the postsynaptic apparatus changes from a flat surface to an invaginated membrane with gutters and folds. This structural change is also accompanied by alterations in molecular components and their relative positions; AchR subunit composition shifts from an embryonic ($\alpha_2\beta\gamma\delta$) to an adult form ($\alpha_2\beta\varepsilon\delta$) and voltage- and ligand-gated channels, and their associated cytoskeletal elements, segregate into discrete alternating domains. Pre-terminal Schwann cells myelinate axons and terminal Schwann cells, which at birth form a loose cap over nerve terminals, constrain their domains by separately capping each terminal bouton. At this stage Schwann cells become nerve-independent for their survival. Although studies using transgenic mice lacking Schwann cells (Lin et al., 2000) suggest that this glial cell is not necessary for navigation of axons to their targets or initial steps of neuromuscular junction formation, in early postnatal development Schwann cell become essential for the survival of motor neurons (Woldeyesus et al., 1999).

1.3- STRUCTURE OF AXONS AND NEUROMUSCULAR JUNCTIONS IN ADULTS

1.3.1- Myelinated nerve fibre

The myelinated nerve fibre constitutes a unique acquisition of vertebrate evolution, allowing the fast propagation of action potentials along the axons at low metabolic costs. In addition, it represents one of the most extraordinary examples of cell-cell inter-relationships, in which axons and Schwann cells depend on each other to develop and maintain their structural organisation.

Myelinating Schwann cells that have acquired an adult phenotype are organised in distinct subcellular domains, which in turn remodel axons into highly polarised structures. In this section, I will review these defined domains in the Schwann cell and the axon, domains that have profound implications for the electrophysiology of the nerve fibre as discussed in later sections.

Compact myelin

Schwann cells synthesize the myelin sheath. This is interrupted by nodes of Ranvier at regular intervals. Each internode comprises the myelin sheath manufactured by a single Schwann cell (Webster, 1971). One of the major biochemical characteristics that distinguishes myelin from other cellular membranes is its high lipid to protein ratio: 70-80% lipids and 20-30% proteins (Garbay et al., 2000). This characteristic and the exclusion of almost all the conductive extracellular and cytoplasmic material during myelin compaction, confers ideal electrical insulating properties, crucial for the fast propagation of the action potential (reviewed below).

At the ultrastructural level, transverse sections of the myelin sheath exhibit a well ordered structure of alternating dark and light lines spiralling around the axon. The fusion of the cytoplasmic leaflets of the Schwann cell plasma membrane give rise to the major electron dense line (major dense line) and the close apposition of the extracellular leaflets of consecutive membrane spirals forms two electron dense lines spaced at a distance of 2.5 nm referred to as intraperiod line (Fig. 4).

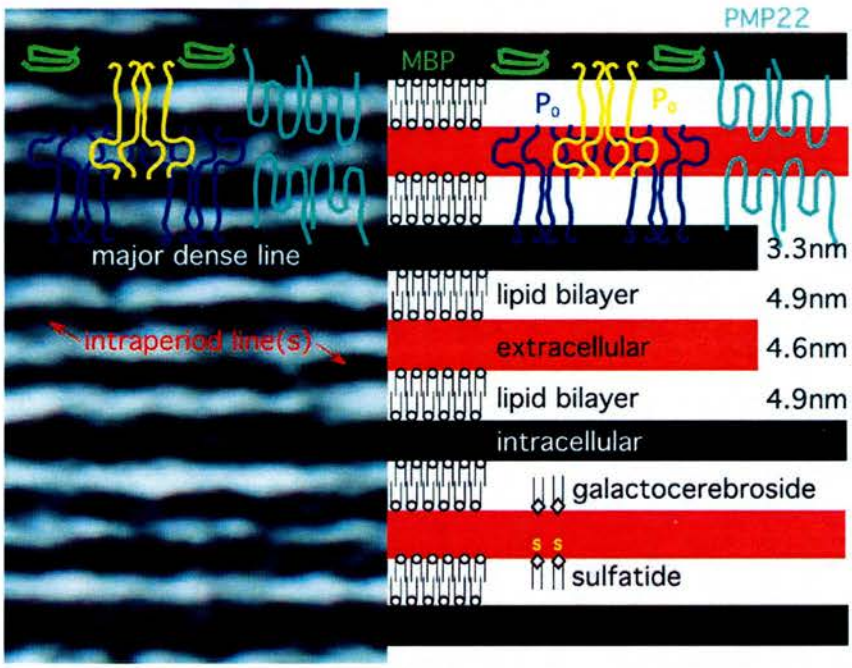

Figure 4. Ultrastructure of compact myelin and proteins involved on their stabilisation.
In the left side, a high power electron micrograph of compact myelin; a diagramatic representation is presented in the right side, including proteins involved in the structural organisation of the compact myelin sheath (after Scherer and Arroyo, 2002).

Cytoplasmic component of the Schwann cell

The cytoplasm of the Schwann cell is arranged as a complex channel network that runs longitudinally along the internode both in the outer or abaxonal side as well as in the inner region of the myelin sheath. In addition, Schmidt-Lanterman incisures run transversely through the myelin sheath. This arrangement provides a continuous connection between all cytoplasmic compartments of the Schwann cell, probably required for signal communication between axons and Schwann cells and metabolic support of the entire cell (Fig. 3).

Santiago Ramón y Cajal, using silver staining methods, was the first to describe the structural arrangement of the abaxonal Schwann cell cytoplasm (Ramón y Cajal, 1933) (Fig. 5A). He proposed that this network of cytoplasm was required for the efficient transport of nutrients along the internode to the more distal regions of the Schwann cell. The cytoplasmic domains are rich in filamentous actin and microtubules and their membranes contains caveolin-1 (Mikol et al., 1999), a protein involved in the formation of caveolae, which are invaginations of the plasma membrane known to regulate signal transduction and cholesterol transport (van Deurs et al., 2003). Regions devoid of cytoplasm are located between cytoplasmic rich domains, in close apposition with the outermost loop of compact myelin (Ushiki and Ide, 1987)(Fig. 5B and C). These regions are characterised by the presence of the protein L-periaxin in association with dytroglycan-related protein 2 (DRP2) (Sherman et al., 2001)(Fig. 5D). DRP2-periaxin associates with the dystroglycan receptor which links the extracellular matrix to the Schwann cell cytoskeleton (reviewed below). At the inner side of the myelin sheath (adaxonal side), the Schwann cell periaxonal plasma membrane is separated from the axon by a 12 to 14 nm periaxonal space and closely apposed to the myelin sheath except for a single cytoplasmic channel that traverses the entire internode. The connection between the adaxonal and abaxonal cytoplasmic compartments is provided by Schmidt-Lanterman incisures, cytoplasmic channels that run spirally through the myelin sheath. The role of incisures as conduits for metabolic material to the myelin sheath has been proposed. In agreement with this role, the number of incisures along the internode increases with fibre diameter (Hiscoe, 1947), suggesting that there exists an upper limit to the amount of myelin that can be maintained in a single region

between two incisures. In addition, radial diffusion of small ions has been reported to occur through gap junctions formed by the protein connexin-32 and linking apposed membranes of Schmidt-Lanterman incisures (Balice-Gordon et al., 1998).

Nodes of Ranvier

The node is the region of the nerve fibre devoid of myelin where the axonal membrane is exposed to the extracellular space (Fig. 6A). Voltage-gated sodium (Na^+) channels are highly concentrated in the axolemma in this region, and are instrumental in the local regeneration of the action potential that allows saltatory conduction of the nerve impulse (Fig. 6B). In addition to Na^+ channels, several transmembrane and cytoskeletal proteins are localised to the nodal axolemma, forming multiprotein complexes that link ion channels with the cortical cytoskeleton of the axon. The cytoskeletal protein ankyrin-G binds directly to Na^+ channels and βIV-Spectrin (Bouzidi et al., 2002) and also interact with two members of the neural cell adhesion molecules (neural CAM), NrCAM and neurofascin-186 (Garver et al., 1997). It has been shown that βIV-spectrin regulates the clustering of Na^+ channels at the nodes by providing a link between the Na^+ channel complex and the actin cytoskeleton (Komada and Soriano, 2002).

The length of the node is proportional to axonal diameter and can vary from less that 1 μm to more than 5 μm. Compared with the axonal diameter in the internodal region, the axonal diameter at the node is smaller, especially in large nerve fibres. The decrease in axonal diameter results in an increase in the density of microtubules, membranous vesicles and neurofilaments. The reduced neurofilament spacing arises as a results of neurofilament sidearm extension by a decrease in neurofilament phosphorylation (Mata et al., 1992). At the nodal gap, the Schwann cell extends cytoplasmic processes from the outer region of the cell, known as microvilli (Fig. 6C). Microvilli are connected between adjacent Schwann cells via tight junctions (Poliak et al., 2002) and closely appose the nodal axolemma (Ichimura and Ellisman, 1991). In addition to filamentous actin, microvilli are enriched in the homologous cytoskeletal-associated proteins, ezrin, radixin and moesin (ERM proteins) (Scherer et al., 2001). These Schwann cell processes are important for the formation of the nodal domains during development (Gatto et al., 2003). In addition, microvilli could

be involved in the communication between adjacent Schwann cells and in the maintenance of a microenvironment for the regeneration of the action potential at the node (Mi et al., 1996).

Paranodal region

Flanking the node of Ranvier, the compact myelin sheath opens and forms a cytoplasmic corridor that spirals around the axon and tightly associates to the axolemma by junctional complexes, known as axoglial junctions. Observed in longitudinal sections they appear as cytoplasmic loops derived from each turn of the myelin wrap (Fig. 6A). Paranodal loops are held together by autotypic adherens junctions (Fannon et al., 1995) and are communicated between each other by gap junctions (Meier et al., 2004).

Paranodal loops are separated from the axolemma at a distance of 2.5-3.0 nm by septate-like densities with a defined molecular composition. The axonal membrane at the axoglial junction contains the proteins Caspr and contactin that function as heterodimers interacting with the glial protein neurofascin-155 (Fig. 6B). Genetic inactivation of Caspr, contactin and neurofascin-155 in mice (Bhat et al., 2001; Boyle et al., 2001; PJ Brophy, unpublished observations) shown that these proteins are essential for the formation of the axoglial junction and the efficient conduction of the action potential, acting as barriers for ion diffusion away from the node and by spatially separating Na^+ and K^+ channels between the node and the juxtaparanode, respectively.

Juxtaparanode

The juxtaparanodal region is located under the compact myelin sheath adjacent to the innermost paranodal loop. The axonal membrane at this region is enriched in delayed rectifier K^+ channels, Kv1.1 and Kv1.2, their β subunits and a protein complex responsible for the localisation of these channels at the juxtaparanode (Fig. 6B). This complex is formed by the association of K^+ channels with Caspr2 through an as yet unidentified PDZ-domain containing protein. Caspr2 binds to the GPI-anchored protein TAG-1, which in turn may homodimerise in *trans* with TAG-1 protein located in the Schwann cell plasma membrane. This complex is responsible for the

accumulation of K^+ channels at the juxtaparanodal axolemma, as targeted disruption of Caspr2 or TAG-1 results in the dispersion of these channels through the axonal internode (Poliak et al., 2003; Traka et al., 2003). Although the physiological role of K^+ channels in the adult nerve fibre is not fully understood, it has been shown that their presence is critical for stabilisation of the action potential in branch points of the myelinated fibre near the neuromuscular junction (Zhou et al., 1999) and it has also been suggested that they may provide a protective function in partially demyelinated nerve fibres (Poliak and Peles, 2003). K^+ channels may also be mediating the communication between the axon and the glial cell as an activity dependent signal by the movement of potassium ions to the periaxonal space that are removed by connexin-29 hemichannels located at the adaxonal membrane of the myelinating Schwann cell (Altevogt et al., 2002).

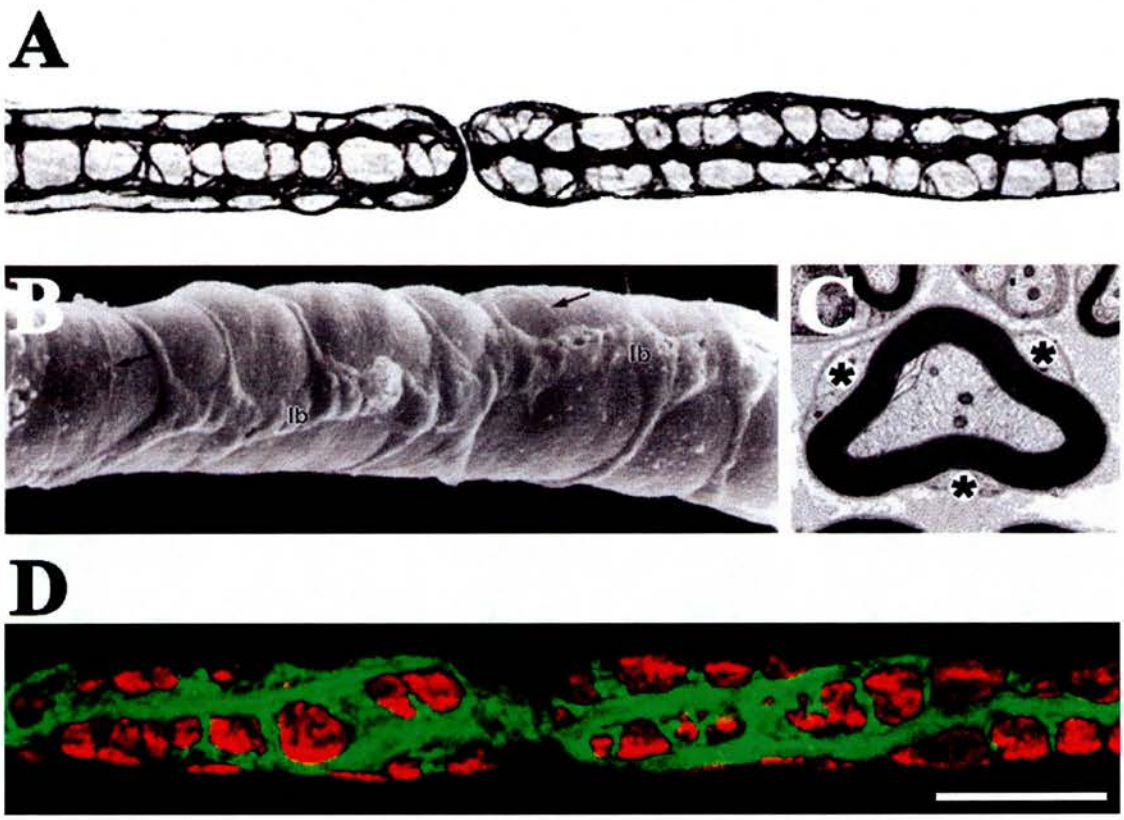

Figure 5. Cytoplasmic component of the abaxonal region of the Schwann cell. **(A)** Silver staining of nerve fibers by Santiago Ramón y Cajal (Ramón y Cajal, 1933) reveals the heterogeneity of the Schwann cell cytoplasm as bands that originate in the perinuclear regions and runs longitudinally along the Schwann cell. These longitudinal domains are connected by transverse trabeculae. **(B)** Scanning electron micrograph of the surface of a myelin forming Schwann cell showing the longitudinal arrangement of the cytoplasmic channels with fine trabecula connecting them (after Ushiki and Ide, 1987). **(C)** In electron microscope transverse sections, cytoplasmic channels appears as regions that protrude from the outermost wrap of the myelin sheath (asterisks) separated by appositions between the adaxonal surface of the myelin sheath and the Schwann cell plasma membrane. **(D)** Immunostaining of teased fibers with fluorescent-conjugated phalloidin (green) and an antibody against DRP2 (red). Schwann cell cytoplasmic domains revealed by Phalloiding staining are excluded from DRP2 positive patches. Scale bar, 20 μm.

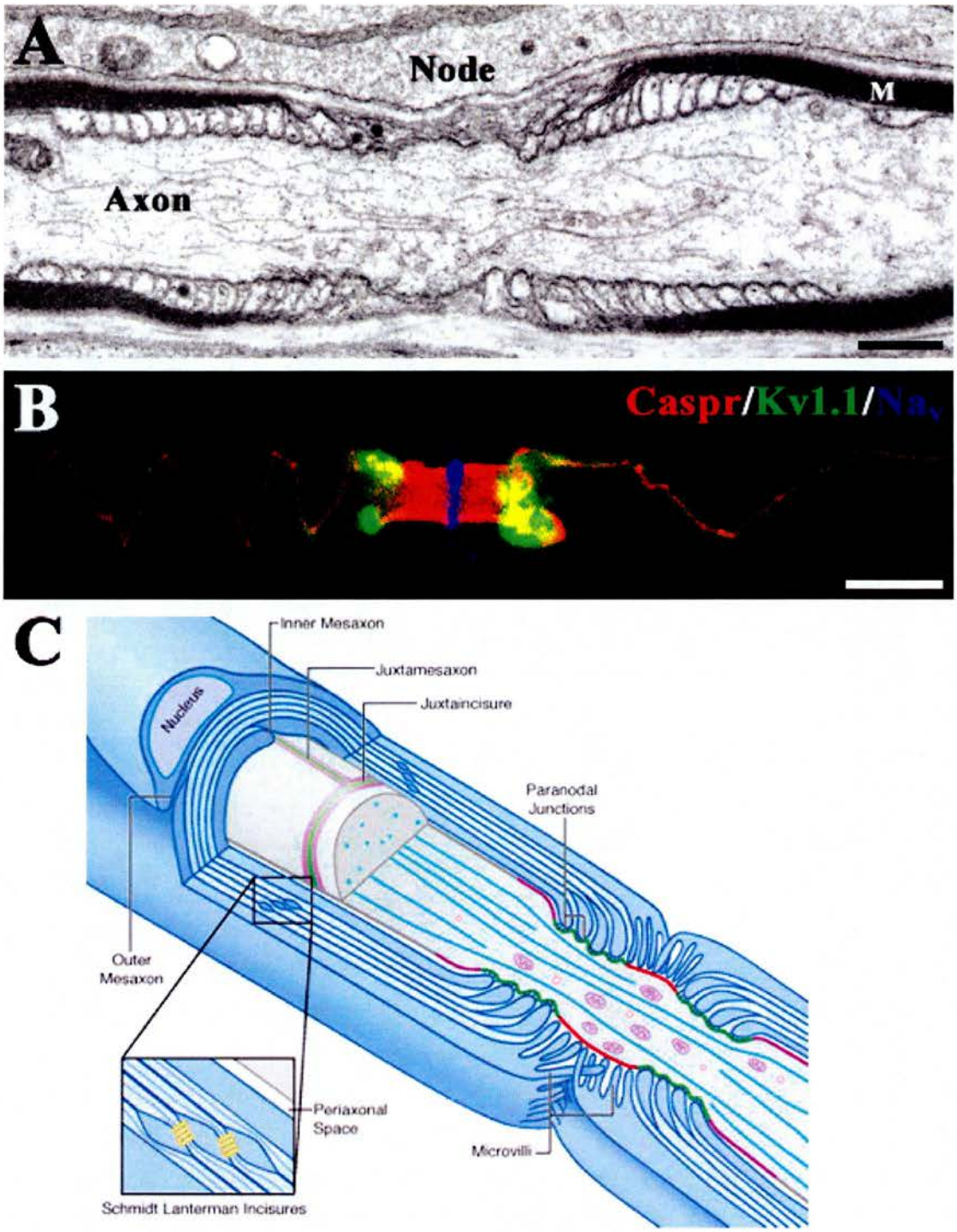

Figure 6. Structure of the node of Ranvier.
(A) Electron micrograph of a longitudinal section through a myelinated nerve fiber at the level of the node. M, myelin sheath. Scale bar, 0.1 μm. **(B)** Immunocytochemistry in a single teased nerve fiber using antibodies against sodium channels (blue), Caspr (red) and potassium chanels (green), which localise in the node, paranode and juxtaparanode, respectively. Scale bar, 10 μm. **(C)** Diagramatic representation of the node and adjacent domains (After Salzer, 2003).

1.3.2- Neuromuscular junction

Only two cells are required in order to produce a natural muscle contraction; one that generates the mechanical force and a second that triggers this action. Actually, the presence of a contractile unit (muscle fibre) and a trigger (motor neuron) is sufficient to perform this contractile activity in an artificial cell-culture system.

The cellular complexity exhibited by the real system provides in addition the capacity to modulate synaptic structure and function and to restore their original conformation following different mechanical or pharmacological insults. Therefore, an extensive analysis of the cellular components in the muscle may serve to reveal unresolved aspect of NMJ development, maintenance and plasticity that may also be relevant to understand synaptic structure and function in general, elsewhere in the nervous system. In the present section, I will not only describe the cells present in the neuromuscular regions, but also include in the following description, the diversity of cell-types which populate extrasynaptic domains. In addition, I will describe a particular situation in which the plasticity of the neuromuscular system is revealed, including the cellular reactions involved in this response.

Neuromuscular region

The neuromuscular synapse is a region in which different cells converge to form special cellular modifications in close spatial apposition. Proteins are concentrated in zones that lie in register between the pre- and postsynaptic regions to ensure a rapid and efficient transmission of the action potential.

The mechanical functions of the skeletal muscle are performed by syncytial myofibers (muscle fibres), which contains a specialized contractile apparatus maintained by large numbers of postmitotic nuclei. Each muscle fibre is innervated, normally in its middle region, by a single motor axon. In this region, representing only the 0.1% of the myofibre cell surface, the membrane invaginates and forms the so called junctional fold (Sanes and Lichtman, 2001). Nicotinic acetylcholine receptors (AchR) are concentrated at the crest of the folds, whereas other proteins, including sodium channels, are enriched in the depths of the folds. This arrangement is thought to increase the efficacy of synaptic transmission. The segregation in the radial axis of the postsynaptic region also applies to other proteins, including

cytoskeletal components, receptors, signalling and adhesion proteins (Sanes and Lichtman, 1999). In order to maintain these spatial and functional specialisations, the pattern of gene expression by subsynaptic (end-plate) nuclei, lying beneath the postsynaptic membrane, differs from nuclei located in extrasynaptic portions of the muscle fibre (Duclert et al., 1996).

Motor axon terminals locate above junctional folds and form specialised structures for transmitter release termed synaptic boutons, in which synaptic vesicles, filled with the neurotransmitter acetylcholine (Ach) cluster in specialisations of the presynaptic membrane, referred to as active zones (Fig. 7). The exquisite register of active zones with the mouths of the postjunctional folds ensures that the neurotransmitter acetylcholine secreted into the synaptic cleft will encounter a high concentration of AchR in the post-synaptic membrane, thus facilitating synaptic transmission.

Myelin-forming Schwann cells associate with pre-terminal regions of axons. In the end-plate region, a non-myelinating type of Schwann cell, commonly referred to as terminal Schwann cell (tSC) caps terminal branches and synaptic boutons with a high degree of registration to the pre- and postsynaptic specialisations (Fig. 7). Although once considered as passive elements in neuromuscular dynamics, terminal Schwann cells have now been recognized as a highly active element of the neuromuscular junction. They respond to the state of innervation by structural and biochemical changes, but are also sensitive to the level of activity exhibited within their neuromuscular junction (Castonguay and Robitaille, 2001; Jahromi et al., 1992). In neuromuscular junctions where tSC have been ablated, nerve terminals retract and neurotransmitter release is reduced (Reddy et al., 2003), underscoring the role of tSC in the maintenance of synaptic structure and function.

In addition to the cellular components of the NMJ, a basal lamina surrounds each muscle fibre, which traverses the synaptic cleft and ensheathes terminal and myelin-forming Schwann cells. Muscle basal lamina components are similar to those present in basal lamina throughout the body (e.g. collagen, laminin, heparan sulfate proteoglycans) but in the muscle their isoform composition, especially laminin proteins, exhibit spatially- and temporally-restricted expression (Patton et al., 1997; Sanes et al., 1990). The molecular constitution of the extrasynaptic basal lamina

differs from the synaptic one and even in the synaptic region, the basal lamina composition changes markedly between different domains (i.e. synaptic cleft, junctional folds and Schwann cell). Basal laminae play important roles in the formation and maintenance of the neuromuscular synapse. In synaptogenesis, the basal lamina promotes differentiation of axons into nerve terminals, mediates adhesion of nerve to muscle and concentrates several molecules required for postsynaptic differentiation and the normal function of the neuromuscular synapse (e.g. acetylcholinesterase) (Sanes and Lichtman, 1999). In addition, basal lamina components maintain the integrity of the nerve-muscle apposition by their adhesive properties but also actively repelling terminal Schwann cells from the synaptic cleft (Noakes et al., 1995).

Extrasynaptic region

Neuromuscular synapse cell components differentiate in order to perform their specific activities described above; they withdraw from the cell cycle and exhibit a special pattern of gene expression. With some exceptions, this differentiation process is permanent; therefore, the capacity to repopulate these cells depends on the presence of a stem cell compartment. The extrasynaptic region has been widely recognized to serve as the source of several populations with stem cell characteristics, which are not only the cellular source for growth, repair and maintenance of skeletal muscle, but can also contribute to alternative non-muscle lineages (Bailey et al., 2001). One of the most studied lineages of myogenic progenitors are muscle satellite cells, located close to the muscle fibre, between the sarcolemma and the basal lamina (Hawke and Garry, 2001). This cell population remains mitotically quiescent in the unperturbed state of the muscle, but in response to stimuli such as myotrauma, they proliferate and start to express proteins related to the skeletal muscle lineage (Kuschel et al., 1999). Subsequently, activated satellite cells fuse to each other to form myofibers.

In addition, skeletal muscle contains a population of pluripotential stem cells, referred to as the side population (SP). This cell lineage is distinct from satellite cells (Seale et al., 2000) and can give rise to myogenic satellite cells and differentiate into all major blood lineages (Jackson et al., 1999). Another population of stem cells was

recently identified in the interstitial spaces of skeletal muscle using the stem cell marker CD34 (Qu-Petersen et al., 2002). This population was isolated and displayed the capacity to reconstitute muscles and differentiate into vascular endothelial cells.
The muscle extrasynaptic compartment, mainly studied because it constitutes a reservoir of stem cell populations, also has to be considered as the arena in which axons and glial cells navigate during synaptogenesis and neuromuscular system regeneration in order to reach the appropriate target structure. Therefore the study of cell populations, other than stem cells, located in these areas could shed light onto unresolved mechanisms involved in these processes.

Neuromuscular plasticity

The adult neuromuscular synapse exhibits a remarkable capacity for functional and structural adaptation in response to different stimuli. From the diversity of stimuli that can elicit a plastic response by the neuromuscular apparatus, the destruction of a portion of the motor supply of the muscle -termed partial denervation- has been used as an experimental paradigm owing to its capacity to evoque a wide range of structural changes in the neuromuscular system, which allow us to study the contribution of NMJ-associated cells in remodelling processes. Partial denervation followed by reinnervation also leads to a transient state of polyneuronal innervation, resembling early postnatal life, providing the opportunity to study processes involved in the transition from multiple to single innervation.
Following partial denervation, terminal Schwann cells (tSC) grow into the synaptic cleft, surrounding fragments of degenerating nerve terminals and positioning themselves in register with postsynaptic specializations (Balice-Gordon, 1996; Son et al., 1996). In addition, tSC elaborate extensive processes along the muscle surface. This "activated" phenotype of tSC is also characterized by the novel expression of the growth-associated protein GAP-43 (Woolf et al., 1992) and nestin (Kang et al., 2001). Some processes extended by reactive tSC reach innervated end-plates inducing the sprouting of motor axons and guiding them to the denervated synapses (Son and Thompson, 1995) where they establish functional synapses (Fig. 8). Reinnervation by the original motor pool creates a condition in which several motor neurons transiently innervate the same muscle fibre (Brown and Ironton, 1978),

recapitulating the situation that occur in early postnatal NMJ maturation but differing in several ways. First, regenerating axons find a well differentiated postsynaptic target, in contrast to the primary differentiation of muscle fibres that developing motor axons encounter. Second, Schwann cells normally follow developing axons, serving as guides for regenerating axons. Following a process of synapse elimination, neuromuscular synapses may recover the characteristic of a single motor axon innervating a muscle fibre, although some polyneuronal junctions can persist, perhaps indefinitely (Barry and Ribchester, 1995).

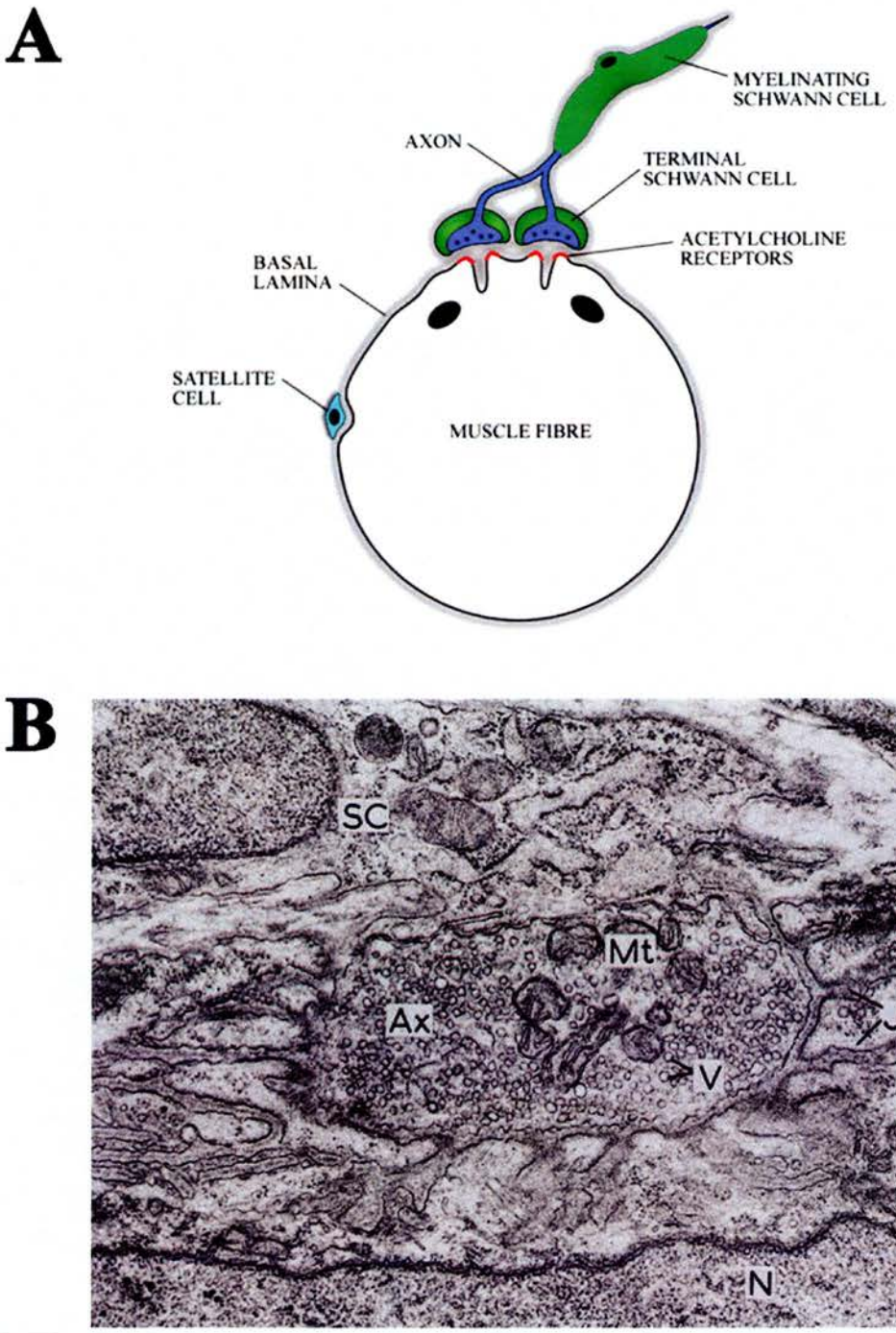

Figure 7. Structure of the neuromuscular junction.
(A) Diagram representing a transverse view of a muscle fiber and associated cells in the neuromuscular junction and extrasynaptic area. **(B)** Electron micrograph reveals the complex structure of the neuromuscular junction and some of the cell components represented in the diagram; S, terminal Schwann cell; Ax, axon terminal; Mt, mitochondria; V, synaptic vesicles; N, nuclei; (After Landon, 1975).

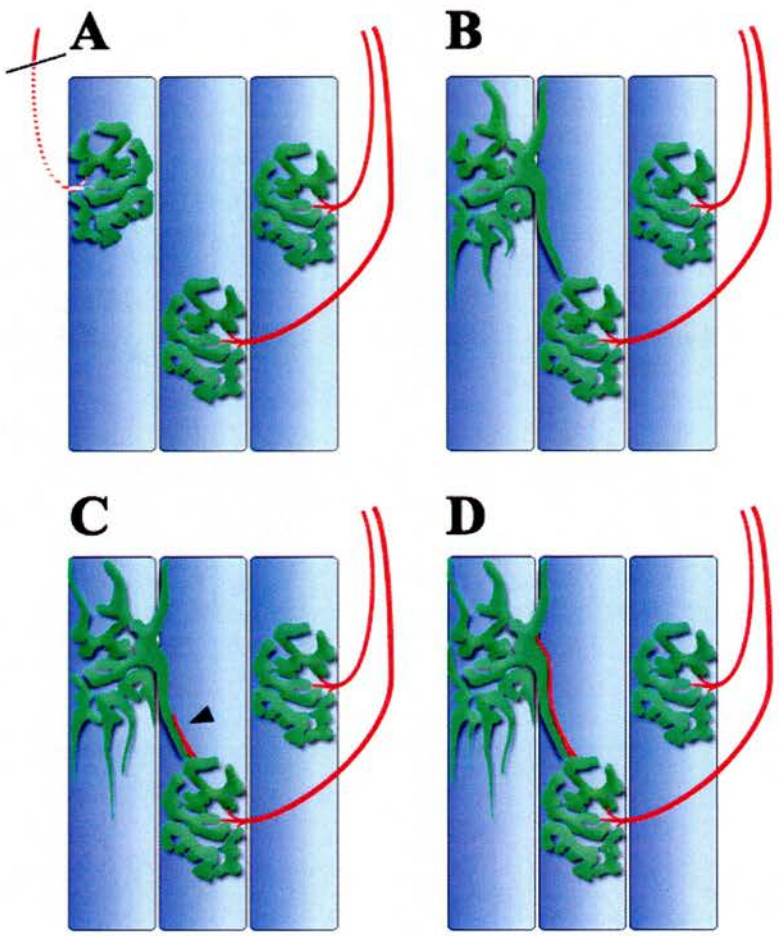

Figure 8. Response of neuromuscular-associated cells to partial denervation.
(A) Denervation of a portion of the muscle motor supply (black line) leads to degeneration of the distal portion of the transected axon. **(B)** Terminal Schwann cells from the denervated end-plate begin to extend processes, eventually reaching an innervated junction. **(C)** The nerve terminal is induced to sprout by contact with the terminal Schwann cell sprouting (arrowhead). The nerve sprout is guided by the terminal Schwann cell "bridge", reaching the denervated junction **(D)**.

1.4- ELECTROPHYSIOLOGY OF THE PERIPHERAL NERVOUS SYSTEM

Qu. 24. Is not Animal Motion perform'd by the Vibration of this Medium, excited in the Brain by the Power of the Will, and propagated from thence through the folid, pellucid and uniform Capillamenta of the nerves into the Muscles, for contracting and dilating them?

Newton (*Optiks*, second edition 1718)

Although Newton's question described reasonably well the thread of events required for animal motion, it was not until the development of the science of electricity and Galvani's research in animal electricity during the 1780's that the nature of the "Vibration" was uncovered. Subsequently, important advances in electrophysiological techniques, complemented with ultrastructural investigations using electron microscopes have increased our understanding of the electrophysiological properties of the myelinated fibre and the morphological parameters involved in its regulation. This structure-function relationship of the peripheral nervous system will be discussed in the following section with special reference to the myelinated nerve fibre and the neuromuscular junction.

1.4.1- Myelinated axons and the conduction of the action potential

Large calibre axons in the peripheral nervous system are surrounded by the myelin sheath, which is interrupted at regular intervals by nodes of Ranvier. This structural arrangement profoundly affects the electrical properties of the nerve fibre, allowing fast conduction of the action potential with considerable economy of space and energy.

The myelin sheath presents a much higher transverse resistance and lower capacitance than a normal cell membrane, reducing the current flow across the internodal axonal membrane. In addition, voltage-sensitive ion channels are heterogenously localised along the axon, with a high density of voltage-sensitive sodium (Na^+) channels at the node (approximately $1000/\mu m^2$) and a much lower density along the internodal region under the myelin sheath ($<25/\mu m^2$) (Ritchie and

Rogart, 1977)(Fig. 6B). As a result of these characteristics of the myelinated fibre, the regeneration of the action potential takes place only at the nodes as a consequence of the movement of Na ions into the cell (down its electrochemical gradient) through voltage-sensitive Na^+ channels. The local current generated at the node spreads electrotonically (passively) through the relatively low-resistance axoplasm with a small decrease in amplitude as a result of the insulation provided by the myelin sheath. This local current then activates Na^+ channels in the subsequent node. Nodes of Ranvier are analogous to the amplifiers that were situated along sub-Atlantic telephone cables: telephonic signals decrease in size as a result of leakage across the cable, but are regenerated at regular intervals by the amplifiers. The high velocity of local current spread along the axon and the regeneration of the action potential limited to the nodes results in a high conduction velocity of the action potential (in the range of 20 to 120 m/s). Unidirectionality of the action potential is ensured by the inactivation and refractory period of Na^+ channels following their voltage-induced activation. The discontinuous nature of the action potential regeneration in the myelinated fibres was verified experimentally by Tasaki and Huxley & Stämpfli in the 1940s by showing that the inward current flow in individually dissected nerve fibres was restricted to the nodes (Huxley and Stampfli, 1949; Tasaki, 1939)(Fig. 9). They named this form of conduction of the action potential as "saltatory" (from the Latin *saltare*, to jump). As stated above, fast K^+ channels ($K_v1.1$ and $K_v1.2$) are expressed at low densities in the nodal axon membrane (Devaux et al., 2004), and present at high densities in the juxtaparanodal region (Wang et al., 1993). In addition, Na^+/K^+-ATPase molecules are present in the nodal axolemma, where they maintain ionic homeostasis and are responsible for electrogenic hyperpolarization (Gordon et al., 1990).

The organisation of the myelinated fibre has significant implications for nervous system structure. Conduction velocity in nonmyelinated fibres is proportional to the square root of axonal diameter or to the fourth root of its cross-sectional area. In order to double the conduction velocity, the area of the fibre must increase by a factor of sixteen. In myelinated fibres, the conduction velocity is directly proportional to fibre diameter and can feature fast conduction velocity without a considerable increase in axonal size. In this way the myelinated nerve bundle can

carry more information per unit time, allowing fine muscular control. In addition, the above conduction velocity-diameter relationship predicts that above a critical diameter of about 1 μm, myelinated fibres can conduct action potentials faster than unmyelinated fibres of the same diameter, this prediction is consistent with the fact that axons with diameters above 1 μm are generally myelinated (Rushton, 1951).

Parameters influencing nerve conduction velocity in the myelinated nerve

Theoretical and experimental work have shown that four parameters of the myelinated fibre can influence the conduction velocity of the action potential, i.e. axonal diameter, myelin thickness, internodal length and the tightness of the axoglial junction at the paranodal region.

The influence of axon diameter and the myelin thickness can be explained by three passive conduction properties or cable properties of the axon, i.e. internal resistance of the axon (r_i), membrane resistance (r_m) and membrane capacitance (c_m). If r_i is high, the spread of the local current is slower, if r_m is high, the local current will spread faster. In addition, the velocity of the action potential will depend on the rate at which the membrane capacitance (c_m) ahead of the action potential can be charged, therefore if the c_m is high, it will take longer and more current to charge the capacitor and the action potential will travel slower. The parameters r_m, r_i and c_m are all related to the radius of a fibre,

$$r_m \propto 1/2\pi\text{radius}$$

$$r_i \propto 1/\pi\text{radius}^2$$

$$c_m \propto \text{radius}$$

Therefore, if the axon increase in diameter r_m and r_i decreases, the internal resistance decreases faster relative to the membrane resistance, increasing the velocity of conduction. Increase in axonal diameter will also increases c_m, but this increase is proportional to the increase in the radius while the decrease in r_i is proportional to the radius squared. Myelin thickness also influences two of these parameters; r_m is directly and c_m inversely proportional to the thickness of the myelin sheath. Hence,

as myelin thickness increase, r_m increases and c_m decreases, both parameters change in a way that positively influence the conduction of the action potential.

In theory, internodal length (IL) should influence nerve conduction velocity as the presence of more nodes in a given segment (decrease IL) increases the action potential regeneration events, thus increasing the time for the action potential to travel along the nerve fibre. This has not been experimentally verified, as both axonal diameter and myelin sheath thickness positively covaries with internodal length. Simulations of action potential conduction in myelinated fibres have been used to address this issue (Brill et al., 1977; Moore et al., 1978). These have shown that nerve conduction velocity is independent of the IL from changes around 1500 μm, but becomes dependent at shorter internodal lengths (25-750 μm).

The sensitivity of nerve conduction velocity to the structural state of the axoglial junction has been studied in the contactin null mice (Boyle et al., 2001). Myelinated nerve fibres in these mice show an absence of axoglial junctions that result in widened paranodal gaps between the axolemma and the glial paranodal loops; axonal diameter, myelin thickness and internodal length appears normal. Nerve conduction velocity in contactin null nerves is severely reduced. As the authors indicate, the increased paranodal gap probably increases the capacitance at the paranodal junction and decreases the resistance through the paranodal junction with a concomitant loss of current flowing back through the paranode instead of spreading longitudinally towards the downstream node.

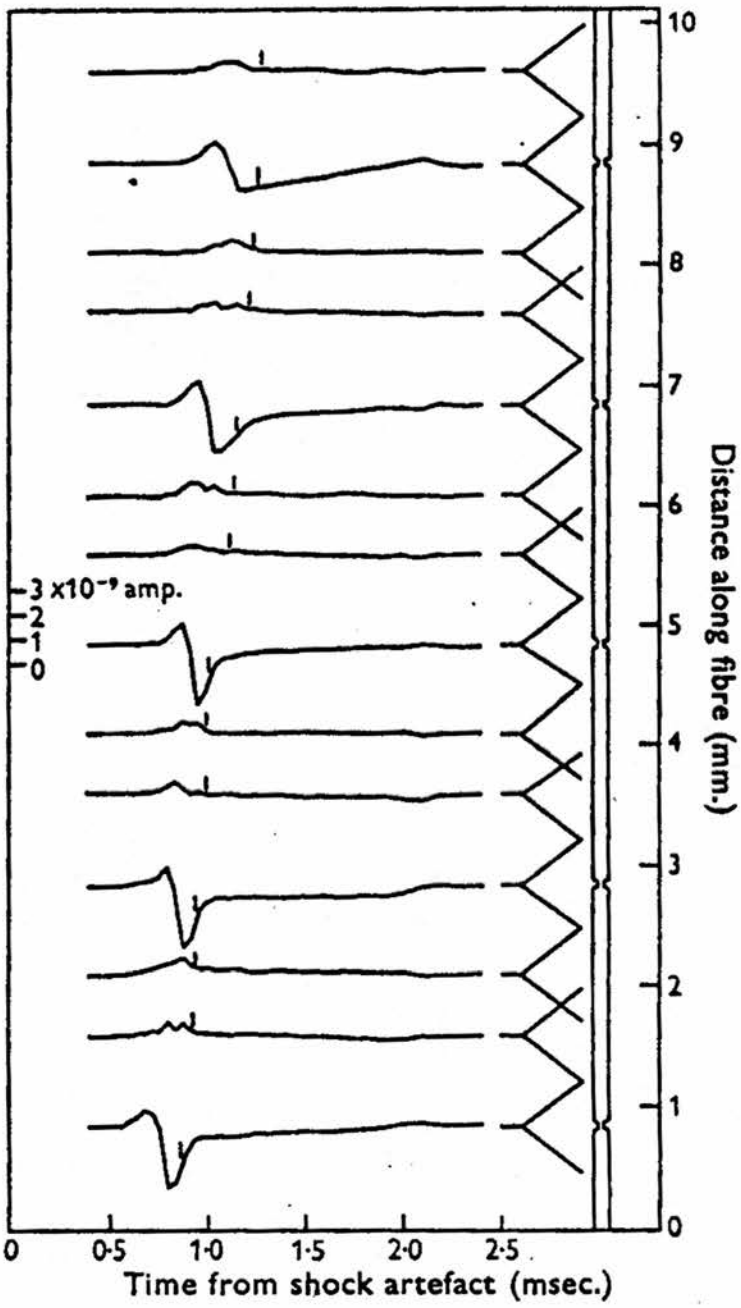

Figure 9. Discontinuous nature of the action potential regeneration in myelinated fibers.

Figure from the classic article by Huxley & Stämpfli (Huxley and Stampfli, 1949). Its shown membrane currents at different positions along a nerve fiber represented diagramatically on the rigth. Notice that only in the nodal regions a significant current is recorded. Inward current is plotted downwards.

1.4.2- Propagation of the action potential at the neuromuscular junction

In their distal domains, myelinated motor axons and their associated Schwann cells undergo profound structural changes that contrast with the homogeneous structure in proximal regions. On entering the muscle, motor nerve fibres branch to innervate a variable number of muscle fibres, correlating with the degree of precision required by the muscle to achieve its function. The number of muscle fibres innervated by a single motor axon is referred to as motor unit. Thus, a muscle requiring fine control display a large number of smaller motor units; the contrary situation is implemented in muscles that perform broad movements or posture sustainment.

Following the primary branching, the motor axon contacts the muscle fibre in a specialised area know as the motor end plate (Fig. 10). At this site, the tip of the motor axon branches profusely, with each branch ending in a specialized terminal structure of the axon referred to as synaptic bouton. These boutons contain vesicles loaded with the neurotransmiter acetylcholine. Axons lose their myelin sheath as they approach the vicinity of a motor end-plate, right before the terminal branching. Myelin-forming Schwann cells near the branching point are characterised by short internodal lengths that decrease proportionally more than either axonal diameter or myelin thickness (Quick et al., 1979). This feature should increase the safety factor for nerve conduction of the action potential in regions of fibre branching, where the safety factor for conduction is relatively low (Smith, 1980).

Action potential regeneration in the last node of Ranvier spreads electrotonically to the presynaptic terminal, where an active Na current is generated exclusively in the region after the last myelinated segment where Na^+ channels are concentrated (Brigant and Mallart, 1982; Mallart and Brigant, 1982). Inward Na current depolarises the terminal region by electronic spread causing the opening of voltage-dependent calcium (Ca^{2+}) channels. Inward flow of Ca^{2+} initiates a sequence of events that results in the mobilization of synaptic vesicles, their fusion with presynaptic membrane and release of acetylcholine (Ach) into synaptic cleft by exocytosis.

Release of Ach to the synaptic site take place as a result of a complex calcium-dependent mechanism that docks and opens neurotransmitter-filled vesicles into the synaptic cleft. It involves several proteins located in synaptic vesicles and at precise

sites on the terminal plasma membrane, known as active zones. During synaptic vesicle exocytosis, the synaptic vesicle SNARE (v-SNARE) synaptobrevin 2, forms a complex with two target SNAREs (t-SNAREs), syntaxin 1 and SNAP-25, on the presynaptic plasma membrane (DeBello et al., 1995). The formation of this SNARE complex drives membrane fusion by pulling synaptic vesicles toward the presynaptic membrane. Finally, synaptotagmin respond to increase in calcium concentration in the nerve terminal, regulating the final steps of vesicle fusion (Mochida, 2000). Acetylcholine released into the synaptic cleft activates receptors leading to post-synaptic depolarization, the end-plate potential (EPP), which activates voltage-gated Na^+ channels in the junctional folds. The resulting action potential is propagated along the muscle fibre membrane, triggering muscle fibre contraction.

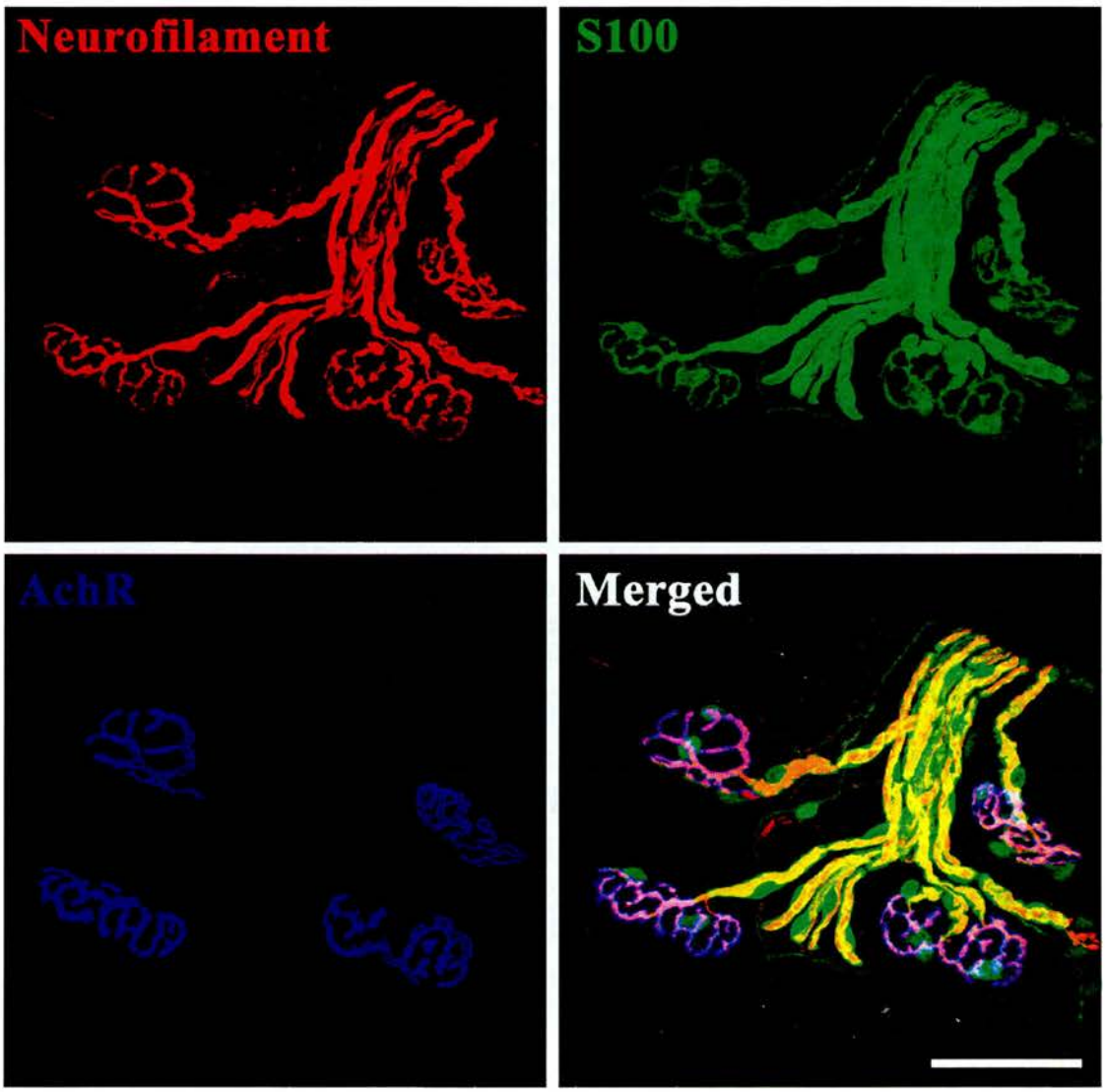

Figure 10. Cellular organization at the neuromuscular junction.
(A) Whole mounts muscle triple immunostaining with antibodies against neurofilament and synaptic vesicle protein (red), the Schwann cell protein S100 (green) together with AChR staining (blue). Individual colour channels are shown in addition to the merged picture. Notice the exact register between axon terminals and acetylcholine receptors; terminal Schwann cells locate above these structures covering the neuromuscular synapse area. Scale bar, 50 μm.

1.5- PERIAXIN NULL MICE AS A MODEL OF CHARCOT-MARIE-TOOTH DISEASE

Charcot-Marie-Tooth (CMT) diseases comprise a group of hereditary neuropathies heterogeneous in their clinical and molecular features. They were first described by Charcot and Marie, in France, and Tooth in England, in 1886. The clinical phenotype of CMT, although showing considerable variability, is characterised by progressive muscle weakness and distal sensory disfunction. Several genes have been associated with CMT and the original classification, mainly based on the disease phenotypic expression has been reformulated; autosomal dominant demyelinating forms are referred as CMT1 and CMT3 and recessive demyelinated as CMT4. The CMT2 subclass constitute those related to axonal gene mutations. A number of animal models representing different forms of CMT diseases have been generated by genetic engineering or have arisen by spontaneous mutation, providing valuable information about the disease mechanisms.

Mutations in periaxin (Prx), a protein expressed exclusively by myelinating Schwann cells in the peripheral nervous system, have been reported to cause demyelinating forms of CMT (Takashima et al., 2002); as these mutations act in a recessive manner, they have been classified as CMT4. Genetic ablation of the periaxin gene in mice has been performed (Gillespie et al., 2000). Periaxin null mice ensheath and myelinate axons in an apparently normal manner, but develop a late onset demyelinating neuropathy, confirming the importance of periaxin in the maintenance of the myelin sheath (Fig. 11). Phenotypically, the mice show tremor, an inappropriate clasping reflex, reduced peripheral nerve conduction velocity and pain behaviour in reflex tests (Gillespie et al., 2000). In addition, molecular analysis of peripheral nerves in wild-type and periaxin null mice have provided relevant information on the molecular organization of periaxin and its associated proteins as described below.

During development, periaxin translocates from the adaxonal region to the abaxonal plasma membrane of the Schwann cell (Scherer et al., 1995), where it localises to appositions between the Schwann cell plasma membrane and the outermost layer of the myelin sheath. Periaxin associates with the dystrophin-related protein 2 (DRP2), a protein restricted to appositions and member of the dystrophin glycoprotein

complex (DGC) (Sherman et al., 2001) (Fig. 5D). In the peripheral nerve fibre and skeletal muscle, DGC links components of the basal lamina to the cortical actin cytoskeleton (Winder, 2001). In Schwann cells, DGC is composed of α- and β-dystroglycan, sarcoglycans, utrophin, a truncated form of dystrophin (Dp116) and DRP2 (Fig. 12). Periaxin, in addition to associates with DRP2, homodimerises by its PDZ domains, which probably contributes to the clustering of the dystroglycan-DRP2 complex to specific regions of the Schwann cell plasma membrane, referred above as appositions. This hypothesis is supported by the observation that without periaxin, DRP2 is mislocalised and reduced in quantity (Sherman et al., 2001). Although important observations have been produced in the periaxin null mice, the link between disruption of the DGC-DRP2 complex and the late onset demyelinating condition has not yet been resolved.

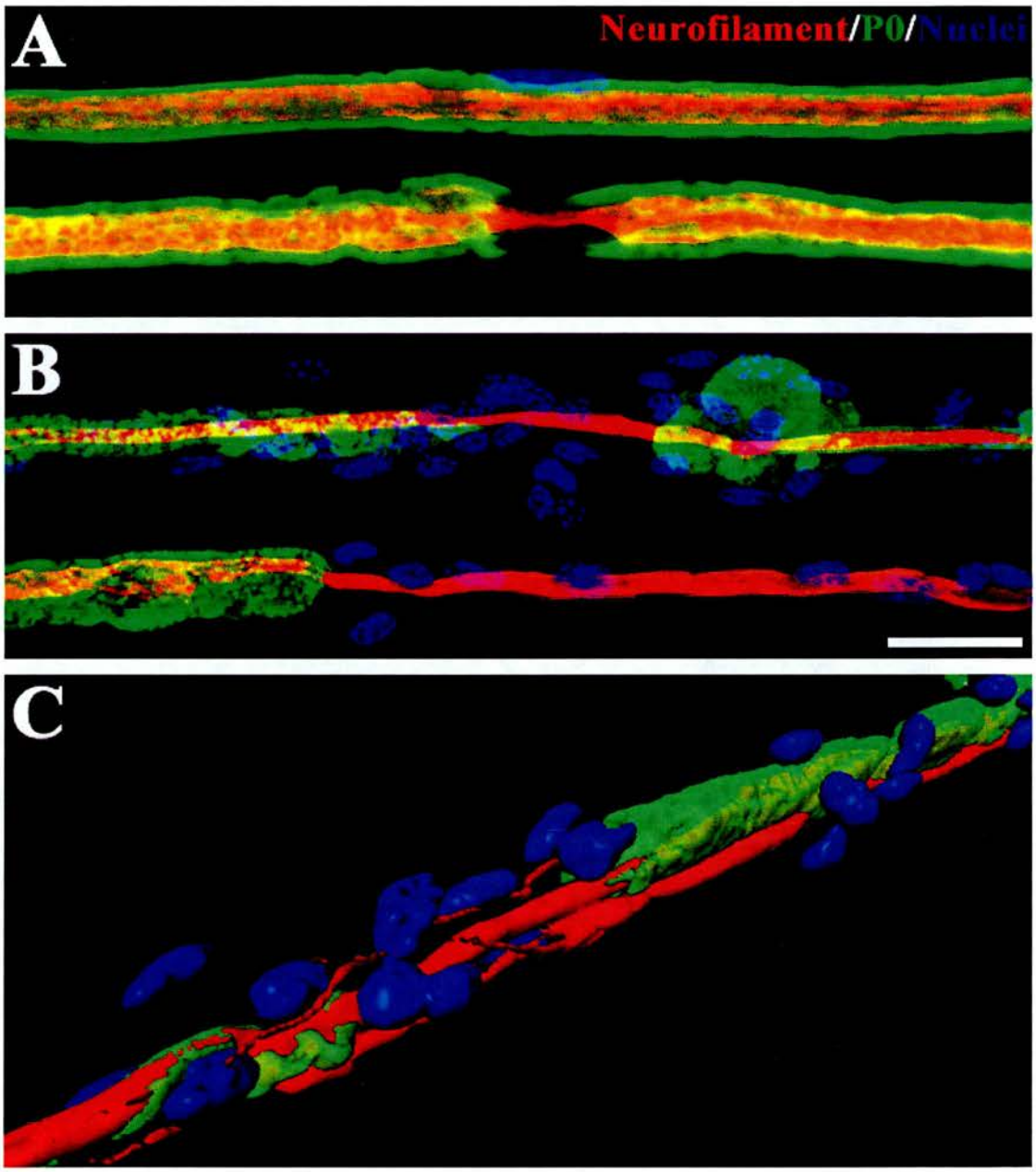

Figure 11. Peripheral demyelination in periaxin null mice.
Teased sciatic nerve fibres from 8-month old wild-type **(A)** and periaxin null mice **(B)** were immunostained for the myelin protein P0 (green), neurofilament (red) and nuclei (blue). The null mutant shows focal thickenings of the myelin sheath flanking demyelinated segments and an increased number of nuclei, corresponding to Schwann cells attempting to remyelinate demyelinated fibres. In **(C)**, a three-dimensional rendering was performed in a periaxin null teased fibre illustrating the presence of sprouts in the demyelinated segment. Scale bar, 20 μm.

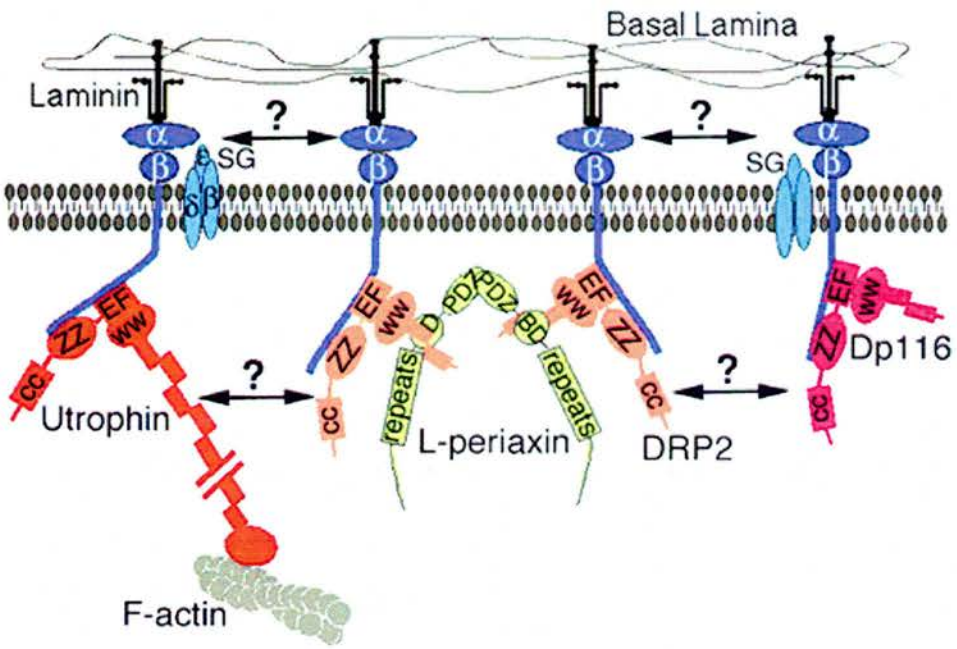

Figure 12. DRP2-Dystroglycan complex in myelin-forming Schwann cells
Schematic representation of the dystroglycan complex (DGC) and associated proteins. DGC links the basal lamina to the cortical actin cytoskeleton. DRP2 associates with DGC and periaxin. Periaxin, in turn, homodimerise by its PDZ domains (after Sherman et al., 2001).

1.5- AIMS OF THE PROJECT

The general aim in this thesis was to examine how the particular relationship between cellular components of the peripheral nerve and the neuromuscular junction are involved in the morphological and electrophysiological characteristics of each of the cellular components (or functional units) under both normal and perturbed conditions. This aim has been approached in three sub-projects, with the following specific objectives.

1- To determine the molecular components involved in the compartmentalisation of the Schwann cell cytoplasm and how this subcellular organisation influences the Schwann cells phenotype; to finally asses how morphological changes in the Schwann cell regulate the conduction of the action potential in myelinated fibres.

2- To characterise the complete cellular configuration of the neuromuscular junction, paying particular attention to cells other than terminal Schwann cells, motor nerve terminals or muscle fibres, and their role in the plastic responses of the neuromuscular system.

3- To determine the consequences of peripheral demyelination for the structure and function of the neuromuscular apparatus, in order to understand the possible contribution of morphological and electrophysiological changes at the neuromuscular junction to the phenotype of demyelinating conditions.

2- RESULTS

2.1- SCHWANN CELL-AXON RELATIONSHIP IN THE REGULATION OF NERVE CONDUCTION VELOCITY

The myelinated nerve fibre in the peripheral nervous system is a functional unit composed of the axon and its associated Schwann cell. The relationship established between these two cells is crucial for the definition of specialised domains along Schwann cells and axons, domains that are involved in fast transmission of the action potential.

During postnatal development myelinating Schwann cells grow extensively in length, at the same time they produce a compact myelin sheath around the axon. Schwann cell growth and maintenance of several distinct structural domains along its length requires an efficient mechanism for trophic support of distal regions. At the same time this mechanism should correctly target components to their proper locations.

Santiago Ramón y Cajal was the first to report that the cytoplasm of Schwann cells is arranged as an intricate reticular array of cytoplasmic channels along the abaxonal region of the cell (Ramón y Cajal, 1933). He speculated that this cytoplasmic arrangement was probably required for trophic support of the entire Schwann cell. More recent studies have shown that between cytoplasmic regions, an ordely pattern of apposition is present between the plasma membrane of the Schwann cell and the outermost loop of the myelin sheath (Sherman et al., 2001). Appositions contain a dystrophin-glycoprotein complex associated with DRP-2 and periaxin, but the role of this complex in the formation of apposition has not been addressed.

In this study, I have explored the possibility that periaxin is directly involved in the structural maintenance of appositions and analysed the role of appositions in the formation of cytoplasmic domains in Schwann cells. The function of the cytoplasmic network has been addressed, providing important information related to the specification of structural parameters related to the axon-Schwann cell unit and the influence these parameters have in saltatory conduction of the action potential.

2.1.1- Cajal Bands in Schwann cells are disrupted in the periaxin null mice

In order to test the hypothesis that periaxin is required in the formation of Schwann cell abaxonal appositions, teased fibres from 3-week old wild-type (WT) and Prx-null (KO) quadriceps nerves were immunostained with an antibody directed to the Schwann cell cytoplasmic protein S100 and examined by confocal microscopy.

As shown in figure 13A, immunolabelling with S100 antibody in WT fibres reveals the longitudinal and transverse cytoplasmic channels in the Schwann cell, henceforth called Cajal bands. In contrast, cytoplasmic channels were absent in periaxin-null Schwann cells, which present a continuous signal from the S100 immunostaining along the Schwann cell (Fig. 13A).

The use of confocal microscopy allows projections to be made along any axis of the acquired 3D volume. This property of the imaging system was used to obtain more information concerning the disruption of Cajal bands in periaxin null Schwann cells. Triple-immunostaining using antibodies against neurofilament, the myelin protein MBP and S100 were applied to teased fibres from 3-week old WT and KO quadriceps nerves and the complete volumes containing individual nerve fibres were obtained by confocal microscopy. With this information, longitudinal projections through the middle of the nerve fibre and transverse projections along the Z-axis were performed. In WT nerve fibres, cytoplasmic bands located outside the myelin sheath, appearing as discontinuous regions in the Z-projections (Fig. 13B). In KO nerve fibres, cytoplasmic domains were arranged as a concentric ring of cytoplasm outside the myelin sheath (Fig. 13C).

Electron microscopy (EM) was used in order to investigate the ultrastructural correlate of the light microscopic results described above. In transverse sections of 3-week old quadriceps nerve, the cytoplasm of myelin-forming Schwann cells in WT nerve fibres showed discrete regions of cytoplasm separated by appositions between the abaxonal membrane of the Schwann cell and the outermost myelin loop (Fig 14A and B). In contrast, KO Schwann cells have no appositions and the cytoplasm appears continuous around an ultrastructurally normal myelin sheath (Fig 14C).

Quantification of the above results was performed by counting the number of apposition per Schwann cell from randomly selected fields of transverse EM

micrographs of 3-week old WT and KO quadriceps nerve (n=3 for each group, 120 fibres per group). At this age, the majority of WT Schwann cells have 3-4 apposition with a small proportion of them having only one (Fig 14D). The highest percentage of KO Schwann cells showed no appositions with a small percentage featuring random contacts between the plasma membrane and the myelin sheath which, although they were scored as appositions in the analysis, were clearly not a defined structure like the WT appositions.

During this analysis it was noticed that the number of appositions in WT Schwann cells appeared to be greater in large diameter nerve fibres. This observation was tested by relating the number of apposition to the corresponding fibre diameter in transverse EM micrographs from 3-week old WT quadriceps nerves. A significant correlation between these two parameters was found (Fig. 15). This result indicates that new appositions and therefore longitudinal cytoplasmic bands, are added as the Schwann cell grow in size, suggesting a trophic support function for Cajal bands in Schwann cells.

Two alternative explanations for the lack of appositions in periaxin-null Schwann cells can be proposed. Periaxin could be involved in the formation of appositions or it could act by stabilising previously formed appositions. These alternatives can be distinguished by analysing the presence or absence of appositions in KO Schwann cells when they first form in WT nerve fibres. Transverse sections of postnatal-day 2 (P2), P4 and P8 from WT and KO quadriceps nerves were analysed by EM. In WT nerve fibres, mixed population of Schwann cells at different stages of axonal ensheathment were found at P2, P4 and P8, ranging from axons in the process of sorting to axons featuring compacted myelin sheaths of different thickness. At P8, the population of myelin- and nonmyeling-forming Schwann cell is almost established, and nerve fibres with thick myelin sheaths can be detected.

The abaxonal cytoplasm of WT Schwann cells with non-compact myelin or with a low number of compact myelin loops appears continuous with no apparent compartmentalisation (Fig 16A). In WT Schwann cells with thicker myelin sheaths, the cytoplasm appears compartmentalised and flanked by appositions between the Schwann cells plasma membrane and the outermost loop of the myelin sheath (Fig. 16B and C), these appositions were characterised by a conserved 14 nm separation

between membranes (Fig. 16G). In KO nerves fibres, the cytoplasm appears continuous in early stages of myelination as in WT fibres (Fig 16D) becoming compartmentalised in Schwann cells with myelin sheaths similar in thickness to WT Schwann cells that have segregated their cytoplasm into discrete regions (Fig. 16E). Nevertheless, appositions that separate cytoplasmic regions in KO Schwann cells have distances of about 30 nm between membrane faces, considerably wider than WT appositions (henceforth referred to as pseudo-appositions, Fig. 16G). In the absence of periaxin, pseudo-appositions are not maintained, since KO Schwann cells with thick myelin sheaths displays a continuous ring of cytoplasm (Fig. 16F).

These results suggest that the initial distribution of cytoplasm and formation of appositions in Schwann cells may be independent of periaxin, which seems more likely to have a role in the stabilisation of preformed appositions.

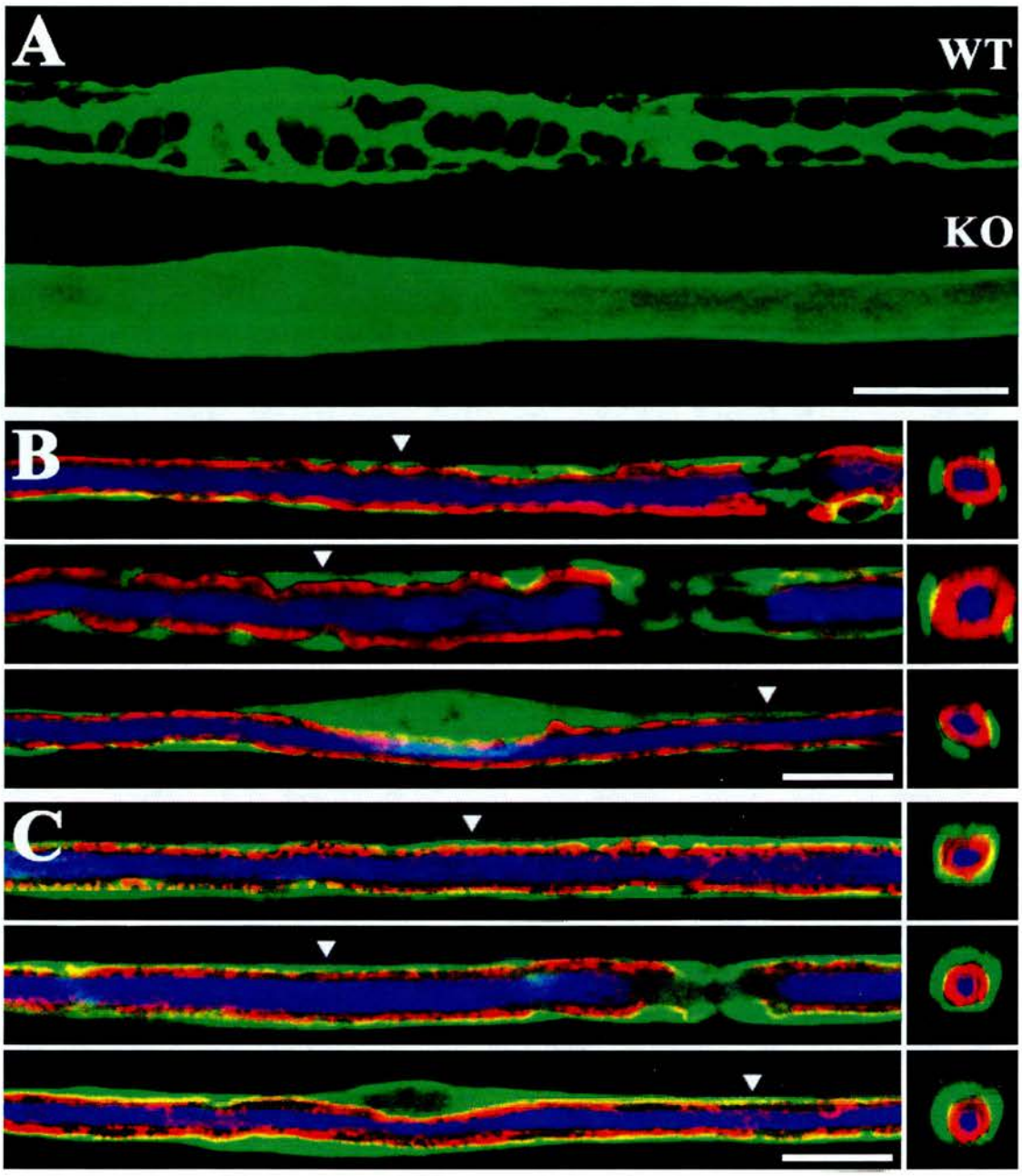

Figure 13. Cajal bands are absent in 3-week old periaxin null Schwann cells
(A) Teased fibers from 3-week old WT and KO quadriceps nerve, labelled with an antibody against the cytoplasmic protein S100. The cytoplasms in WT Schwann cells is arranged in longitudinal and transverse bands. In contrast, the Schwann cell cytoplasms in KO fibers is continuous. In **(B)** and **(C),** teased fibres triple-labelled with antibodies against S100 (green), the myelin protein MBP (red) and neurofilaments (blue) were imaged by confocal microscopy and longitudinal optical section through the middle of the fiber (left) and Z-projections of the entire nerve fiber (right) were produced. **(B)** The WT Schwann cell cytoplasm appears compartmentalised, whereas in KO Schwann cells **(C)** it forms a continuous ring outside the myelin sheath. Scale bars, 20 μm.

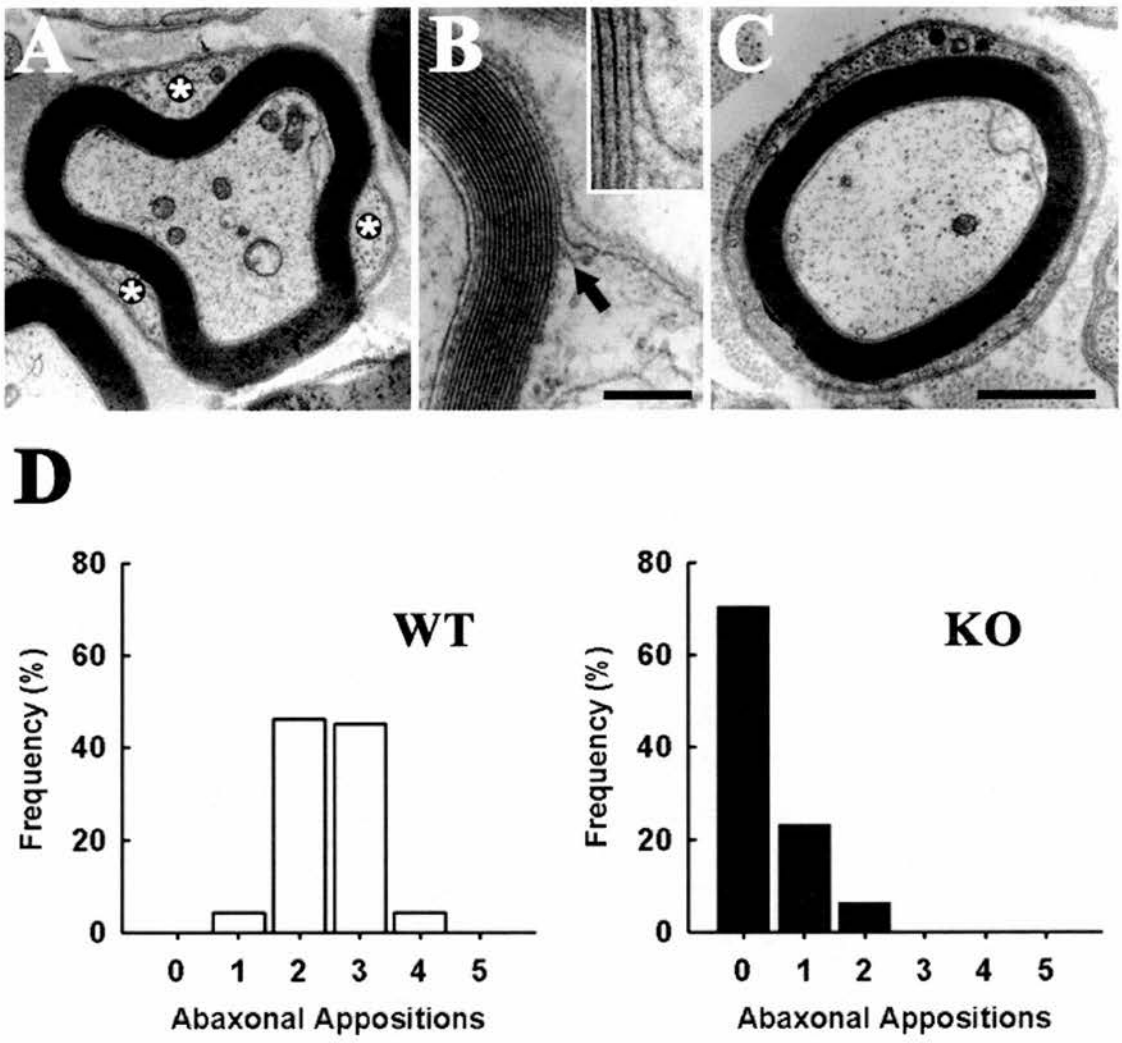

Figure 14. Cajal Bands do not form in the absence of appositions.
Electron micrographs of transverse sections through the quadriceps nerves of WT and KO mice. **(A)** The cytoplasms of WT Schwann cells (asterisks) is delimited by appositions between the Schwann cell plasma membrane and the outermost loop of the myelin sheath. **(B)** Transition region between the Schwann cell cytoplasm and the apposition (arrow). Scale bar, 0.2 μm. A high power view of this region is shown in the inset. **(C)** In KO Schwann cells, the lack of appositions result in a concentric ring of cytoplasm outside the myelin sheath. Scale bar, 1 μm (A and C). **(D)** The quantification of appositions per Schwann cell in 3-week old quadriceps nerves (n=3 and 120 fibers per group) shown the almost complete lack of appositions in the KO (right) compared with the WT (left).

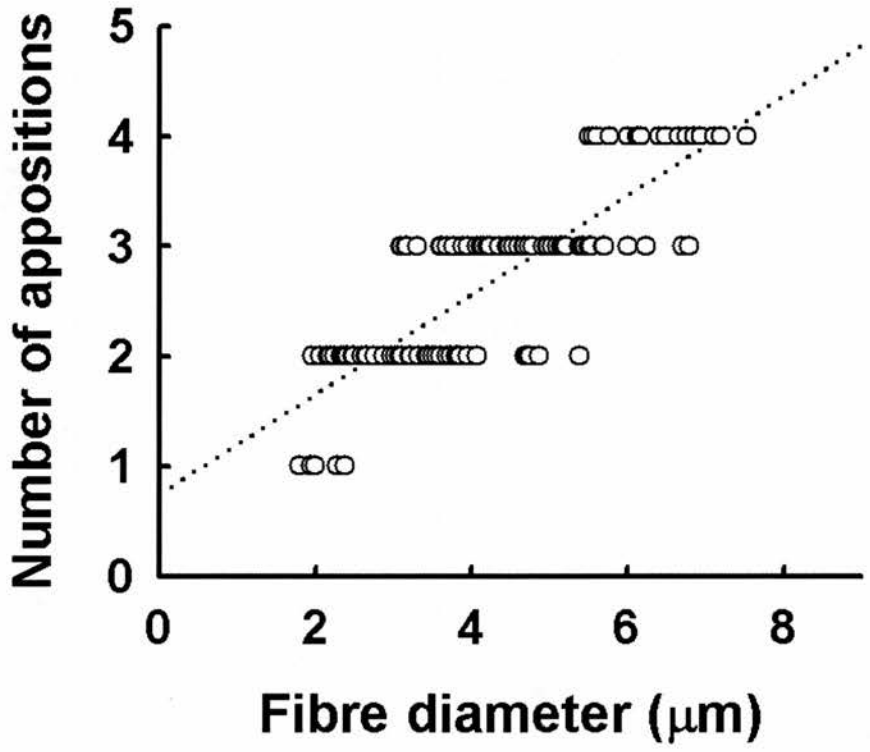

Figure 15. The number of Cajal bands increases relative to the Schwann cell size.

The possibility that the number of appositions, hence Cajal bands, increases relative to the longitudinal (IL) and radial (myelin sheath thickness) size of Schwann cells was investigated by measuring the diameter of individual fibers and the corresponding number of appositions in cross sections from quadriceps nerves of 3 week old WT (n=3, 120 fibers). As shown by linear regression (dotted line), the number of appositions relates to the diameter of the nerve fiber (r^2=0.7).

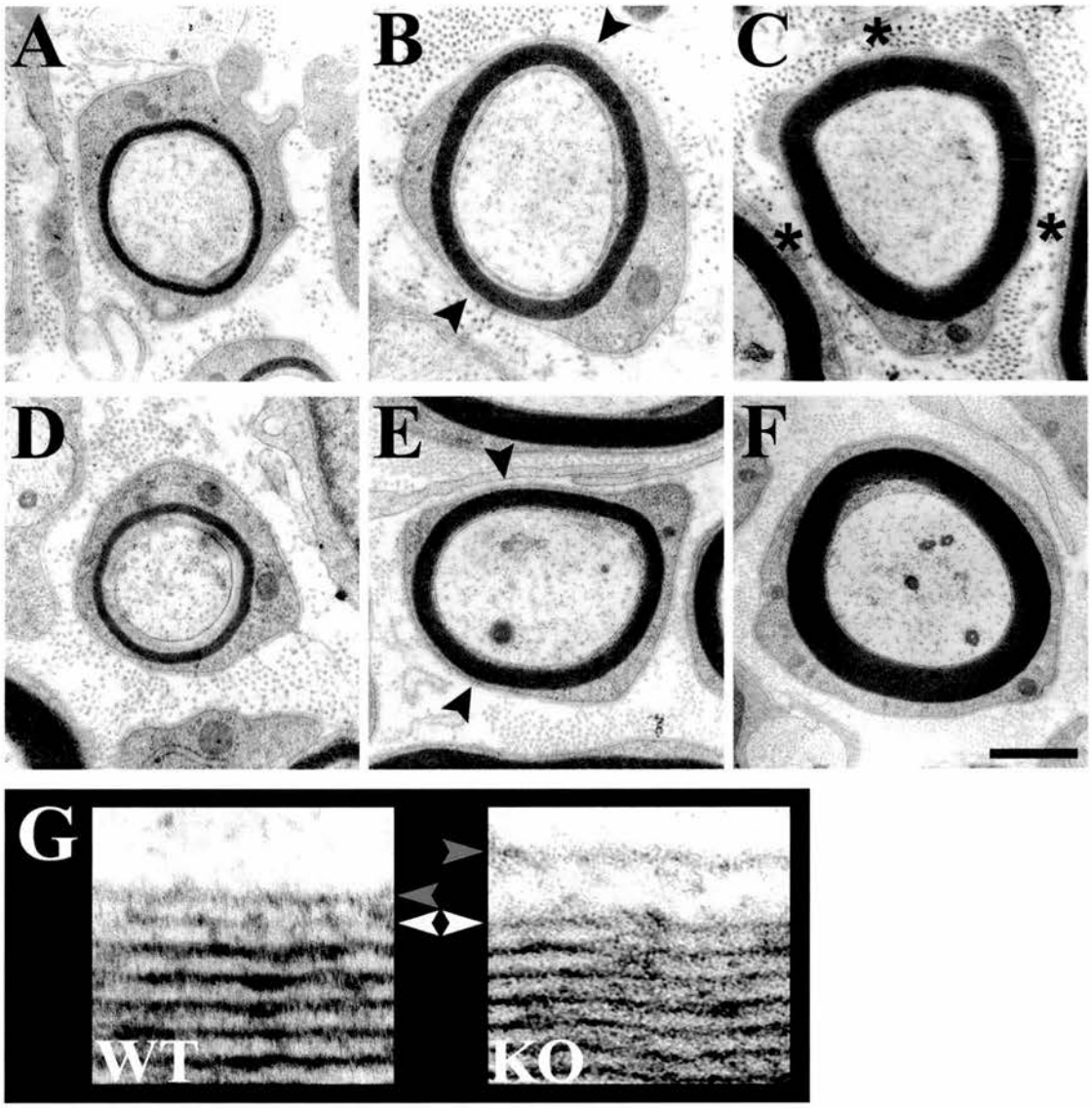

Figure 16. Periaxin is involved in the stabilisation of Schwann cell appositions. Electron micrographs of transverse sections through the sciatic nerve of P6 WT **(A-C)** and KO **(D-F)** mice. In both cases, Schwann cells with thin myelin sheaths have a continuous cytoplasm, **(A)** and **(D)**. As the myelin sheath becomes thicker, appositions (arrowheads) between the Schwann cell plasma membrane and outermost myelin loop segregate the cytoplasms into discrete domains or Cajal bands, **(B)** and **(E)**. In WT Schwann cells, appositions remain as the thickness of the myelin increases (asterisks in **C**), but in Schwann cells lacking periaxin, appositions are not maintained and the cytoplasm rearranges as a continuous domain **(F)**. Scale bar, 1 μm. **(G)** High power view of the apposition region. In WT Schwann cells, the distance between the plasma membrane (red arrowhead) and the apposing membrane (white arrowhead) is approximately 14 nm. In contrast, the distance between these membranes in KO Schwann cells is increased to double of WT values.

2.1.2- Elongation of Schwann cells is impaired in the absence of Cajal bands

Santiago Ramón y Cajal proposed that the cytoplasmic arrangement of Schwann cells could serve a trophic support function for the entire cell (Ramón y Cajal, 1933)(Fig. 5A). Schwann cells elongate extensively during postnatal development, reaching internodal lengths up to a millimetre (mm) long. Hence, according to Ramón y Cajal's proposal, intact Cajal bands should be required for Schwann cell elongation. To test this hypothesis, internodal lengths were measured from WT and KO quadriceps nerves at P2, 1 , 3 and 6 weeks of age (n=3 for each time point per strain). From these nerves, teased fibre preparations were stained with TRITC-phalloidin and DAPI. Nodes were identified by phalloidin staining except for P2 fibres, where nodes are not discernible; at this age the internodal length was taken as the Schwann cell internuclear distance. This correspondence is valid, since Schwann cell nuclei are located in the middle of the nerve fibre. At P2, when myelinated Schwann cells have associated in a 1:1 relationship with segments of the axon, WT and KO internodal lengths were similar (Fig. 17B). In older nerves, KO internodal lengths were strikingly decreased compared to WT (Fig. 17A and B). The elongation rate of WT Schwann cells fitted a rectangular hyperbola (Equation, $Y=A*X/(B+X)$) with parameters (in μm) A=821.2 and B=11.51 (R^2=0.9914), and the elongation rate of KO Schwann cells follows a straight line with a slope of 6.9 ± 0.30 μm/d (r^2=0.996, P=0.0019).

Axonal elongation has been proposed to control the elongation of the associated Schwann cell but the exact relation is still debated (Hildebrand et al., 1996; Hiscoe, 1947; Nilsson and Berthold, 1988), therefore I tested whether the decreased KO internodal lengths was due to abnormal axonal extension. The lengths of quadriceps nerves were measured from spinal cord exit to muscle insertion point (n=3 for WT and KO). Elongation rate of WT and KO quadriceps nerves were similar at all ages examined (Fig 17B). Both, WT and KO nerve growth fitted a rectangular hyperbola with the following parameters (in mm); WT, A=19.74 and B=1.405 (R^2= 0.9901); KO, A= 19.53 and B= 1.396 (R^2= 0.9902). In addition, the growth rate of WT nerves and internodes were not statistically different. These results indicates that in WT nerves, Schwann cells associate with the axon and then grow at the same rate as the

growing nerve. Periaxin-null Schwann cell lacking Cajal bands, had lower growth rates in spite of the fact that their nerves grow at a normal rate. In addition, the linear rate of growth exhibited by KO Schwann cells suggests that the lack of Cajal bands imposes a limit to Schwann cell elongation.

2.1.3- Axonal diameters, myelin sheath thickness and nodal structure are normal in peripheral nerves of the periaxin null mice

The striking reduction in longitudial extension of Schwann cells lacking Cajal bands suggested that these cytoplasmic domains might be involved in the effective trophic support required for cell elongation. I asked whether the myelinating phase in nerves containing Schwann cells lacking Cajal bands was characterised by the attainment of normal parameters in terms of axonal diameters, myelin sheath thickness and nodal architecture.

Axonal diameters were measured from randomly selected fields of transverse EM micrographs of 3-week old WT and KO quadriceps nerves (n=3 for each group, 120 axons per group). The histogram obtained (Fig. 18A) shows that the distribution of axonal diameters at 3 weeks is similar between WT and KO mice. From the same preparations, and including data from transverse EM micrographs of 6-week old WT and KO quadriceps nerve (n=3 for each group, 120 axons per group), the fibre diameter and correspondent axon diameter were measured. Their relation was expressed by the g-ratio (axon diameter/fibre diameter), which reflects a conserved correspondence between the myelin sheath thickness and the axonal diameter. In 3-week old mice, the g-ratio is similar between WT and KO quadriceps nerves but the g-ratio at 6 weeks of age is reduced in the KO compared to the WT (Fig. 18B), reflecting the initial stages of hypermyelination in periaxin-null Schwann cells.

In addition, the amount of the myelin specific protein P0 in an equal segment of the quadriceps nerve was measured at different ages to complement the morphometrical analysis. Segments of 5 millimeters (mm) were removed from WT and KO quadriceps nerves at different ages and subjected to SDS-PAGE electrophoresis, and Western blotted with an antibody against P0 (Fig. 18C). Band intensities were estimated using NIH Image software and expressed as the percentage of the most intense band (Fig. 18D). The quantification of the bands showed that the levels of P0

protein are similar between WT and KO at all ages examined, including 3 and 6 months when hypermyelination and demyelination is well under way in KO quadriceps nerves. Therefore, KO Schwann cell continue to express normal levels of the protein P0, irrespective of the level of disruption in their myelin sheath.

The structure of the node and paranode in KO nerve fibres and the localisation of proteins restricted to these domains were analysed by immunostaining of 3-week old WT and KO tease fibres. As shown in figure 19A, localisation and signal levels of Na^+ channels at the node, Caspr and neurofascin (NFC) at the paranode are similar between WT and KO preparations. The same conclusion applies using antibodies against βIV-Spectrin and α-Dystroglycan, localised at the node and in the Schwann cell membrane, respectively (Fig. 19B). In addition, the levels of several proteins restricted to the node-paranode domains were compared between 3-week old WT and KO nerves by Western blot. Proteins analysed include the axonal and Schwann cell specific isoforms of neurofascin, NF155 and NF186, respectively; βIV-Spectrin and Caspr. The levels of all proteins analysed were similar between WT and KO nerve samples (Fig. 19C). Finally, the ultrastructural organisation of the nodal and paranodal regions of 3-week old WT and KO nerve fibres were examined using EM from longitudinal sections of quadriceps nerves (section and imaging of longitudinal preparations performed by Dr. Diane L. Sherman). The EM micrographs shown that the overall structure of the node and paranode is similar between WT and KO nerve fibres (Fig. 19D). Nodal length, myelin sheath termination and axoglial junctions (Fig. 19D, inset) showed no derangement in the KO nerve fibres.

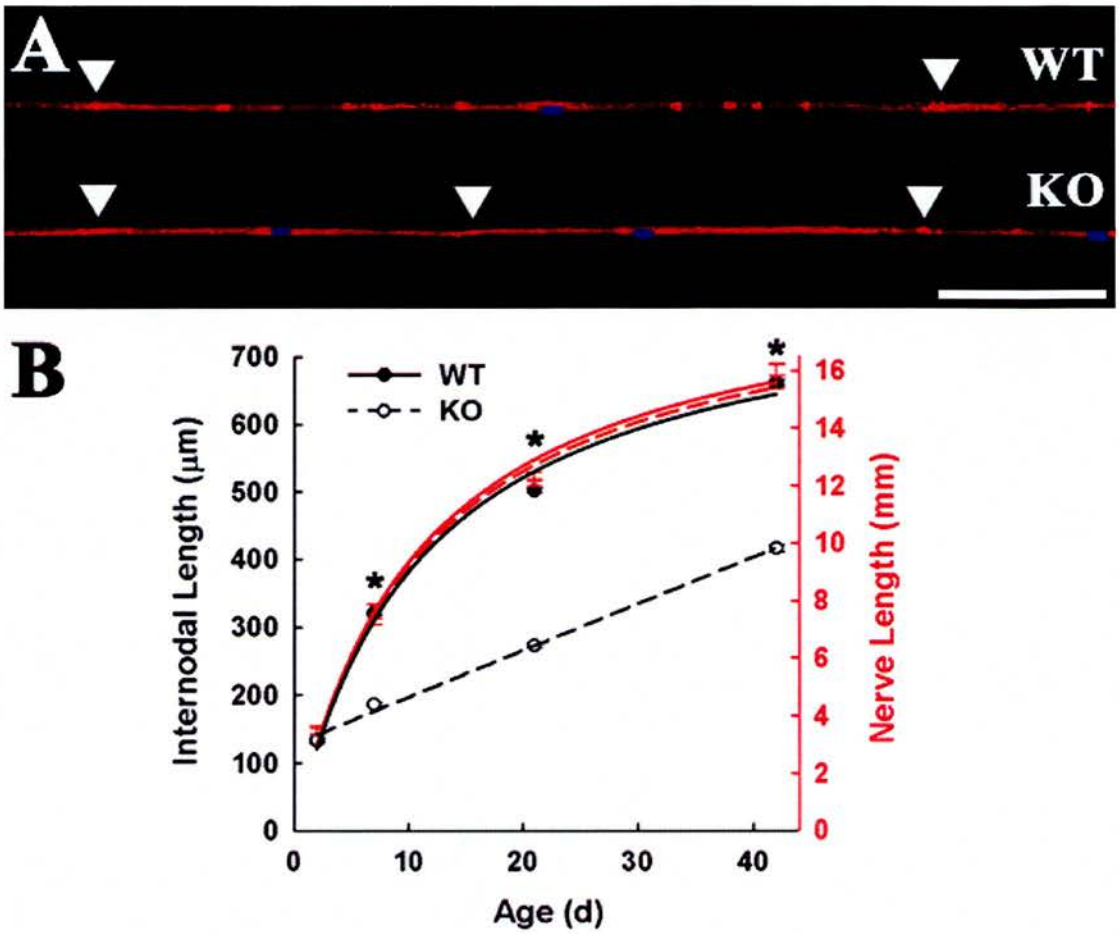

Figure 17. Internodal elongation is decreased in periaxin null Schwann cells lacking Cajal bands.

The time course of internodal length (IL) and nerve length (NL) growth was study in P2, P7, 3 weeks and 6 weeks WT and KO quadriceps nerves. For IL measurements teased fibers stained with TRITC-phalloidin (red) and DAPI (blue) were analysed. Quadriceps nerve lengths were measured from the spinal cord exit to muscle insertion point. **(A)** At 3 weeks, KO internodal lengths measure about the half of WT values. Arrowheads indicate nodes of Ranvier. Scale bar, 100 µm. **(B)** WT and KO internodal lengths are similar at P2, thereafter the WT growth rate (continuous black line) increases following a rectangular hyperbola function and KO growth rate (dashed black line) follows a straight line. The growth rate of quadriceps nerves in both WT and KO mice (continuous and dashed red line, respectively) were best represented by a rectangular hyperbola function. The curves shown no significant differences tested by F-test ($P=0.945$; testing the null hypothesis that there are no significant differences between these curves). From the graph is evident that internodal elongation of WT Schwann cells match precisely the elongation of the nerve at all ages but KO Schwann cells can not extend at the nerve growth rate from P2 to 3 weeks, after this age internodal and nerve growth rates are similar (asterisks, $P<0.0001$; Student's t-test for internodal lengths).

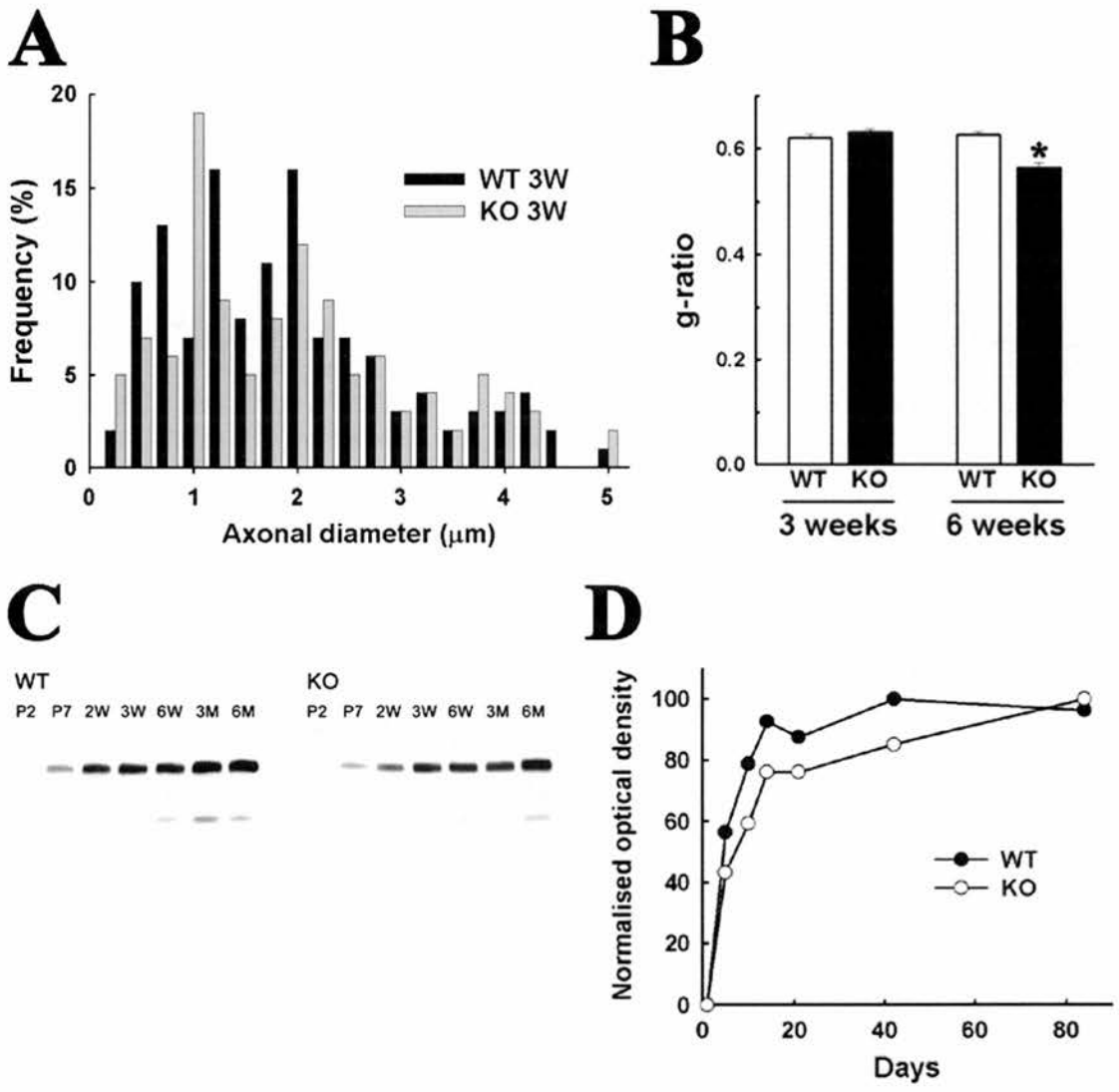

Figure 18. Axonal diameters and the thickness of the myelin sheath are normal in quadriceps nerves from 3-week old periaxin null mice.

(A) Axons in 3-week old KO quadriceps nerves shown a normal diameter distribution compared to the diameter distribution of WT axons (n=3 for each group, 120 fibers per group). **(B)** The g-ratio values, an indication of the myelin sheath thickness in relation to the axonal diameter, of WT and KO nerves fibers from quadriceps nerves are similar at 3 weeks (n=3 for each group, 120 fibers per group). At 6 weeks, KO nerve fibers present a decreased g-ratio compared to WT fibers, indicative of hypermyelination of axons (asterisks, $P<0.0001$; Student's t-test). **(C)** Protein samples from equal lenghts of WT and KO quadriceps nerves obtained at the ages indicated, were blotted with an antibody against the myelin protein P0. At all ages examined, the levels of P0 are similar between strains. The equal level of myelin per unit length in WT and KO quadriceps nerves is shown in graph on **(D)**, obtained by measuring the optical densities from the P0 bands in **(C)** and normalising the higher value.

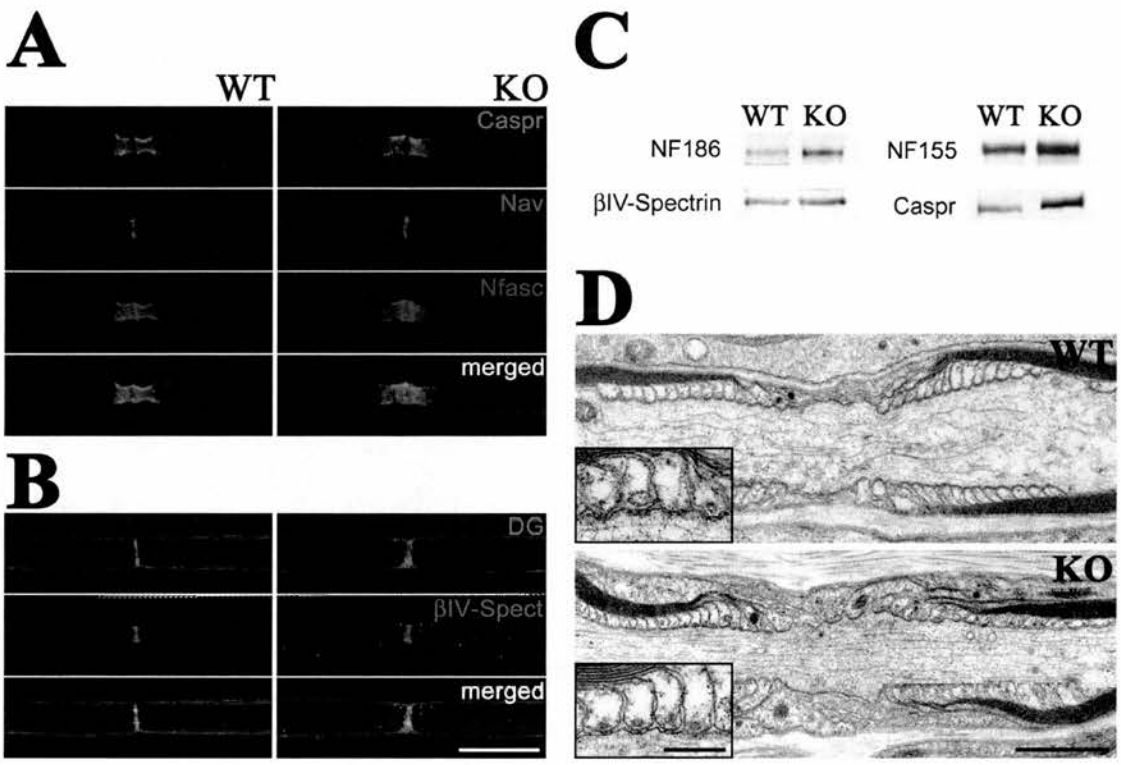

Figure 19. Composition and structure of nodal and paranodal regions in 3-week old WT and KO nerve fibers.

(A) Teased quadriceps nerve fibre triple-labelled with antibodies against Caspr (red), sodium channels (Nav) (green) and both neurofascin-155 and neurofascin–186 (Nfasc) (blue). Localisation for these three proteins in paranodal (Caspr and neurofascin-155) and nodal (sodium channels, neurofascin–186) domains are similar between WT and KO nerve fibers. **(B)** Nerve fibre double-labelled for α-dystroglycan (DG) (red) and βIV-spectrin (βIV-spect) (green). Both, the microvillar protein α-dystroglycan and the nodal marker βIV-spectrin are normally localised in KO nerves fibers. Scale bar, 20 μm. **(C)** Western blot of sciatic nerve extracts (20 μg protein) shown that the levels of the proteins βIV-spectrin, neurofascin-186 (NF186), neurofascin-155 (NF155) and Caspr are increased in KO nerves compared to WT. This increase in the levels of nodal and paranodal proteins in KO nerves is consistent with the approximately double number of these domains per unit length compared to WT. **(D)** Electron micrographs of longitudinal sections from WT and KO quadriceps nerves shown that the ultrastructure of node and paranodes, inluding the formation of axoglial junctions (inset), is similar between strains. Scale bar, 0.2 μm.

2.1.4- Schwann cells specify internodal lengths in a cell-autonomous manner

The decreased elongation rate of periaxin null Schwann cells might reflect an indirect effect, not associated with the growth capacity of the Schwann cell. In order to determine if the ability of Schwann cells to elongate was cell-autonomous, chimeric mice containing mixed populations of WT and KO Schwann cells were generated by injection of embryonic stem (ES) into blastocysts (chimeras were generated by Dr. Diane L. Sherman). Embryonic stem cells from transgenic mice (S129 strain) expressing a tau-GFP fusion protein (Pratt et al., 2000) were injected into WT or KO blastocysts (both derived from C57BL/6 strain) in order to distinguish between Schwann cells populations in the same nerve as the tau-GFP fusion protein is expressed by Schwann cell. Chimeras containing mixed populations of tau-GFP expressing Schwann cells (henceforth referred to as WT^{GFP}) and periaxin null Schwann cells were generated (WT^{GFP}-KO). In addition, chimeras containing WT^{GFP} and WT (C57BL/6 strain) Schwann cells (WT^{GFP}-WT) were generated to test the elongation capacity of tau-GFP expressing Schwann cells compared to WT. Quadriceps nerves of 3-week old chimeras containing an equivalent contribution from each Schwann cell type (n=3 for each chimera type) were selected for the analysis. Internodal lengths were measured from teased nerve preparations stained with TRITC-Phalloidin and DAPI. In WT^{GFP}-WT chimeras, Schwann cells expressing GFP (WT^{GFP}) have internodal lengths similar to WT Schwann cells (Fig. 20A and B). In contrast, KO Schwann cells mixed with WT^{GFP} Schwann cell have reduced internodal length similar to the values exhibited in the pure KO background (Fig. 20A and B). The internodal lengths of both WT^{GFP} and WT Schwann in the chimeric nerves were greater than internodal lengths of WT Schwann cell in a pure C57BL/6 strain (Fig. 20B). This was due to the fact that chimeric mice have longer quadriceps nerves. In contrast, internodal length of KO Schwann cells in a chimeric or pure KO strain were similar (Fig. 20B), in agreement with the previously suggested limited growth capacity of Schwann cells lacking Cajal bands.

In summary, the capacity of Schwann cells to elongate is cell-autonomous but matched the axon grow rate precisely. In contrast, periaxin null Schwann cells lacking Cajal bands have a decreased elongation capacity.

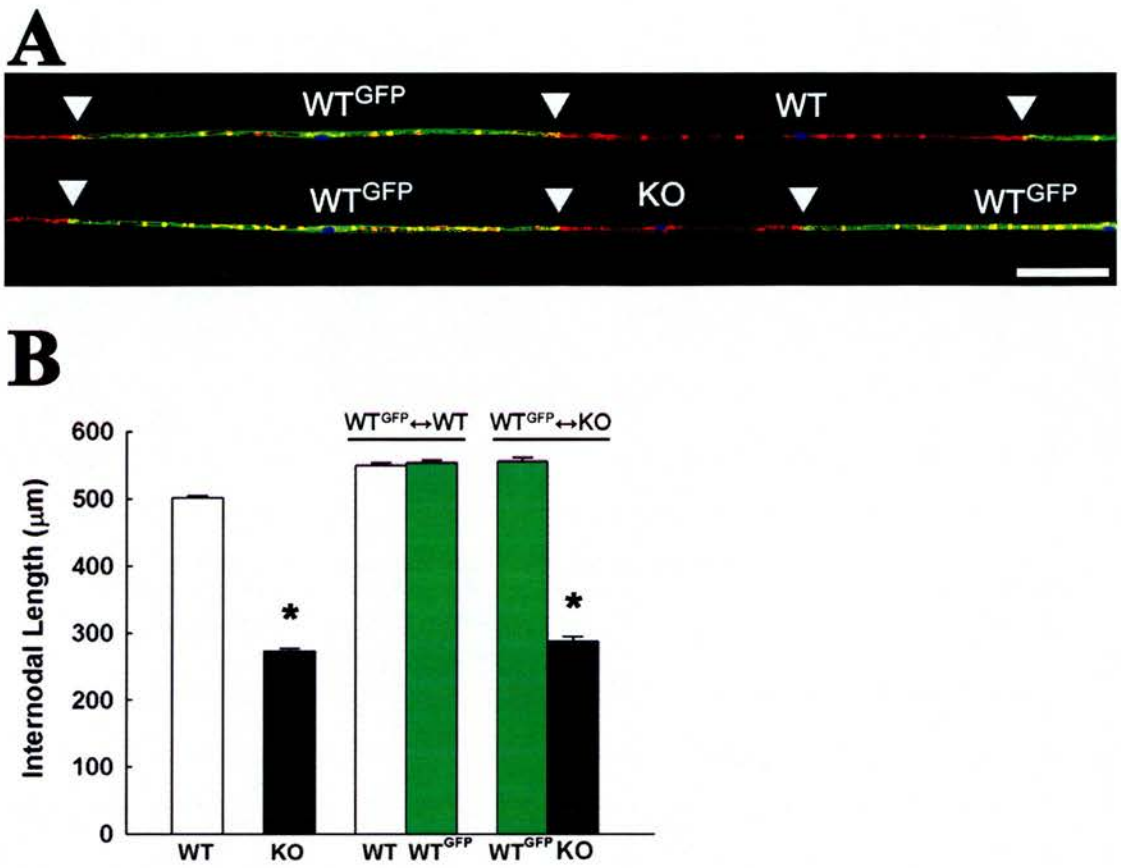

Figure 20. The capacity of Schwann cells to elongate is cell-autonomous
(A) Nerves from 3- week old chimeric mice containing Schwann cells expressing tau-GFP (WT^{GFP}, strain S129) and WT or KO Schwann cells (C57Bl/6 strain) were stained with TRITC-phalloidin (red), and DAPI (blue); in green the signal from GFP. In WT^{GFP}-WT chimeric nerve fibers, WT^{GFP} and WT Schwann cells have similar internodal lengths. KO Schwann cells have reduced internodal lengths in chimeric nerves containing WT^{GFP} Schwann cells. Arrowheads indicates the nodes of Ranvier. Scale bar, 100 μm. **(B)** Quantification of internodal lengths, the first two bars shown the decrease in internodal length of KO nerves compared to WT (*P<0.0001 by Student's t test; n=3). In WT^{GFP}-WT chimeras, internodal lengths are similar, but their values are bigger compared to those in the pure WT nerves (P<0.0001 by Student's t test). In WT^{GFP}-KO chimeras, KO Schwann cells have reduced internodal lengths compared to WT^{GFP} (*P<0.0001 by Student's t test; n=3) but similar to those in the pure KO strain.

2.1.5- Schwann cell cytoplasmic volume is regulated independently of internodal length

Cajal bands restrict the Schwann cell cytoplasms to defined corridors along the abaxonal surface of the Schwann cell. These cytoplasmic domains are formed as a result of appositions scattered along the Schwann cell. One function of appositions might be to reduce the cytoplasmic volume and thereby increase the effective concentration of molecules required for the transport of lipids and proteins to distal regions allowing the Schwann cell to growth at a fast rate and maintain the molecular composition of distal domains. To test if appositions have a role in the specification of Schwann cell cytoplasmic volume, the cytoplasmic content of periaxin-null Schwann cell lacking appositions was measured. A combined electron and light microscopy morphometric approach was used to obtain an accurate value of cytoplasmic volume per individual Schwann cells. Schwann cell cytoplasmic area and the corresponding fibre diameter was measured from randomly selected fields of transverse EM micrographs of 3-week old WT and KO quadriceps nerve (n=3 for each group, 80 nerve fibres per group), the value of fibre diameter was used to estimate the internodal length of the Schwann cell from analysis of the relation between these two parameters performed in teased fibres (Fig. 21A). This value of internodal length was multiplied by the transverse area of cytoplasm to obtain the cytoplasmic volume of individual Schwann cells.

The graph obtained when the cytoplasmic volume per Schwann cell was plotted against axonal diameter (Fig. 21B) indicates that the amount of cytoplasm per Schwann cell in both WT and KO mice is related to axonal diameter with values not statistically different between WT and KO (Fig. 21C), in spite the fact that KO Schwann cell length is reduced to a near half of the WT values at this age (3-week old, see Fig. 19B and 21A). Therefore, the absence of appositions in periaxin null Schwann cells results in approximate double the amount of cytoplasm per cross sectional area (Fig. 21D), a characteristic that might be implicated in their reduced elongation capacity.

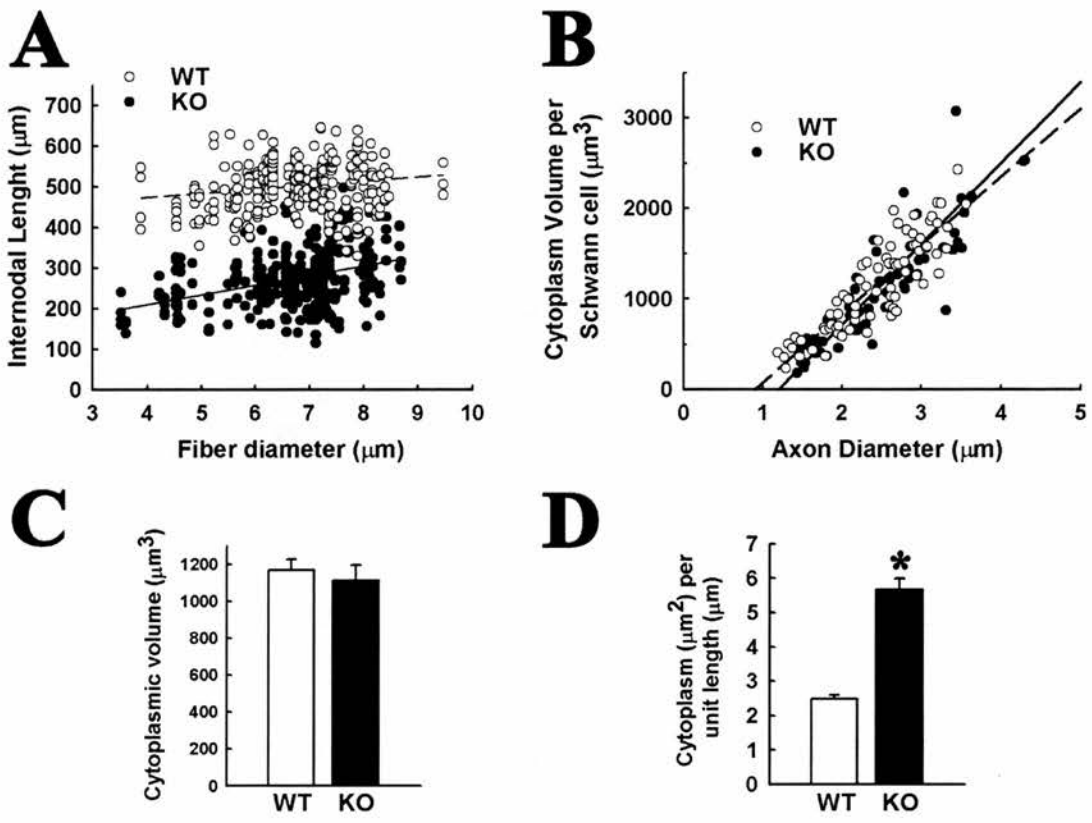

Figure 21. Schwann cell cytoplasm volume is restricted by apposition domains
Cytoplasmic volume of individual Schwann cells together with their internodal lengths and diameter of their associated axon were estimated from light and electron microscope preparations of 3-week old WT and KO quadriceps nerves (see methods, section 4.4, for a detailed explanation of the morphometric analysis performed)
(A) Internodal length and fiber diameter were measured from 3-week old WT and KO teased fibers stained with TRITC-phalloidin (red) and DAPI (blue). These two parameters are related in both WT and KO nerves fibers. But KO internodal lengths are reduced as described before (see figure 17). **(B)** The cytoplasmic volume of both WT and KO Schwann cells correlates with the diameter of the associated axon (linear regression analysis; WT (continous line), r^2=0.76; KO (dashed line), r^2=0.73) and are similar between strains despite the fact that the internodal lengths of KO Schwann cells are decreased by a half of the WT values. **(C)** Mean values of cytoplasmic volume of WT and KO are not significatively differents (Student's t-test) **(D)** The amount of cytoplasms per micron length was estimated from the mean values of cross sectional cytoplasms area. Schwann cells lacking cajal bands have an increase of cytoplasms per unit length compared to WT Schwann cells (asterisks, P<0.0001; Student's t-test).

2.1.6- Microtubule network is disrupted in Schwann cells lacking Cajal bands

The growth capacity of any cell is dependent on the efficient delivery of components to their extending domains. This is particularly important for Schwann cells, which grow at a high rate during postnatal development (extension of ~40 μm per day in the first postnatal week, see figure 17) and which maintain an extensive subcellular structure, namely, the myelin sheath. In order to determine if the microtubule network, known to be involved in the subcellular transport of proteins and mRNA (Rogers and Gelfand, 2000), was altered in Schwann cells lacking Cajal bands, the distribution of microtubules was analysed by double-immunostaining of teased fibres from 3-week old WT and KO sciatic nerves using antibodies against S100 and tubulin. In WT Schwann cells, microtubules are restricted to Cajal bands and extend from the perinuclear region to the paranodal domains (Fig. 22A). In contrast, the microtubule network in the KO appears deranged, becoming punctate as it approaches the paranodes (Fig. 22B). Destabilization of microtubules in WT Schwann cells was produced using topical colchicine treatment in 3-week old animals (see methods). After 3 days of recovery, microtubules start to rearrange in the perinuclear area (Fig. 22C) indicating that microtubule depolymerisation using this protocol is reversible.

2.1.7- Localisation of MBP mRNA is affected in periaxin null Schwann cells

Microtubule-dependent transport of RNA granules containing ribosomes and mRNA has been shown to be required for the local synthesis of the myelin protein MBP in the myelin compartment of oligodendrocytes (Carson et al., 1997). To determine if the disruption of microtubules in Schwann cells lacking Cajal bands have any influence on MBP mRNA localisation, 3-week old WT and KO teased nerve fibres were processed for *in situ* hybridization (ISH) using a digoxigenin-labeled probe specific for MBP (ISH protocol performed by Dr. Diane L. Sherman). In WT Schwann cells, MBP mRNA signal localises to the perinuclear area and paranodal regions in agreement with results obtained by Griffiths *et al.* in Schwann cells (Griffiths et al., 1989)(Fig. 23A). In contrast, MBP mRNA in periaxin null Schwann

cells accumulates only in the perinuclear area and no signal can be detected in paranodes (Fig. 23A). To control for specificity of the ISH protocol the MBP sense probe was used. No signal was detected in either WT or KO nerve fibres (data not shown). In addition, the mRNA distribution of the integral membrane protein P0 showed no discernible differences between WT and KO fibres, being located exclusively in the perinuclear region (Fig. 23B).

The relation between microtubule organisation and MBP mRNA localisation was studied by ISH in teased fibres prepared from nerves treated with colchicine followed by a 3 day recovery period, previously shown to effectively disrupt the microtubule network (Fig. 22C). In these fibres, MBP mRNA does not accumulate in the paranodal regions (Fig. 23A), indicating that intact microtubule organisation is required for the proper localisation of MBP mRNA to Schwann cell distal domains.

ISH results were subjected to a semiquantitative analysis using MATLAB software. Bright field images were acquired and inverted as shown in figure 23A; between 9 to 12 individual Schwann cells (from node to node) for each group (WT, KO and colchicine treated teased fibres) were cropped from the original images and normalised in their longitudinal lengths. These images were imported to MATLAB and processed by a custom made code to generate a surface plot representing the mean pixel intensity of the MBP signal along the internode for each group. The graphs obtained (Fig. 23C) extend to a semiquantitative domain the observations generated by the ISH protocol described above, i.e. Schwann cells lacking Cajal bands do not properly localise MBP mRNA to distal domains, probably as a consequence of the disruption of the microtubule network. These observations, in turn, might explain the decreased capacity for growth of periaxin null Schwann cells.

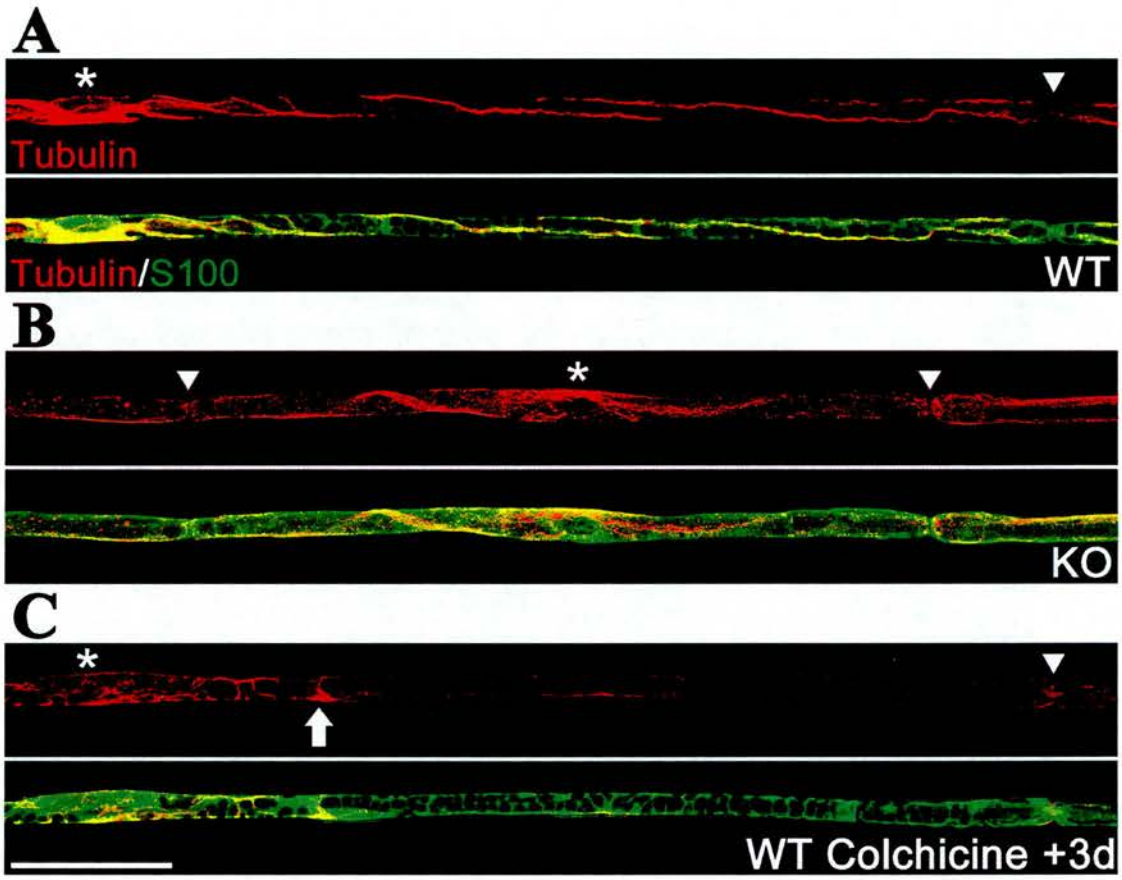

Figure 22. Disruption of the microtubule network in Schwann cells lacking Cajal bands.

Teased fibers from 3-week old WT and KO peripheral nerves were double-immunostained using antibodies against tubulin (red) and S100 (green). **(A)** In WT Schwann cells, microtubules extend through S100 immunostained Cajal bands, from the perinuclear area up to the paranodal domains. **(B)** In KO Schwann cells lacking Cajal bands, the microtubule network becomes disorganised as it approach the paranodes. Treatment of WT nerves with colchicine *in vivo* results in complete microtubule depolymerisation. After three days of recovery **(C)**, microtubules reform and extend from the perinuclear region (arrow indicates recovery front). Nuclei and nodes of Ranvier are indicated by asterisks and arrowheads, respectively. Scale bar, 50 μm.

Figure 23. The microtubule network is required for the proper localisation of MBP mRNA to the paranodal regions (figure in the next page)

MBP and P0 mRNA were detected in 3-week old WT and KO nerves by *in situ* hybridization using digoxigenin-labelled probes (ISH protocol performed by Dr. Diane L. Sherman). Bright field images were inverted for clarity. Nuclei and nodes of Ranvier are indicated by asterisks and arrowheads respectively.

(A) MBP mRNA in WT Schwann cells accumulates in the perinuclear and paranodal regions. In KO Schwann cells lacking Cajal bands, high signal intensity is detected in the perinuclear region and decrease toward the paranodes. After microtubule disruption using colchicine following 3 days of recover, MBP mRNA is restricted to the perinuclear region. **(B)** In KO Schwann cells, P0 mRNA is localised in perinuclear areas as in WT Schwann cells. Scale bar, 50 μm.

In **(C)** a semi-quantitative analysis of the MBP mRNA signal is presented. For this analysis, brigth field images as shown in **(A)** were cropped from node to node. The longitudinal size of individual Schwann cells were normalised in length and imported to MATLAB software as two-dimensional matrix of numbers representing pixel intensity. For each group a three dimensional array was created by concatenating the individual images in the Z dimension. From this array, the mean value of pixel intensity in the Z dimension was calculated for each pixel resulting in a two dimensional matrix of mean pixel intensity. This new matrix was used to generate a surface plot of the mean pixel intensity matrix of the MBP signal with the Z axis representing mean pixel intensity (colormap of intensity values is shown in the left).

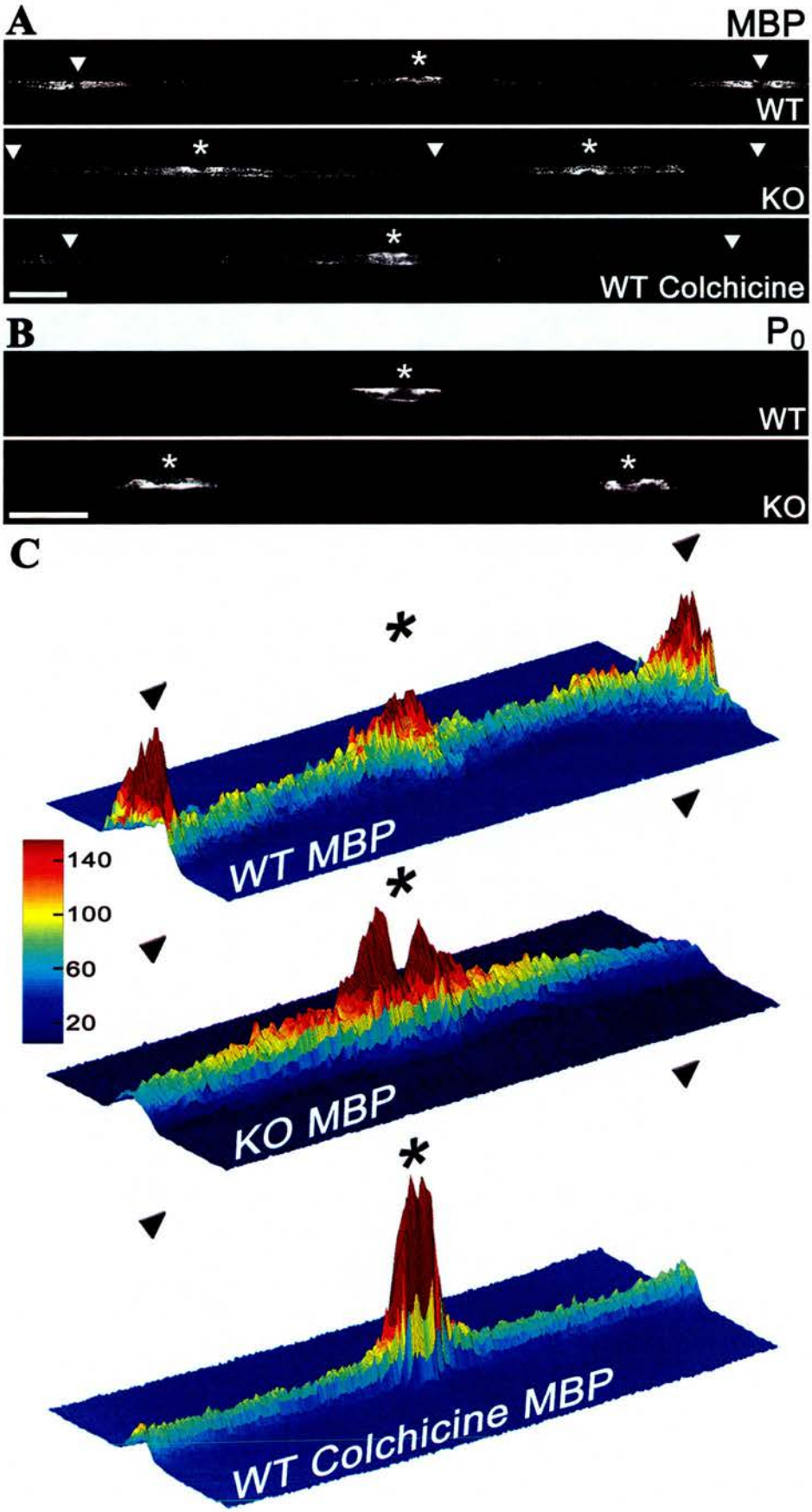
A
MBP
WT
KO
WT Colchicine
B
P0
WT
KO
C
140
100
60
20
WT MBP
KO MBP
WT Colchicine MBP

2.1.8- Nerve conduction velocity is sensitive to internodal length values

The difference in internodal lengths between WT and KO Schwann cell offers a unique opportunity to asses experimentally whether nerve conduction velocity (NCV) is sensitive to changes in internodal length, an influence that has been proposed only on theoretical grounds. This experimental verification can be performed due to the fact that 3-week old periaxin null nerve fibres exhibit normal parameters known to influence nerve conduction velocity, including axonal diameter (Fig. 18A), myelin sheath thickness (Fig. 18B), nodal architecture (Fig. 19A-C), and the proper localisation of Na^+ channels (Fig. 19A).

Nerve conduction velocity was measured from acutely isolated quadriceps nerves from 3-week old WT, KO and WT^{GFP}-KO chimeras (n=4 for WT and KO, n=3 for chimeras). From these nerve preparations, the time from the stimulus artifact to the peak of the compound action potentials, representing the mean conduction velocity of the largest active population of nerve fibres, was measured and nerve conduction velocities estimated as described in methods (section 4.5.1). Nerve conduction velocities in KO quadriceps nerves were significantly reduced compared to WT values (Fig. 24A-B), and chimeric nerves containing an equal proportion of WT and KO Schwann cells present intermediate values in agreement with theoretical predictions (WT, 21.9±1.2; KO, 9.9±0.6; chimeras, 14.6±0.3; mean (m/s) ± SEM).

In addition to the experimental results described above, the dependence of nerve conduction velocity on internodal length was addressed using a model of mammalian motor nerve fibres that includes detailed geometrical and electrical parameters (Figure 24C). This model, implemented in NEURON v4.3.1 (Hines and Carnevale, 1997), was shown to reproduce experimental data on the excitation properties of the nerve fibre (McIntyre et al., 2002). The geometric parameters of the modelled nerve fibre were adapted from the original model based on morphological measurements of 3-week old WT and KO quadriceps nerves from longitudinal and transverse EM sections. The following values were obtained:

Axon diameter=3.0 μm

Node diameter=1.7 μm

Paranode initial diameter=1.7 μm

Juxtaparanode diameter=3.0 μm

Internode diameter=3.0 μm

Juxtaparanode length=33 μm

Number of myelin lamellae=60

Using these parameters, nerve conduction velocity was studied at internodal lengths between 125 to 1750 μm. Significant decrease in nerve conduction velocity was found when the internodal distance decrease from 500 μm to 250 μm (Fig. 24D), values that correspond to the internodal lengths of 3-week old WT and KO nerve fibres, respectively. At internodal length values above 500 μm, nerve conduction velocity becomes less sensitive to this parameter.

The model outcome is in agreement with the experimental results obtained, being an additional confirmation of the sensitivity of peripheral nerve conduction velocity to internodal length.

2.1.9- Motor coordination is impaired in periaxin null mice

The consequences of reduced nerve conduction velocity in the behaviour of periaxin null mice was investigated by testing their motor coordination using the RotaRod. Three-week old WT and KO mice (n=6 for each group) were trained in the RotaRod one day before the trial. The test was performed at two different revolutions per minute (rpm), and was terminated either when the animals fell from the rod or at 60 seconds. At 24 rpm, both WT and KO mice perform equally; but at 32 rpm, the performance of KO mice was significantly poorer than WT mice (Fig. 24E). This result strongly suggest that the decreased nerve conduction velocity of KO nerves by more than 50% of the WT values affect negatively the animals motor coordination capacity.

2.1.10- Normal Cajal bands, internodal lengths and nerve conduction velocities in the CMTX mice

Periaxin null mice display a late-onset demyelinating condition that starts at around 6 weeks of age. In order to ensure that the reduced internodal lengths and nerve conduction velocity in periaxin null nerve fibres were specific for this mutation and

not a consequence of unidentified abnormalities related to their late demyelination, I performed analysis on another mouse mutant that displays late-onset demyelination, connexin-32 knock-out mice (CMTX) (Anzini et al., 1997). Studies on Cajal band organisation, internodal length and nerve conduction velocity were performed in quadriceps nerves of 3-week old CMTX mice using the same protocols described in the previous sections. Cajal bands in CMTX Schwann cells, revealed by immunostaining with an antibody against S100, appear normal (Fig. 25A). The same applies to internodal lengths and nerve conduction velocities as shown in figures 25B and C, respectively. Therefore, the results described for the periaxin null mice are specific for this mutation and not associated with their late onset-demyelination condition.

Figure 24. Nerve conduction velocity is sensitive to Schwann cell internodal length (figure in the next page).
(A) Traces of compound action potential from 3-week old WT and KO quadriceps nerves. **(B)** Nerve conduction velocities were measured from 3-week old WT, KO and chimeric quadriceps nerves. KO nerve conduction velocity is decreased when compared to the WT values. The conduction velocity of chimeric nerves, containing equal proportions of WT and KO Schwann cells (57.1 ± 3.1% KO Schwann cells, n=3; mean ± s.e.m.), have intermediate values. The sensitivity of nerve conduction velocity to changes in internodal length was studied using a model of the myelinated nerve fiber (McIntyre et al., 2002) implemented in NEURON. This model includes detailed representation of geometrical parameters of the myelinated nerve fiber **(C)** that for our simulation, were obtained from morphometric measurements of 3 week-old mouse quadriceps nerve. The electrical parameters of the nerve fibre were as in the original model. **(D)** Nerve conduction velocity is sensible to internodal distances in the shorter ranges, becoming insensible to this parameter at longer internodal lengths. **(E)** Motor coordination was assessed in 3-week old WT and MO mice by using the RotaRod test. No difference in WT and KO motor coordination was observed at low revolutions per minute (rpm), but KO motor coordination is significantly impaired at 32 rpm

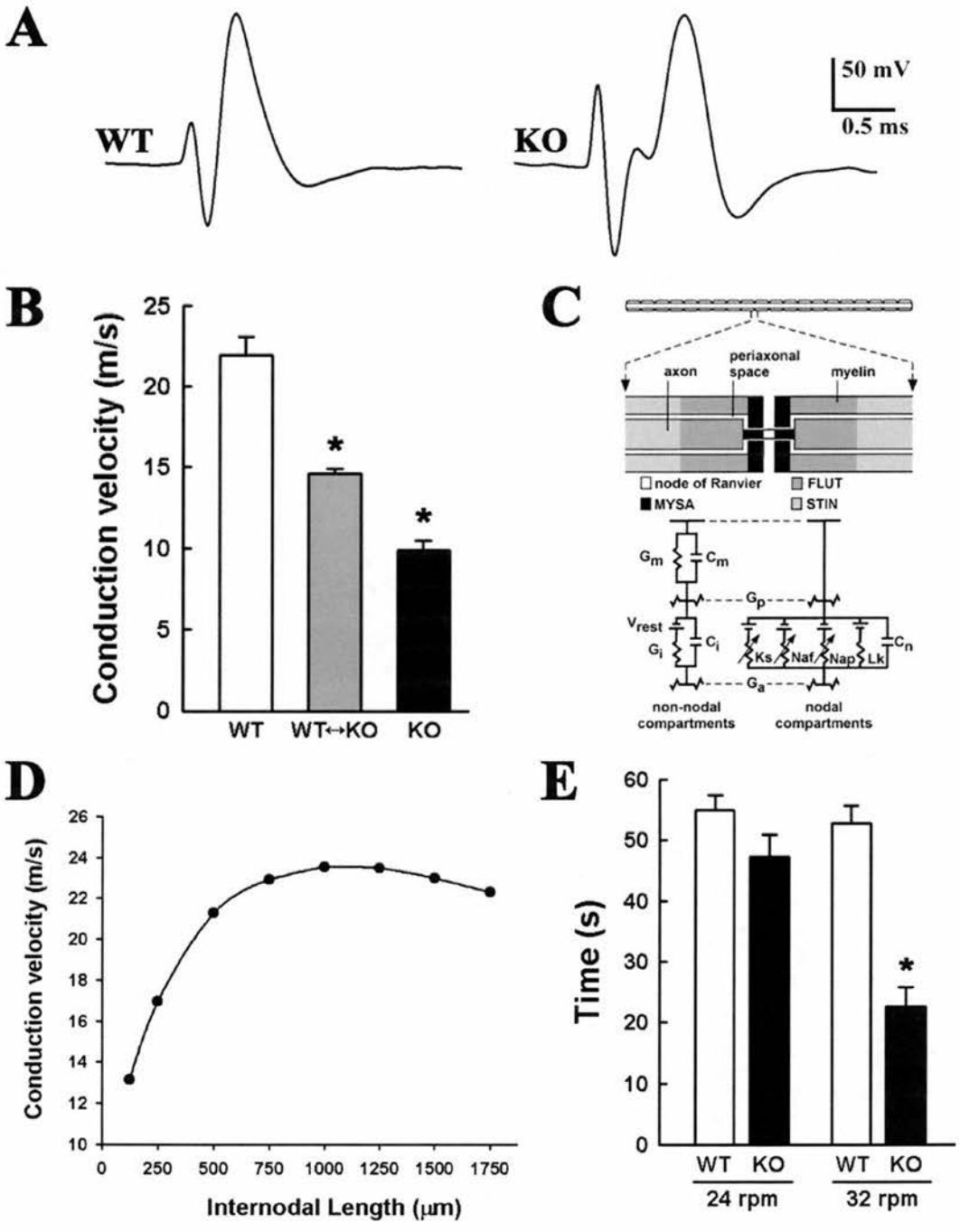
A
WT
KO
50 mV
0.5 ms
B
Conduction velocity (m/s)
25
20
15
10
5
0
*
*
WT
WT↔KO
KO
C
periaxonal space
axon
myelin
node of Ranvier
FLUT
MYSA
STIN
Gm
Cm
Gp
Vrest
Gi
Ci
Ks
Naf
Nap
Lk
Cn
Ga
non-nodal compartments
nodal compartments
D
Conduction velocity (m/s)
26
24
22
20
18
16
14
12
10
0
250
500
750
1000
1250
1500
1750
Internodal Length (μm)
E
Time (s)
60
50
40
30
20
10
0
*
WT
KO
WT
KO
24 rpm
32 rpm

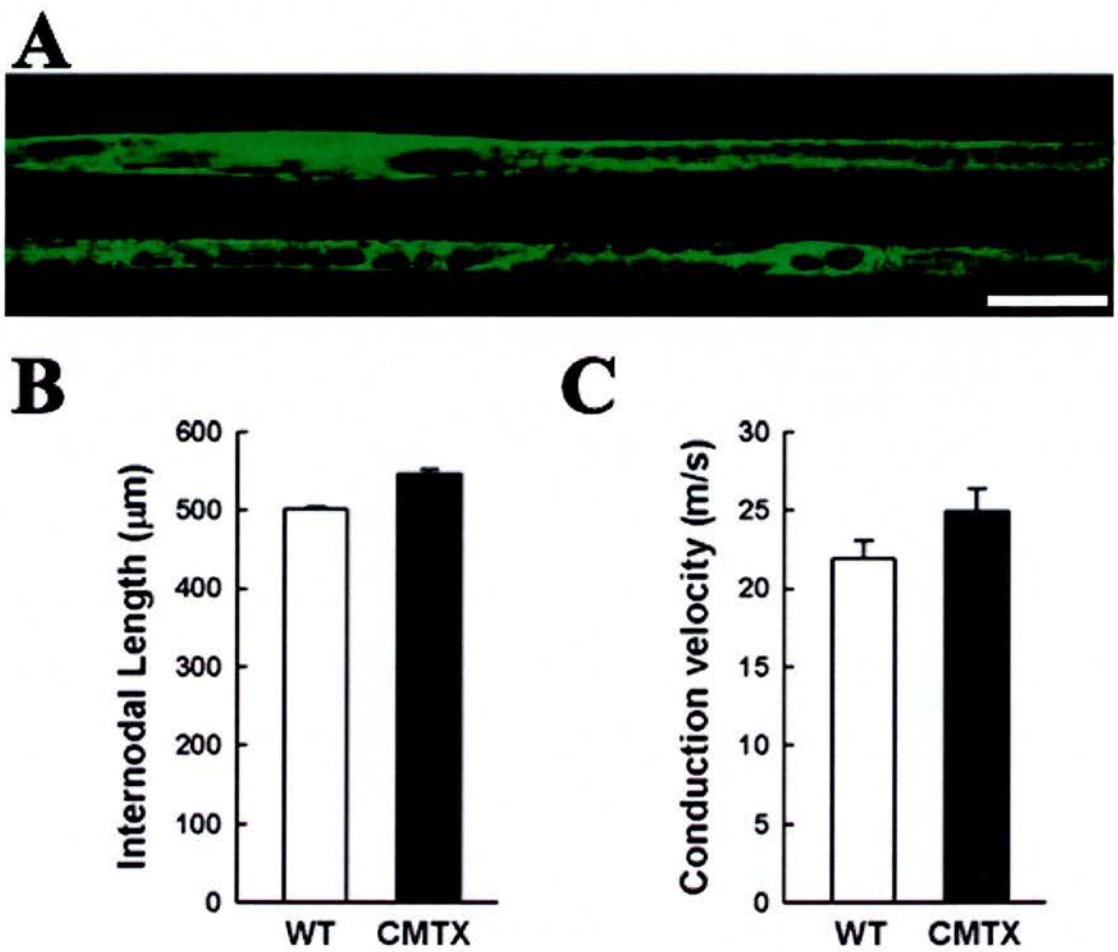

Figure 25. CMTX mice have Cajal bands, normal internodal lengths and WT nerve conduction velocities.

(A) Schwann cells from the CMTX have normal Cajal bands as revealed by immunofluorescence using an antibody against S100. Scale bar, 20 μm.

(B) Internodal lengths are similar between WT and CMTX mice, and the same applies to the nerve conduction velocity **(C)**.

2.1.11- Summary

In this chapter I have shown that periaxin is required for the stabilisation of particular Schwann cell domains, referred to as appositions and addressed the consequences of their disruption for the structure and function of the peripheral nerve fibre.

Appositions are involved in the restriction of Schwann cells cytoplasm to longitudinal bands we termed Cajal bands to acknowledge Santiago Ramón y Cajal first description of this subcellular organisation. Cajal band numbers increase as Schwann cells grow in the longitudinal and radial axis. This suggests a trophic support function for these Schwann cell cytoplasmic domains, as first proposed by Ramón y Cajal. Deletion of periaxin in Schwann cells results in absence of appositions and Cajal band disruption. In mutant nerve fibres, axonal diameters, myelin sheath thickness and domain structure of the nodal-paranodal regions were normal. However, the cell-autonomous capacity of Schwann cells to grow longitudinally as the axon extends is reduced. As a consequence, Schwann cell internodal lengths in 3-week old KO nerves are reduced to a half of the value of age matched WT mice. In Schwann cells lacking Cajal bands, the microtubule network is disorganised and consequently the microtubule-dependent transport of MBP mRNA to the paranodes is disrupted. Disruption of microtubule-based transport of components to distal domains in KO Schwann cells might explain their reduced capacity to growth. Reduced internodal lengths in KO nerve fibres results in slower nerve conduction velocities and defects in motor coordination. Importantly, these results represent the first experimental verification of the relation between internodal length and nerve conduction velocity.

2.2- CELL ORGANISATION AT THE NEUROMUSCULAR JUNCTION

The neuromuscular junction is normally represented as a composite of three main cell types: muscle fibre, motoneuron and terminal Schwann cell (Fig. 7). In addition to these well-known cells at neuromuscular junctions, fibroblasts have been reported to be located near the neuromuscular area (Weis et al., 1991). However, no extensive studies have been performed to define the exact location of these cells nor is their involvement in the formation and restoration of neuromuscular synapses understood. In this section I describe, using a novel antibody, a supopulation of cells located at the neuromuscular junction. From their close association with other cellular components of the neuromuscular junction, their development, their response to nerve injury and paralysis these cells appear to be an integral component of the neuromuscular junction. The results reported here have important consequences for the neuromuscular junction field as a new cell component should be considered in all future analyses of neuromuscular structure and function.

2.2.1- 2166 antibody reveals a novel neuromuscular synapse-associated cell

The 2166 antibody was raised in rabbit against an epitope of the oligodendrocyte-specific protein Tspan-2. When the antibody was tested by immunohistochemistry in mouse brain tissue and Western blot, it failed to recognise the protein Tspan-2 (data not shown). Remarkably, immunohistochemical staining with the 2166 antibody in whole muscle preparations revealed a variety of non-neuronal, non-glial, non-muscle cell types. The pattern of staining using this antibody is filamentous, forming a lasso around the cell nucleus and extending into fine processes. The cells identified were located in muscle interstitial spaces, associated with the intramuscular nerves and in close apposition to the neuromuscular junction.

Based on morphological characteristics and position relative to the neuromuscular synapse, several cell types were classified; 2166^{+} cells in the muscle fibre surface feature a bipolar shape with extensions running along the longitudinal axis of the

muscle fibre (Fig. 26A); the same description applies to a 2166^{+} population associated with intramuscular capillaries (Fig. 26B).

At the neuromuscular junction, 2166-positive cells extend processes coincident with the synaptic specialisations revealed by rhodamine-conjugated α-Bungarotoxin (BTX), a specific ligand for AchR (Fig. 26C). These cells were present in all neuromuscular junctions examined from different skeletal muscles (triangularis sterni, diaphragm, soleus, EDL, FDB, and DL). Staining transverse muscle sections with laminin and 2166 antibody, together with BTX showed that neuromuscular junction associated 2166 cells (NMJ^{2166+}) localise outside the basal lamina (Fig. 26D). This evidence proves that these cells are not terminal Schwann cells, nerve terminals or muscle fibres.

2.2.2- Protein recognised by the 2166 antibody

The staining pattern obtained in different tissues and cell lines using the 2166 antibody suggests that the protein recognised represents a component of the subcellular cytoskeleton. In order to identify the protein recognised by the 2166 antibody, protein homogenates derived from cerebellum of 3-week old mice were separated into soluble and cytoskeletal fractions by ultracentrifugation. Cerebellum tissue was used as the 2166 antibody produced a bright staining by immunofluorescence (data not shown), suggesting a high expression of the protein recognised by the 2166 antibody in this tissue. The samples were resolved by SDS-page electrophoresis, transferred to nitrocellulose membranes and blotted with the 2166 antibody. The antibody recognised a band of approximately 47 KDa only in the cytoskeleton fraction (Fig. 27A). This band was identified in Coomassie blue stained SDS gels, excised and analysed by mass spectrometry. The results from this analysis revealed that the 2166 antigen corresponds to tubulin. To confirm this, purified tubulin from bovine brain was resolved by SDS-page electrophoresis and as a control, cytoskeletal fractions of mice cerebellum were run in the same gel. Proteins were transferred to nitrocellulose membranes and blotted with the 2166 antibody or an antibody against tubulin. The 2166 antibody failed to reveal a band in the lanes corresponding to purified tubulin but did so in lanes corresponding to the cytoskeletal fraction of cerebellum homogenates (Fig. 27B). The tubulin antibody in

turn, recognised a band with corresponding size in the purified tubulin fraction (Fig. 27C). Taken together, a plausible explanation of these results are that the 2166 antibody recognises a post-translational modification of tubulin expressed in cerebellum and exclusively by a subpopulation of cells at the neuromuscular junction.

2.2.3- Identity of neuromuscular associated 2166+ cells

To resolve whether NMJ^{2166+} cells represent a novel population of neuromuscular synapses or whether they belong to a previously described cell population, double immunostaining with a battery of cell type-specific antibodies, together with the 2166 antibody was applied in muscle tissue.

To rule out the possibility that NMJ^{2166+} cells represent terminal Schwann cells, either in normal or activated states, immunostaining was performed using antibodies against S100 and nestin/GFAP, respectively. As shown in figure 28A, NMJ^{2166+} cells were located above terminal Schwann cells, the latter revealed by immunostaining with the S100 antibody. NMJ^{2166+} cells were also GFAP and nestin immunonegative (Fig. 28B and C, respectively) markers for activated states of terminal Schwann cells (Georgiou et al., 1994, Kang et al., 2001). In addition, Schwann cells are located inside the basal lamina which is not the case for NMJ^{2166+} cells (Fig. 26D). These results clearly indicate that NMJ^{2166+} cells represent a cell population that is distinct from terminal Schwann cells.

Staining with antibodies directed to three different markers for satellite cells, i.e. NCAM, desmin and M-cadherin known to be expressed by quiescent and proliferative phenotypes of satellite cells (Irintchev et al., 1994; Yablonka-Reuveni et al., 1999), showed that NMJ^{2166+} cells do not represent this cell type (Fig. 28D-F). NMJ^{2166+} cells also do not represent macrophages as revealed by immunolabelling using the macrophage marker antibody F4/80 (data not shown). The possibility that NMJ^{2166+} cells might represent fibroblasts was studied because a population of "perijunctional fibroblast" was previously identified near rat neuromuscular junctions (Gatchalian et al., 1989). Since these authors based their assertion using an antibody against the Thy-1 protein as a fibroblast marker, the same monoclonal antibody was used in rat and mouse muscle preparations. However, no signal from

cells near or above the neuromuscular junction was obtained; but axons, known to express the Thy-1 protein were immunolabeled, representing a positive control for the antibody efficacy (Fig. 28G).

Since Thy-1 is expressed only by a subpopulation of fibroblast, the negative labelling of NMJ^{2166+} cells obtained with this antibody do not completely rule out their fibroblast lineage. As a broad and less specific marker for fibroblasts, an antibody against the rat isoform of prolyl-4-hydroxylase (rPH), an enzyme involved in the synthesis of collagen, was used for immunofluorescence in whole mounts of rat TS muscles, together with the 2166 antibody and BTX. Positive staining for rPH localised to 2166-positive cells above the NMJ (Fig. 29A). This result indicates that NMJ^{2166+} cells probably represent a subpopulation of fibroblasts associated with the neuromuscular synapse. Hence, I shall refer to these cells as junctional fibroblasts. This assumption may not be accurate as several cell types have the capacity to synthesise collagen, including endothelial cells and myelin forming Schwann cells.

A stem cell population located in interstitial spaces of skeletal muscle was identified and isolated by its expression of the hematopoietic stem cell marker CD34 (Tamaki et al., 2002). Nevertheless, no reference was made in this publication to the localisation of the CD34-positive cells in relation to the neuromuscular junction. Therefore, immunolabelling of TS muscle preparations using an antibody against CD34, together with the 2166 antibody and BTX staining was performed.

Remarkably, junctional fibroblasts appeared positive for CD34 with the expected surface staining (Fig. 29B). The immunostaining for CD34 reveals additional aspects about the morphology of 2166-positive cells and their relation to the neuromuscular junction. Junctional fibroblasts cover and extend outside the neuromuscular region and appears to contact the muscle fibre outside the end-plate perimeter (Fig. 29B and C).

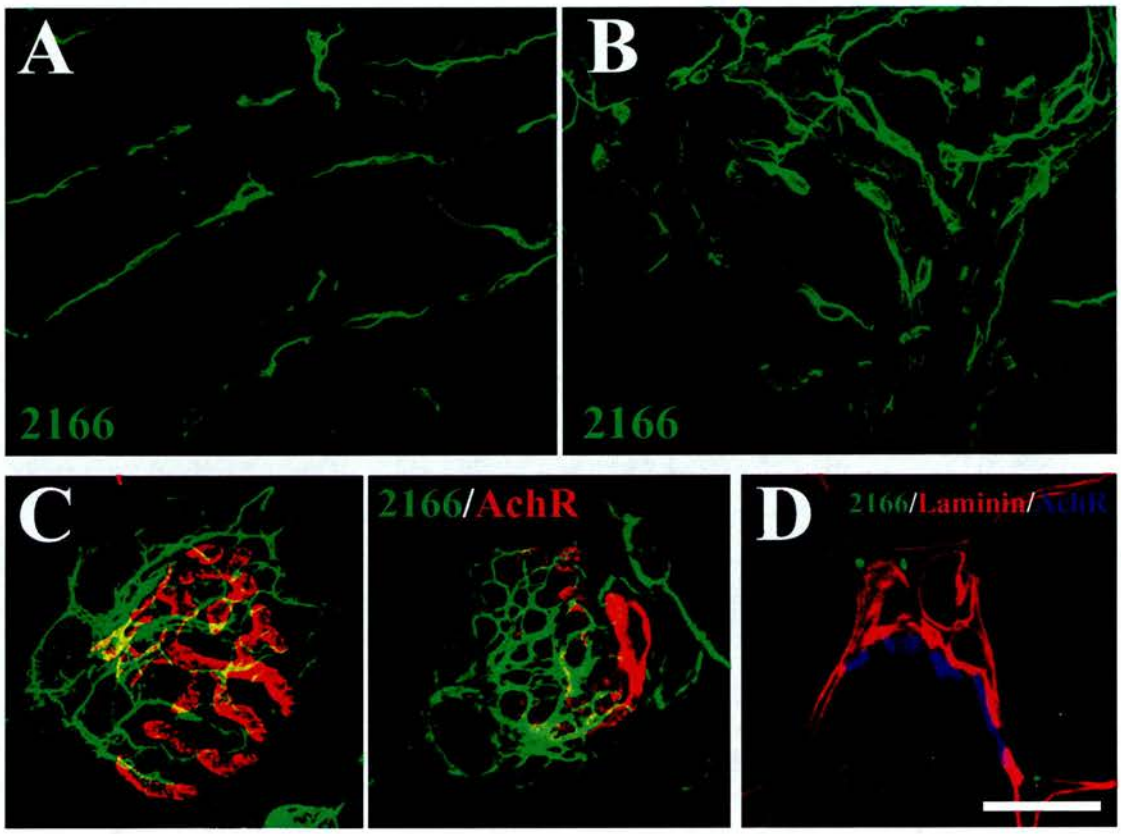

Figure 26. Localisation of 2166$^+$ cells in skeletal muscle.
Immunohistochemistry of whole mounts TS muscle using the 2166 antibody reveals bipolar cells located in the muscle surface **(A)**, and associated with an intramuscular capillary **(B)**. In the neuromuscular junction, identified by AchR staining (red), 2166$^+$ cells (green) are restricted to the synapse area **(C)**. 2166$^+$ cells in the neuromuscular junction locates outside basal laminae, as revealed by staining transverse muscle sections with 2166 (green dots) and laminin antibodies (red), together with AchR staining **(D)**. Scale bar, 80 μm in A and B; 30 μm in C; 50 μm in D.

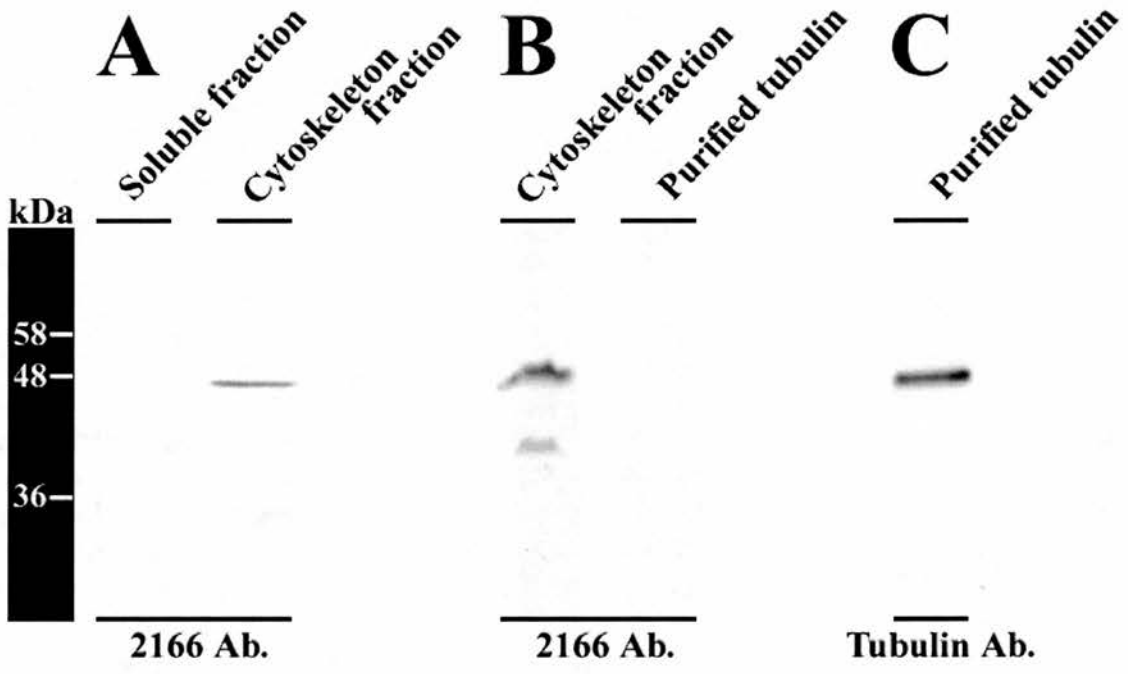

Figure 27. Characterisation of the 2166 antigen.
(A) Western blot analysis using the 2166 antibody; a single band of ~47 kDa is detected in the cytoskeletal fraction from mouse cerebellum. **(B)** The 2166 antibody fails to recognise any antigen in samples containing purified tubulin. As a positive control, a tubulin antibody reveals a strong band in the purified tubulin sample **(C).**

Figure 28. 2166^+ cells represent a novel cell population of skeletal muscle (figure in the next page)

A battery of antibodies was used together with 2166 in order to resolve whether 2166^+ cells represent a known cell population. **(A)** 2166^+ cells are distinct from terminal Schwann cell as revealed by double immunostaining with antibodies against S100 (green), 2166 (red) and AChR staining (blue). **(B)** GFAP, a protein expressed by "activated" terminal Schwann cells is not expressed by 2166^+ cells, inset: positive control from the same preparation showing GFAP signal from myelinated Schwann cells. **(C)** Nestin, a second marker for "activated" Schwann cells is not expressed by 2166^+ cells. **(D, E)** Two markers for proliferating satellite cells, desmin and NCAM, are not immunodetected in 2166^+ cells. **(F)** Immunostaining with M-Cadherin antibody reveals a satellite cell (arrowhead), but no positive staining is found in the neuromuscular junction, identified by laminin immmunosignal (arrow). **(G)** Immunostaining for Thy1 protein, expressed by neurons and a subpopulation of fibroblast, shown that 2166^+ cells do not represent this later cell type. Scale bar, 25 μm in A, B and G; 35 μm in C-E and F.

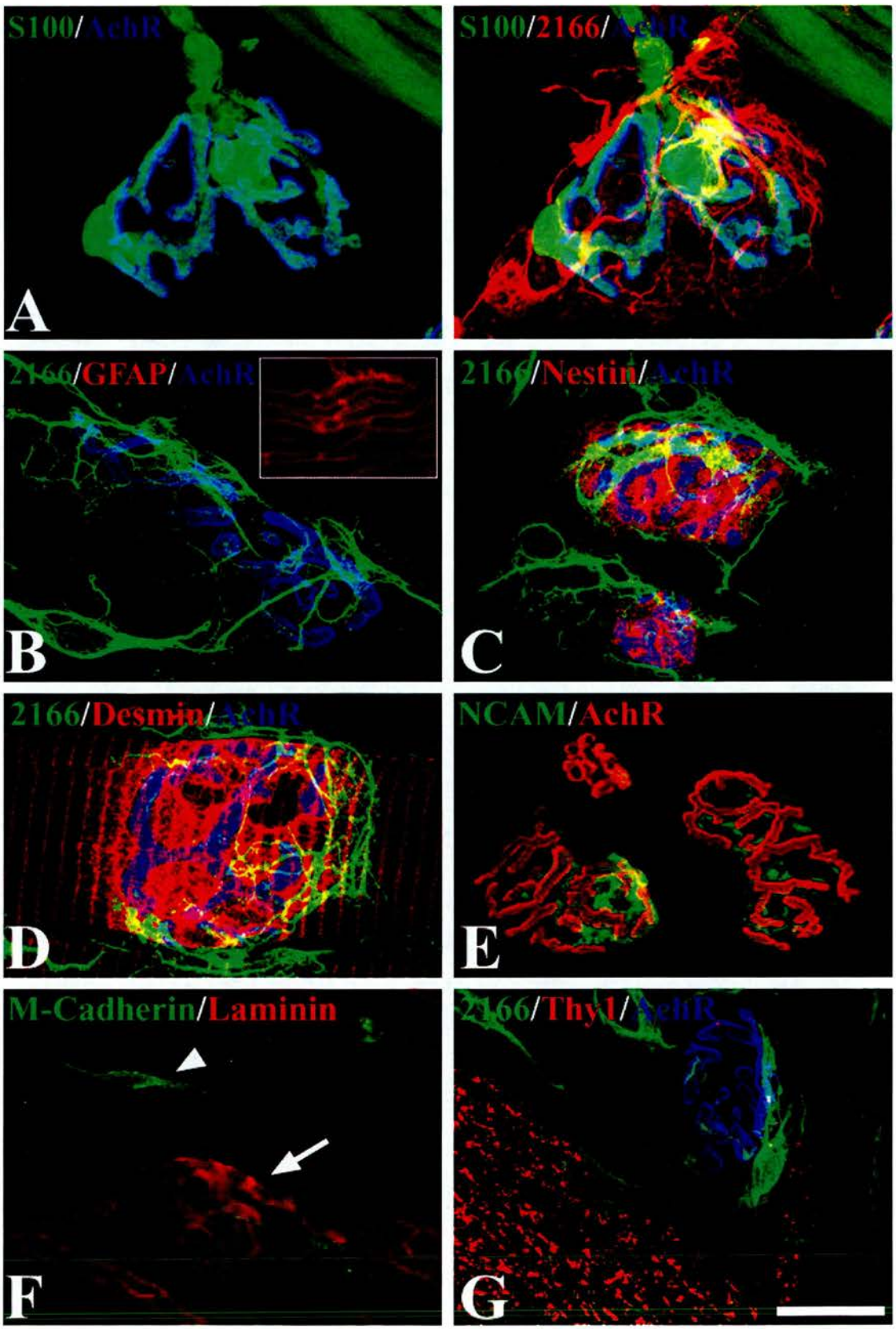
S100/AchR
A
S100/2166/AchR
2166/GFAP/AchR
B
2166/Nestin/AchR
C
2166/Desmin/AchR
D
NCAM/AchR
E
M-Cadherin/Laminin
F
2166/Thy1/AchR
G

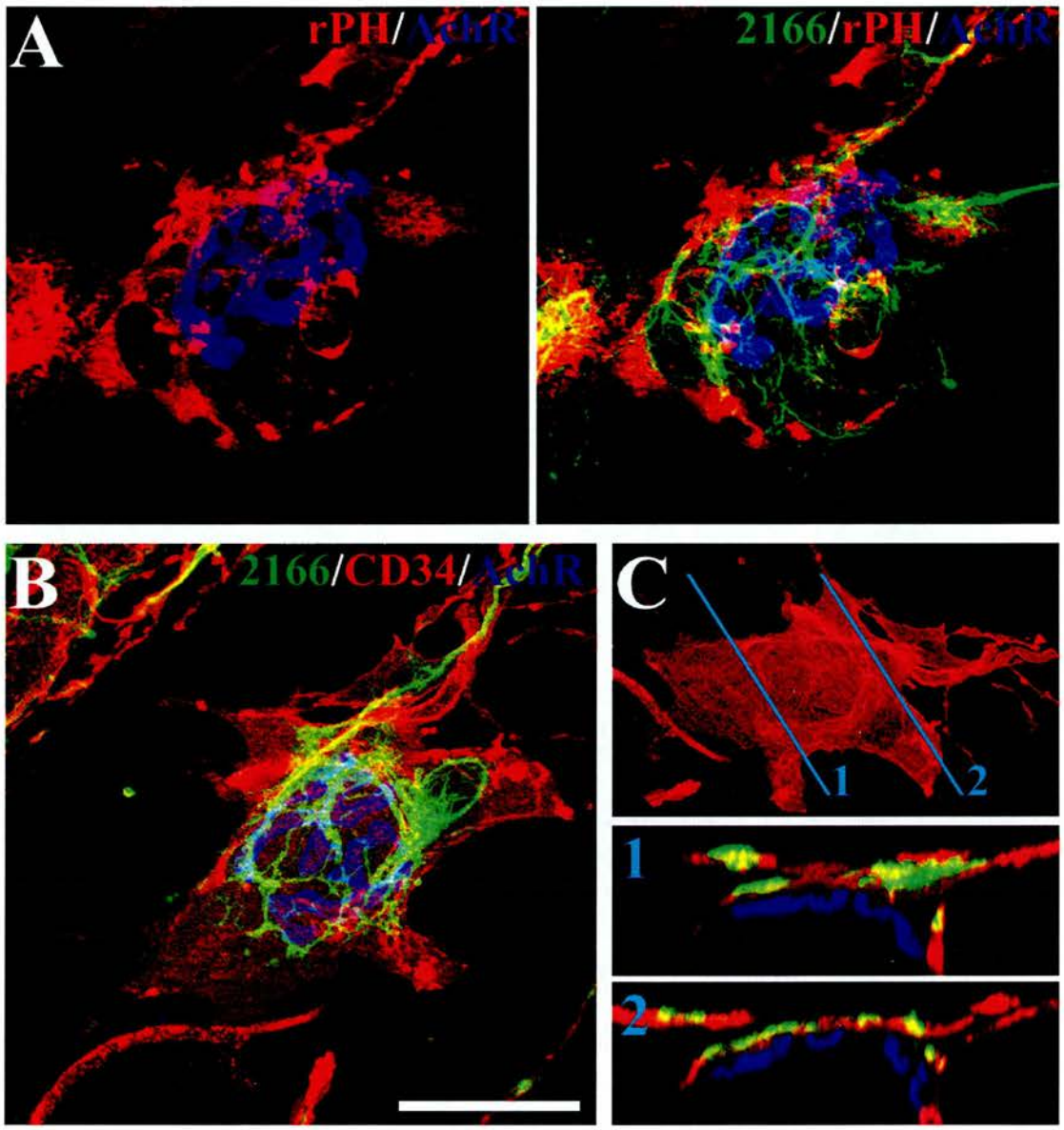

Figure 29. 2166$^+$ cells at the neuromuscular junction probably represent a subpopulation of fibroblasts.

(A) Immunostaining with antibodies against the fibroblast specific protein prolyl-4-hydroxylase (rPH, red) and 2166 (green) together with AChR staining (blue) reveals that 2166$^+$ cells are rPH positive. **(B)** Double immunostaining with antibodies against the membrane protein CD34 (red) and 2166 (green) together with AChR staining (blue), shown that 2166$^+$ cells cover the entire neuromuscular junction. Scale bar, 50 μm. **(C)** Projections in the Z-axis were performed from the whole volume of the neuromuscular junction shown in **B**. In the the upper panel, cyan lines and numbers indicate the places where projections, shown in lower panels, were made in relation to the CD34 staining; color-code of antibodies as in **B**.

2.2.4- Junctional fibroblasts become restricted to the neuromuscular junction during development

Junctional fibroblasts in adult skeletal muscle are highly restricted to the neuromuscular junction area. In order to characterise the sequence of event that leads to their specific localisation, immunostaining using antibodies against 2166, neurofilament and AchR staining was performed at different times during postnatal development of the mouse TS muscle. At P1, cells positive for 2166 immunolabelling were homogenously distributed along the TS muscle with no clear pattern of distribution (Fig. 30A). Between P5 and P10, 2166-positive cells become restricted to the central band of the muscle, region characterised by the localisation of neuromuscular synapses as revealed by AchR staining (Fig. 30B-C). In TS muscles of 4-week old mice, 2166-positive cells become restricted to the neuromuscular junction (Fig. 30D). The number of junctional fibroblasts associated with the neuromuscular junction was quantified in adult TS muscles immunostained with the 2166 antibody and the nuclear staining DAPI (n=5, 100 neuromuscular junctions analysed). As shown in the histogram (Fig. 30E), all neuromuscular junctions possess at least one junctional fibroblasts with some of them exhibiting three junctional fibroblast above their area.

2.2.5- Early response of 2166 cells to denervation and paralysis of the neuromuscular system

Denervation and paralysis of muscle fibres results in a series of biochemical and structural changes in terminal Schwann cells (Hassan et al., 1994; Reynolds and Woolf, 1992; Woolf et al., 1992). As junctional fibroblasts are intimately associated with terminal Schwann cells, the physical and temporal relation between the response elicited in junctional fibroblast and terminal Schwann cells following denervation or paralysis was studied in TS muscle from adult mice.

Partial denervation of TS muscles was performed as described in methods (section 4.6.2). The technique used allows one to denervate only a region of the muscle, a region that can be clearly identified by the segmental innervation that characterises the TS muscle. Partially denervated TS muscles were immunostained with an

antibody against nestin, a marker of "reactive" terminal Schwann cells, the 2166 antibody and fluorescent-conjugated BTX.

In innervated neuromuscular junctions, nestin is expressed only by muscle fibres in the postsynaptic region and junctional fibroblasts are restricted to this area (Fig. 31A). One day post-denervation, the 2166^{+} junctional fibroblasts extended processes away from the neuromuscular region (Fig. 31B). However, terminal Schwann cell were still negative for nestin (Fig. 31B). At junctions denervated for three days, terminal Schwann cells became nestin positive and extended processes along the muscle surface. Some of the processes were seen to be associated with the 2166-positive outgrowths (Fig. 31C). The response of junctional fibroblasts was local. Thus, innervated NMJs in the same muscle as denervated ones, were covered by junctional fibroblasts circumscribed to the AchR cluster region.

Junctional fibroblasts have a fast response after denervation of the associated neuromuscular junction, characterised by their extension of processes. After two days, terminal Schwann cells became reactive and apparently extend along 2166-positive processes. This order of events suggests that junctional fibroblasts might have a role in guiding the growth of terminal Schwann cells by either physical or molecular clues.

To further examine their role in Schwann cell sprouting, paralysis of the TS muscle was performed by injection of botulinum toxin (type A) in the interstitial spaces, below intercostal muscles. This toxin produces paralysis by blocking transmitter release from the nerve terminals. Paralysis was confirmed by stimulating the innervation of the TS muscle following dissection. In all cases, no contractile response was obtained when the injected TS muscle was stimulated, whereas stimulation of the uninjected muscles produced a vigorous contractile response.

After one day of muscle paralysis, junctional fibroblasts sprouted at a level similar to the denervation-induced response (Fig. 32A). This response was also present after 6 days of muscle paralysis (Fig. 32B). Nevertheless, terminal Schwann cells do not become nestin positive at 6 days post-paralysis (Fig. 32B). The lack of terminal Schwann cells response might reflect the possibility that the TS is a "fasyn" type of muscle. These muscle types, identified by Pun *et al.* (Pun et al., 2002), has been

shown to be insensitive in terms of Schwann cells response or nerve sprouting following muscle paralysis by botulinum toxin.

2.2.6- Junctional fibroblasts response to muscle atrophy in the R6/2 mice

The response of junctional fibroblasts was also examined in atrophic TS muscles of a mouse model of Hungtinton disease, the R6/2 mouse, which is a transgenic for the first exons of the human huntington gene, including about 150 CAG (polyQ) repeats. In this mutant, muscle fibres show electrophysiological characteristics of denervated or paralysed muscle (Ribchester et al., submitted). However, terminal Schwann cells remain unreactive as revealed by positive S100 and negative nestin immunostaining and the presence of nerve terminal sprouting is not detected. Immunostaining was performed in TS muscles from two severely affected 15-week old R6/2 mice using the 2166 antibody and an antibody against neurofilament together with AchR staining. Junctional fibroblasts sprouting was similar to the response exhibited following denervation or paralysis of the muscle (Fig. 32C and D). Taken this result together with the effects of denervation and paralysis, it appears that the response of junctional fibroblasts following paralysis or muscle atrophy is not sufficient to trigger terminal Schwann cell reaction. This suggests that the role of junctional fibroblast as guidance cues for reactive terminal Schwann cell sprouts is permissive rather than instructive.

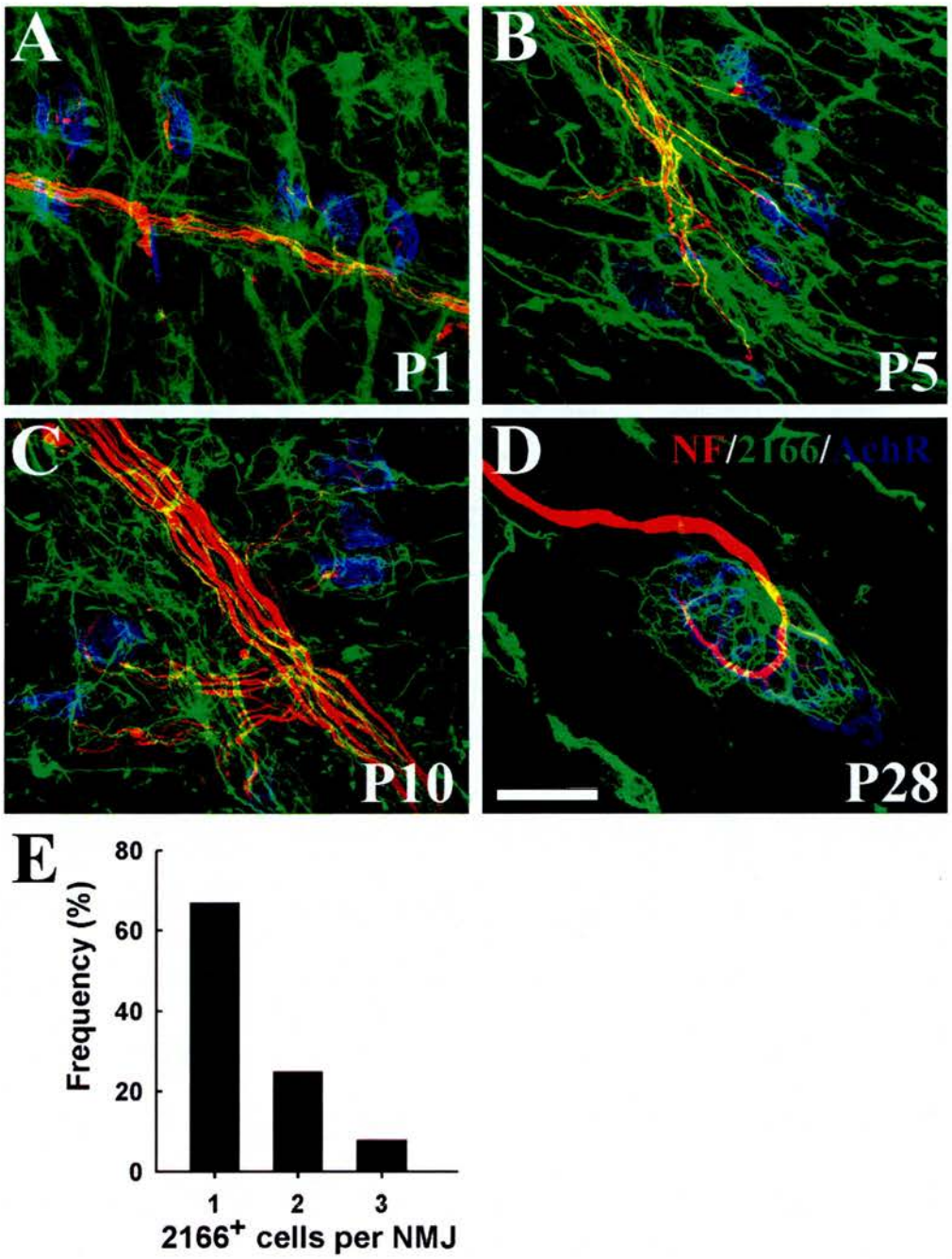

Figure 30. Junctional fibroblasts become restricted to the motor endplate band during postnatal development.

Double immunostaining using antibodies against neurofilament (NF, red), 2166 (green) and AChR staining (blue) was performed in whole mounts of triangularis sterni (TS) muscle at different postnatal ages. In post natal day (P) 1, 2166-positive cells are located homogeneously above the muscle fibers **(A)**. At P5 and P10, junctional fibroblasts become concentrated to the central regions of the muscle **(B-C)**, and at P28 they are restricted to the neuromuscular junction **(D)**. Scale bar, 30 μm in A-C; 20 μm in D. **(E)** In adult mouse TS muscle, every NMJ includes between one and three 2166^{+} cells.

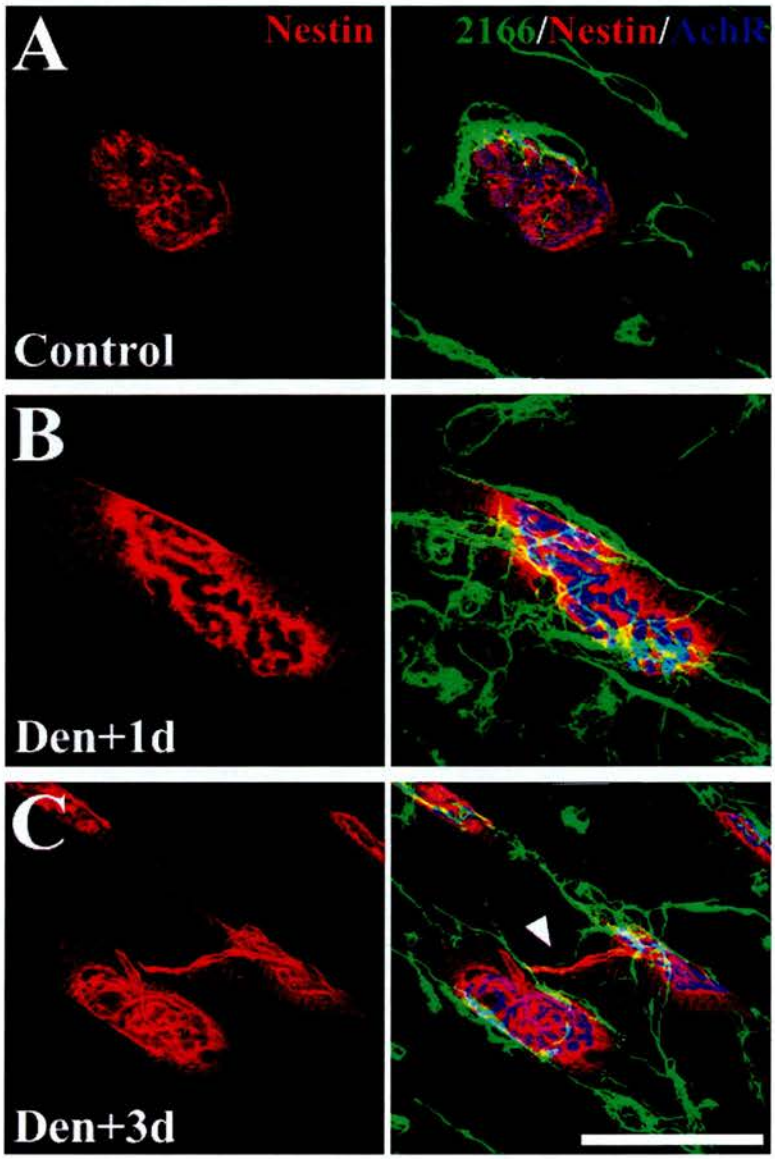

Figure 31. Junctional fibroblast reaction following partial denervation.
TS muscles were partially denervated and the response of terminal Schwann cells and junctional fibroblasts (2166^+ cells) was studied by immunostaining for nestin (red, left panel) and 2166 (green, right panel), respectively.
(A) In innervated neuromuscular junctions, nestin is expressed only by muscle fibers and 2166^+ cells are restricted to the BTX positive area (blue). **(B)** At one day post denervation, 2166^+cells sprout extensively away from the endplate, but terminal Schwann cells remains nestin negative. **(C)** At three days post denervation reactive terminal Schwann cells express nestin and nestin positive processes can be seen associated to 2166^+ sprouts (arrowhead). Scale bar, 30 μm.

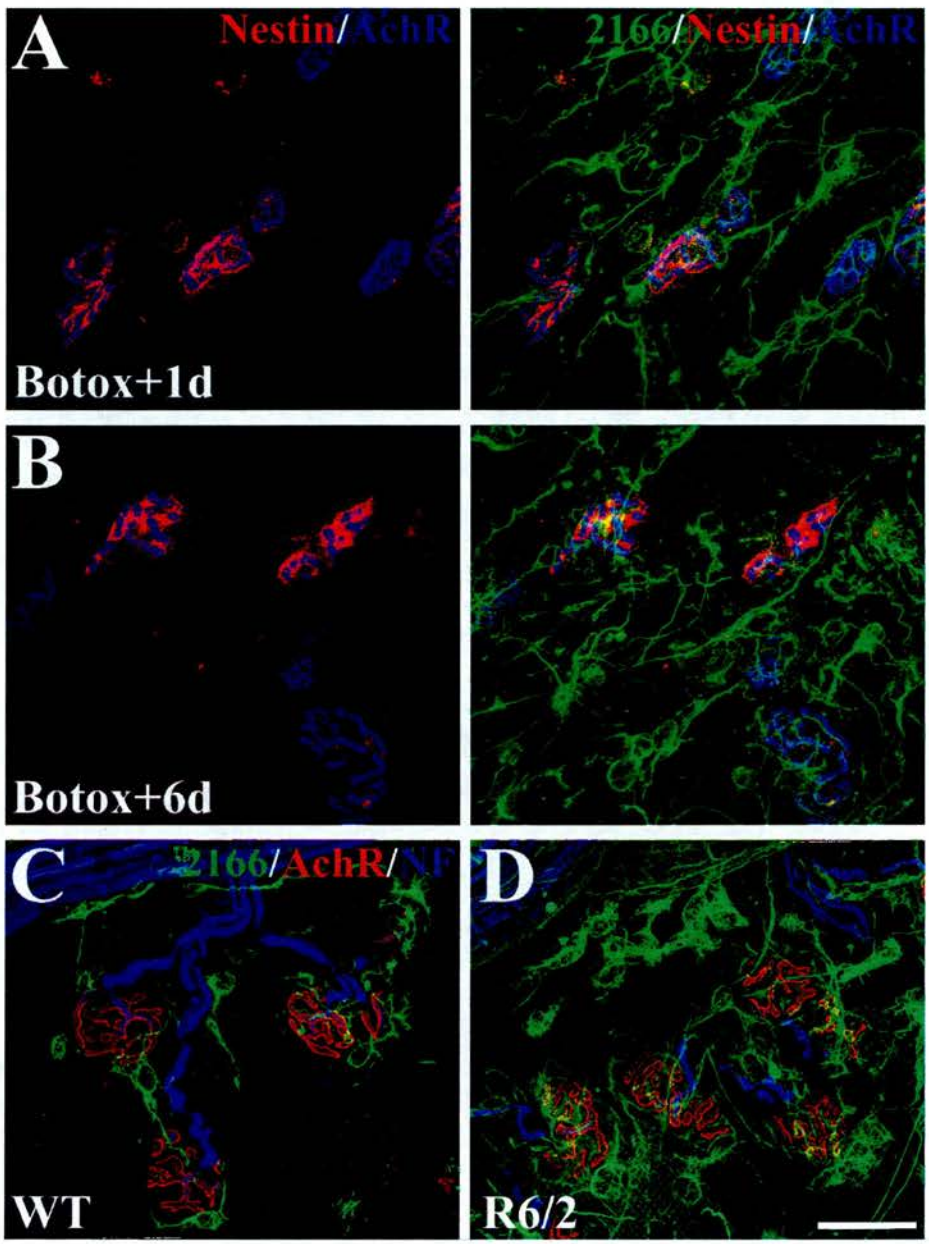

Figure 32. Junctional fibroblast but not terminal Schwann cells react after paralysis.

A-B, TS muscles were paralysed with botulinum toxin (type A) and the response of terminal Schwann cells and junctional fibroblasts (2166^{+} cells) was studied by immunostaining for nestin (red, left panel) and 2166 (green, right panel), respectively. After one **(A)** and six **(B)** days of paralysis, junctional fibroblasts sprout extensively but terminal Schwann cells remains nestin negative. **(C)** TS muscle from WT (left panel) and severely affected R6/2 mice (right panel) were immunostained for 2166 (green) and neurofilament (blue), together with AchR staining (red). The spread of junctional fibroblasts in R6/2 TS muscle appears similar in extent to botulinum-paralysed muscles. Scale bar, 50 μm.

2.2.7- Tenascin-C is expressed in neuromuscular junctions after denervation

Tenascin-C is expressed after denervation by muscle associated fibroblasts in the central band of neuromuscular junctions (Gatchalian et al., 1989). In addition, denervated muscles of the tenascin-C null mice shown delayed reinnervation of neuromuscular junctions (Cifuentes-Diaz et al., 2002). Therefore, activated junctional fibroblasts after denervation could be the source of tenascin-C, which may then acts as a permissive extracellular matrix component responsible for the efficient extension of terminal Schwann cells activated by other molecular cues. In order to the test this possibility, the expression of tenascin-C after denervation and the cellular source of its expression were investigated by immunocytochemistry. TS muscles from WT adult mice were partially denervated and processed for immunofluorescence 1, 2 and 3 days after the procedure. Innervated and denervated regions of TS muscles were immunostained using an antibody against tenascin-C, the 2166 antibody and AchR staining using fluorescent-conjugated BTX. No positive immunostaining for tenascin-C was detected in innervated neuromuscular synapses (Fig. 33A). In neuromuscular junctions denervated for three days, junctional fibroblasts reacted as described previously and a strong immunosignal for tenascin-C is present in regions restricted to the neuromuscular area (Fig. 33B). After 6 days of denervation, tenascin-C expression had started to spread from the neuromuscular perimeter. At this stage, tenascin-C positive regions localised on the surface and following the same axis of the muscle fibres; and 2166-positive cells lay in register with tenascin-C immunopositive regions (Fig. 33C).

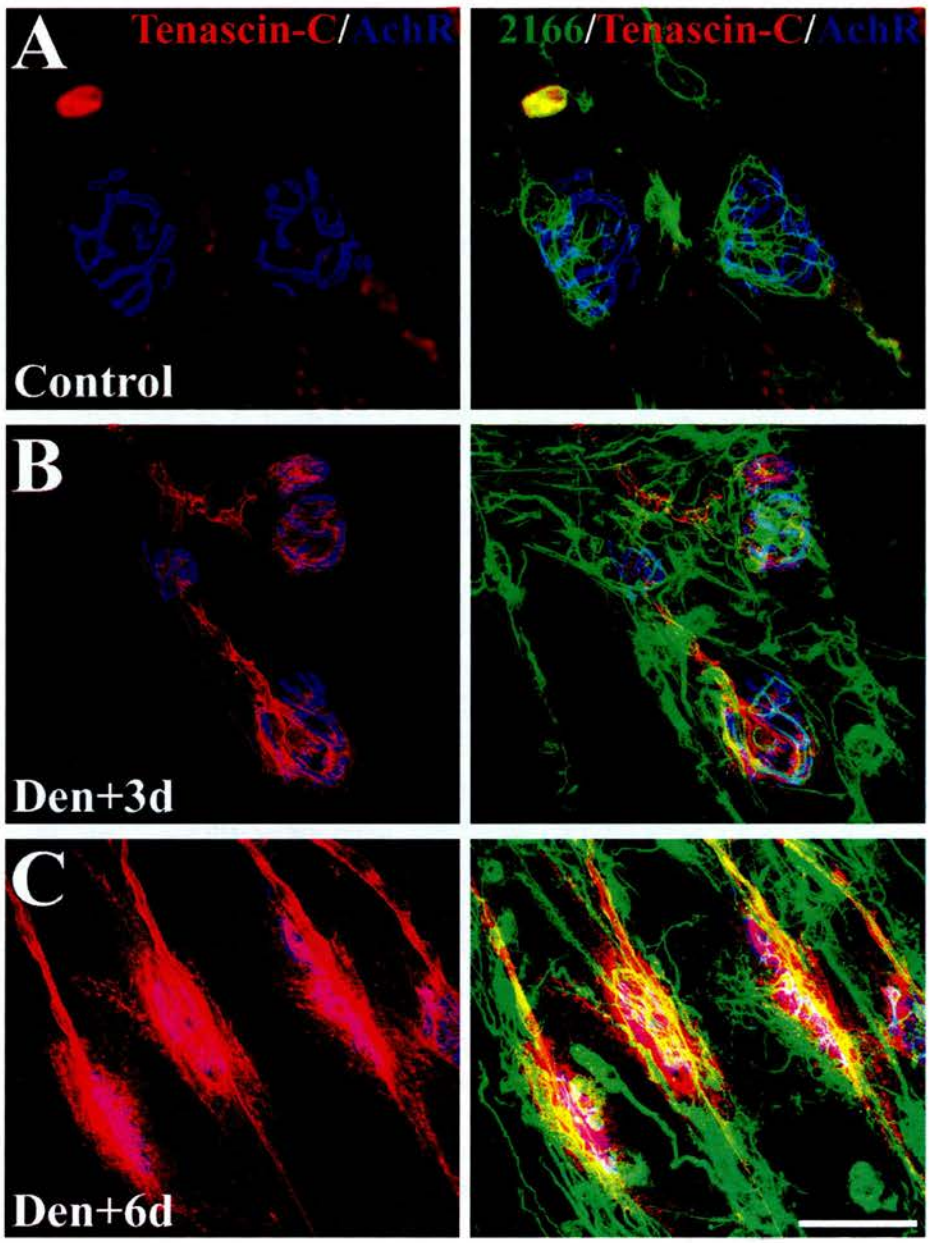

Figure 33. Tenascin-C is expressed in the neuromuscular junction after denervation.

TS muscles were denervated and immunostained with antibodies against tenascin-C (red), 2166 (green), together with AchR staining (blue). **(A)** In innervated NMJs, no tenascin-C signal is detected. **(B)** After 3 days post-denervation 2166-positive cells form extensive sprouting and tenascin-C is detected in the NMJ area and proximal nerve fiber. **(C)** At 6 days post-denervation, tenascin-C signal spread from the synaptic area and localised in register with 2166-positive cells. Scale bar, 50 μm.

2.2.8- Summary

In addition to the well-known cells at neuromuscular junctions (motor nerve terminals, Schwann cells and muscle fibres) I have identified a subpopulation of cells in mouse and rat skeletal muscle using the novel 2166 antibody. The antigen of this antibody is probably a postranslational modification of tubulin determined by mass spectrometry, Western blot and immunocytochemistry. 2166^{+} cells are highly restricted to the synaptic area, above the motor endplate. In adult mouse triangularis sterni (TS) muscle, every NMJ includes between one and three of these cells which are closely associated with terminal Schwann cells, but located outside the basal lamina. The 2166^{+} cells were immunonegative for cell-type specific markers including S100, N-cadherin, F4/80, Thy1, NCAM, desmin and nestin; ruling out any identity with Schwann cells, muscle satellite cells or macrophages. 2166^{+} cells were positive for prolyl-4-hydroxylase, an enzyme involved in the synthesis of collagen, suggesting that junctional fibroblasts belong to a fibroblast or endothelial cell lineage. They also stained positive with an antibody against CD34, a marker of endothelial and stem cells previously identified in skeletal muscles.

During postnatal development, junctional fibroblasts arise from a more diffuse, larger population and become restricted to the motor endplate band. In order to gain insights on the function of junctional fibroblast, their response to partial denervation, paralysis and muscle atrophy was examined. One day after denervation, junctional fibroblasts extend processes profusely. By 3 days, terminal Schwann cells began to extend sprouts that associate with the pre-formed junctional fibroblast sprouts. Following paralysis and muscle atrophy, junctional fibroblasts extend processes but terminal Schwann cells remain in the neuromuscular junction in a non-activated state.

Taking together, these results suggests that junctional fibroblasts are a specific cellular component, involved in the orchestrated cellular responses that occur during plastic changes at the neuromuscular synapse.

2.3- CONSEQUENCES OF DEMYELINATION FOR THE STRUCTURE AND FUNCTION OF NEUROMUSCULAR JUNCTIONS

The protein periaxin is expressed by myelinating Schwann cells, where it is concentrated at the abaxonal surface of myelin as the sheaths mature. Mice lacking a functional Periaxin gene initially produce compact myelin, but later demyelinate. Phenotypically, the mice show tremor, inappropriate clasping reflexes, reduced peripheral nerve conduction velocity and neuropathic pain behaviour. In demyelinating diseases, the phenotypic changes observed are usually attributed to segmental demyelination in the nerve fibre. But the consequences of demyelinating conditions to the neuromuscular junction have not been studied systematically. Recent studies suggest that transgenic mutations which selectively affects the formation or stability of the Schwann cell myelin sheath, have a secondary impact on motor neuron structure and function, specially at motor nerve terminals (Yin et al., 2004). This is the focus of the present section in the context of the periaxin null mice. The studies reported here examine possible changes in the functional and structural characteristics of the neuromuscular synapse as a consequence of demyelinating disorders in order to evaluate the contribution of the motor end-plate plasticity to the phenotype of demyelinating conditions.

2.3.1- Morphological abnormalities in periaxin-null nerve terminals are associated with pre-terminal demyelination of nerve fibres

Immunohistochemistry together with confocal microscopy was used to compare the morphological features of axons, myelinating and terminal Schwann cells of periaxin null (KO) and control mice (WT).

The morphology of neuromuscular junctions in TS muscles from severely affected KO and age-matched WT mice was study by immunostaining using an antibody against neurofilament together with BTX. In 5-month old WT muscles, axons approach the neuromuscular junction and branch extensively close to the neuromuscular junction. In this region, they form terminal specializations that lie in register with AchR (Fig. 34A). In contrast, axons in 5-month old KO muscles present extensive pre-terminal branching with branch points often located at a considerable

distance from the terminal (Fig. 34B and C). Pre-terminal axons of the periaxin null mice present other abnormalities, including thinning of axon branches and focal swellings (Fig. 34C).

The increased pre-terminal branching and extended branch point distance from the terminal of KO compared with WT motor axons was quantified by measuring the distance from the end-plate to the most proximal branch point (with branches extending to the same NMJ) and the number of branches approaching the neuromuscular junction (n=3 for WT and KO, 50 neuromuscular junctions analysed per group). WT motor axons have on average 1.2±0.1 branches approaching the end-plate compared with 3.1±0.2 branches in the KO (mean±SEM, Fig. 34D). The distance of the most proximal branch point in WT axons was 4.7±1.8 μm compared to a value of 34.3±2.8 μm of KO motor axons (Fig. 34E). This abnormal pattern of innervation exhibited in periaxin null neuromuscular junctions may have arisen during neuromuscular development or in later stages. To discriminate between these two possibilities, 3-week old WT and KO neuromuscular junctions were immunostained with antibodies against neurofilament, together with BTX staining. In these preparations, the morphology and pattern of innervation of WT and KO motor axons were indistinguishable (Fig. 35A) and this was corroborated by the same quantitative analysis described above (Fig. 35B and C).

In order to establish if the abnormalities in KO neuromuscular junctions were a product of the lack of periaxin in terminal Schwann cells in addition to pre-terminal myelin-forming Schwann cells, TS muscles from 5-month old WT mice were immunostained using an antibody against periaxin together with BTX. As shown in figure 35D, periaxin is expressed by myelin-forming Schwann cells located in pre-terminal regions and intramuscular nerve fibres but not in terminal Schwann cells which cap the neuromuscular synapse. Therefore, the morphological changes in KO motor axons are a direct consequence of the lack of periaxin in myelin forming Schwann cells.

The abnormal pattern of innervation of KO motor axons arises after normal formation of the neuromuscular junction and is probably related to pre-terminal demyelination. To test this possibility, 5-month old WT and KO muscles were immunostained with antibodies against the myelin protein P0 and neurofilament

together with AchR staining. In WT neuromuscular junctions, the last myelinated region of the nerve fibres is located before the terminal branch (Fig. 36A). In KO nerve fibres, pre-terminal branches located far from the terminal always associate with regions devoid of myelin (Fig. 36B) that probably represents demyelinated regions that arise during the progression of the periaxin null mice condition. In addition, axonal swelling immunopositive for neurofilaments associates with residually-myelinated regions of the nerve fibre (Fig. 36C and D).

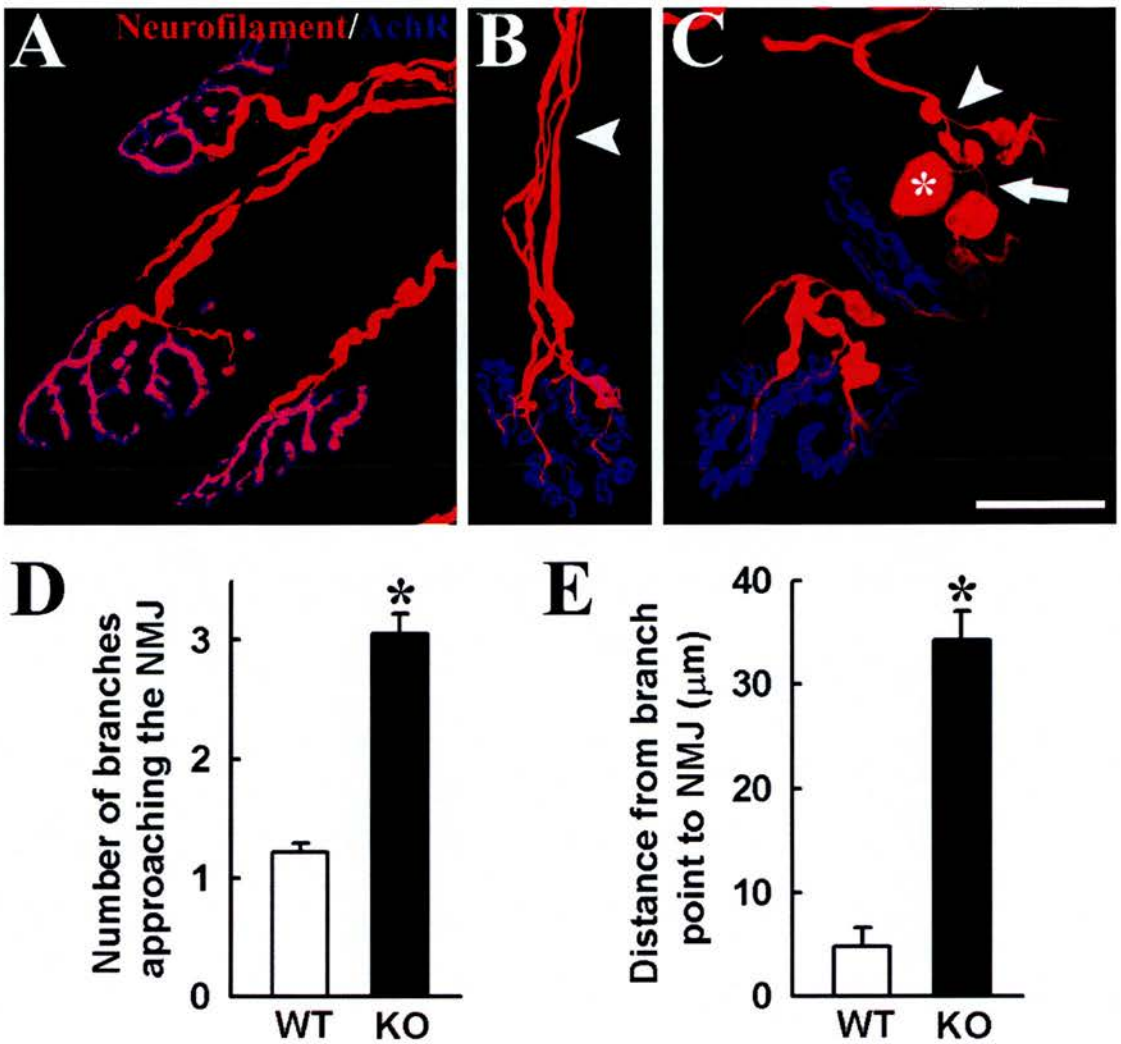

Figure 34. Motor axon abnormalities in the periaxin null mice.
Immunostaining for neurofilament (red) together with AChR staining (blue) shown that in WT neuromuscular junctions motor axons branch extensively when they contact the end-plate region **(A)**. In contrast, preterminal axons of periaxin null mice exhibit several abnormalities **(B)** and **(C)**, including increased number of preterminal axon branches (arrowhead), thinning of axon branches (arrow) and focal swellings (arterisk). More than 80% of periaxin null neuromuscular junctions present these abnormalities but none of these features are found in wild type animals. Scale bar, 30 μm. Quantification of the innervation pattern of WT and KO neuromuscular junctions shown an increase in KO pre-terminal branches contacting the neuromuscular junction compared with the WT values **(D)**. In addition, the distance from the proximal branch point to the neuromuscular junction is increased in KO neuromuscular junctions compared with WT ones **(E)**.

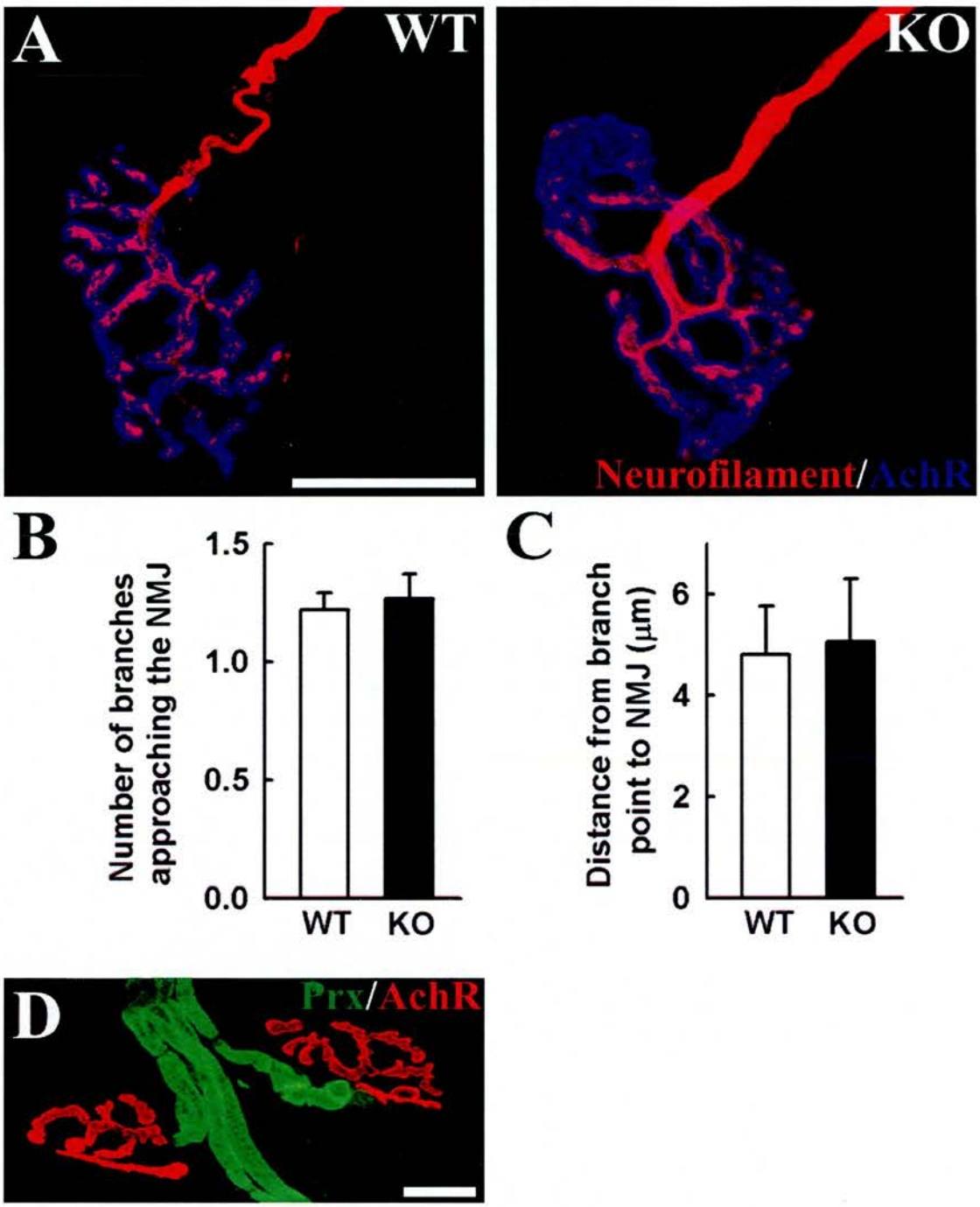

Figure 35. Periaxin null mice develops a morphologically normal neuromuscular junction.

(A) In 3-week old mice, KO neuromuscular junctions appears normal as revealed by immunostaining for neurofilaments (red) and AchR staining (blue). In addition, the number of branches per NMJ **(B)** and the distance from the last branch point to the end-plate **(C)** are not different from WT values. **(D)** Immunostaining for periaxin protein (green) together with AChR staining (red) in wild-type TS muscle shows that periaxin is present in myelinating Schwann cells but not in perisynaptic ones. Scale bars, 20 μm.

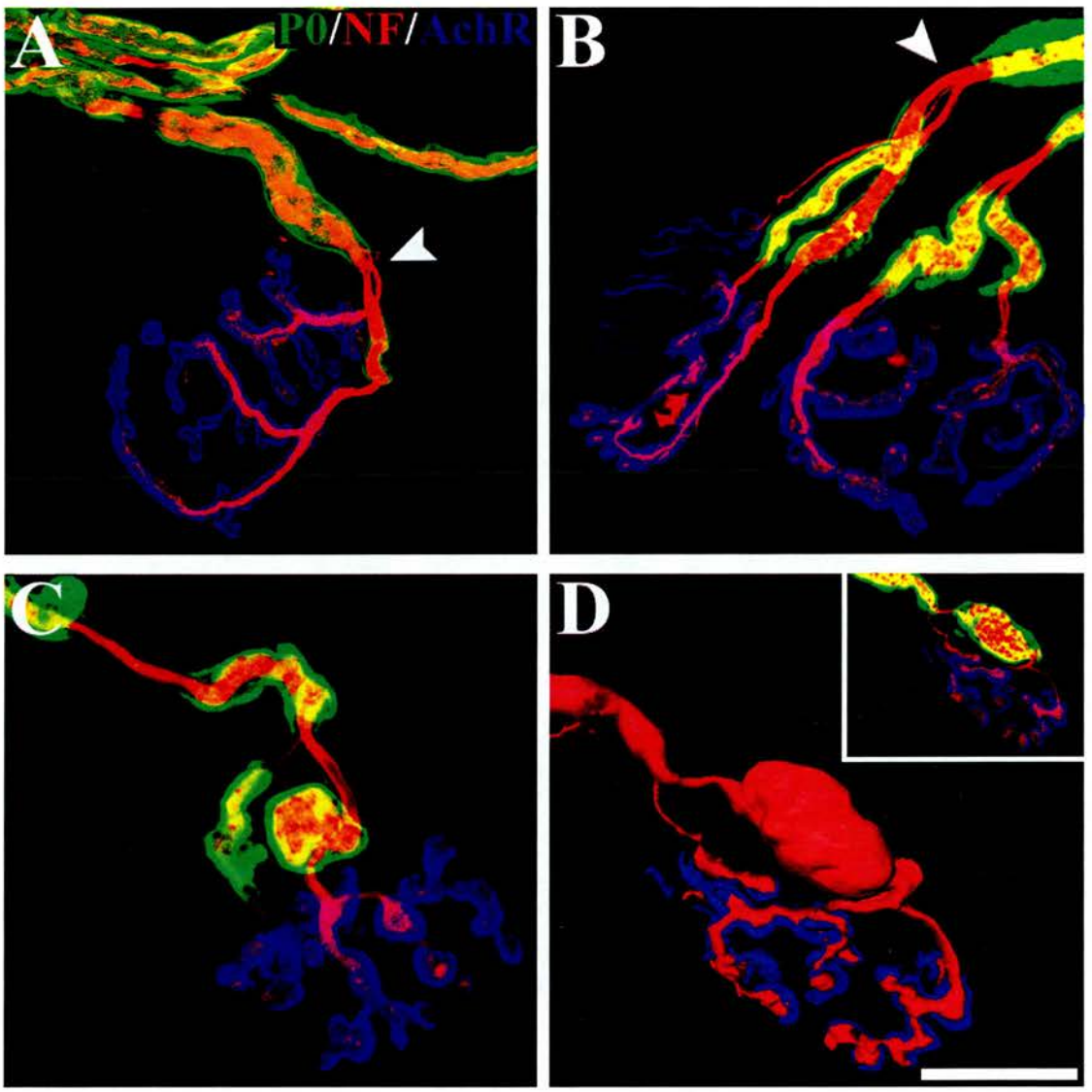

Figure 36. Axon abnormalities are related to preterminal demyelination.
TS muscles from 5-month old WT and KO mice were immunostaining for neurofilament and synaptic vesicle protein (red), myelin protein zero (P0, green) together with AChR staining (blue). In WT neuromuscular junctions, the last myelinated region occurs before the terminal branch **(A)**. In KO mice, preterminal branch-points (arrowhead) are always associated with regions devoid of myelin **(B)**. In addition, neurofilament-rich swellings **(C)** are associated with residually–myelinated regions (P0-positive staining). In **(D)** a 3D rendering was performed showing that the neurofilament-positive swelling is associated with a P0 rich region (inset). Scale bar, 20 μm.

2.3.2- Low frequency stimulation do not reveal any electrophysiological abnormality in periaxin-null neuromuscular junctions

To investigate if the morphological abnormalities in periaxin null neuromuscular junctions result in any physiological changes of the neuromuscular transmission, vital staining with FM1-43 and intracellular recording from muscle fibres were performed in WT and KO muscles.

Active regions of the nerve terminal were identified by vital staining using FM1-43, which incorporates only in recycling synaptic vesicles and can be detected by fluorescent microscopy. TS muscles from 5-month old WT and KO mice were dissected in physiological solution and active terminals loaded with FM1-43 and stained with BTX. In WT neuromuscular junctions, active regions of the nerve terminal, revealed by FM1-43 staining, cover the complete area of AchR staining (Fig. 37A), in KO muscles vital staining revealed no abnormalities in terms of activity of nerve terminals located above the AchR region (Fig. 37A).

Intracellular recording of end-plate potentials (EPPs) was performed in flexor digitorum brevis (FDB) muscle after blocking muscle action potentials with μ-conotoxin (2 μM). EPPs obtained after low frequency stimulation (1 Hz) were recorded in muscles from 2, 4, and 8-month old WT and KO mice (n=3 for each group) and analysed for various parameters. Most mutant junctions showed normal synaptic responses, with similar amplitude, time course and quantal content compared to wild type at all ages examined (Fig. 37B). However, the EPP latency, measured from the stimulus artifact to the start of the rising EPP phase, was increased significantly in KO compared with WT end-plates (Fig. 37C). By 8 months, it was 6.31 ± 0.21 milliseconds (ms) in KO muscles (mean ± S.E.M) compared with 2.56 ± 0.06 ms in WT ($P<0.0001$, t-test). The amplitude and frequency of spontaneous miniature end-plate potentials (MEPPs) were also similar comparing 8-month old WT and KO neuromuscular synapses (Fig. 37D), suggesting normal ACh receptor distribution and function in KO mice.

2.3.3- Failure of neuromuscular transmission in the periaxin null mice after repetitive stimulation

At low frequency stimulation, the neuromuscular transmission in KO muscles appears to be not affected by the morphological abnormalities present in their pre-terminal axons, which include extensive branching. Branch points are known to exhibit low safety factor for the conduction of the action potential in myelinated and unmyelinated axons, especially when subjected to high frequency stimulation. Therefore FDB muscles from 8-month old WT and KO mice were stimulated at a frequency of 30 Hz for 1 second, after blocking muscle action potentials with μ-conotoxin (2 μM). When stimulated at a frequency of 30 Hz, 40% of the KO end-plates responded intermittently, contrasting with the complete response exhibited in WT animals (Fig. 38).

Figure 37. Periaxin null mice have normal end-plate potentials (EPPs) and miniature end-plate potentials (MEPPs) but an increase in latency (figure in the next page).

WT and KO motor end plates were identified using the activity-dependent staining properties of FM1-43 and Rhodamine-α-bungarotoxin to visualise AChR in fresh preparations. This vital FM1-43 staining reveals a normal neuromuscular innervation in periaxin null neuromuscular junctions (**A**; upper panel, WT; lower panel, KO). Scale bar, 20 μm. **(B)** The mean EPP peak amplitude recorded from KO mice at different ages was not significantly different from the mean EPP peak amplitude recorded from the normal strain. The rise time and half decay time of synaptic potentials were also no different between mutant and control strains. **(C)** The latency of EPPs becomes longer with age in KO muscles, probably reflecting the advancement of the demyelinating phenotype. The amplitude and frequency of spontaneous MEPPs were also equal between WT and KO neuromuscular synapses **(D)**; since the quantal size reflects the post-synaptic sensitivity to acetylcholine, these data suggest that ACh receptor distribution and function are also normal.

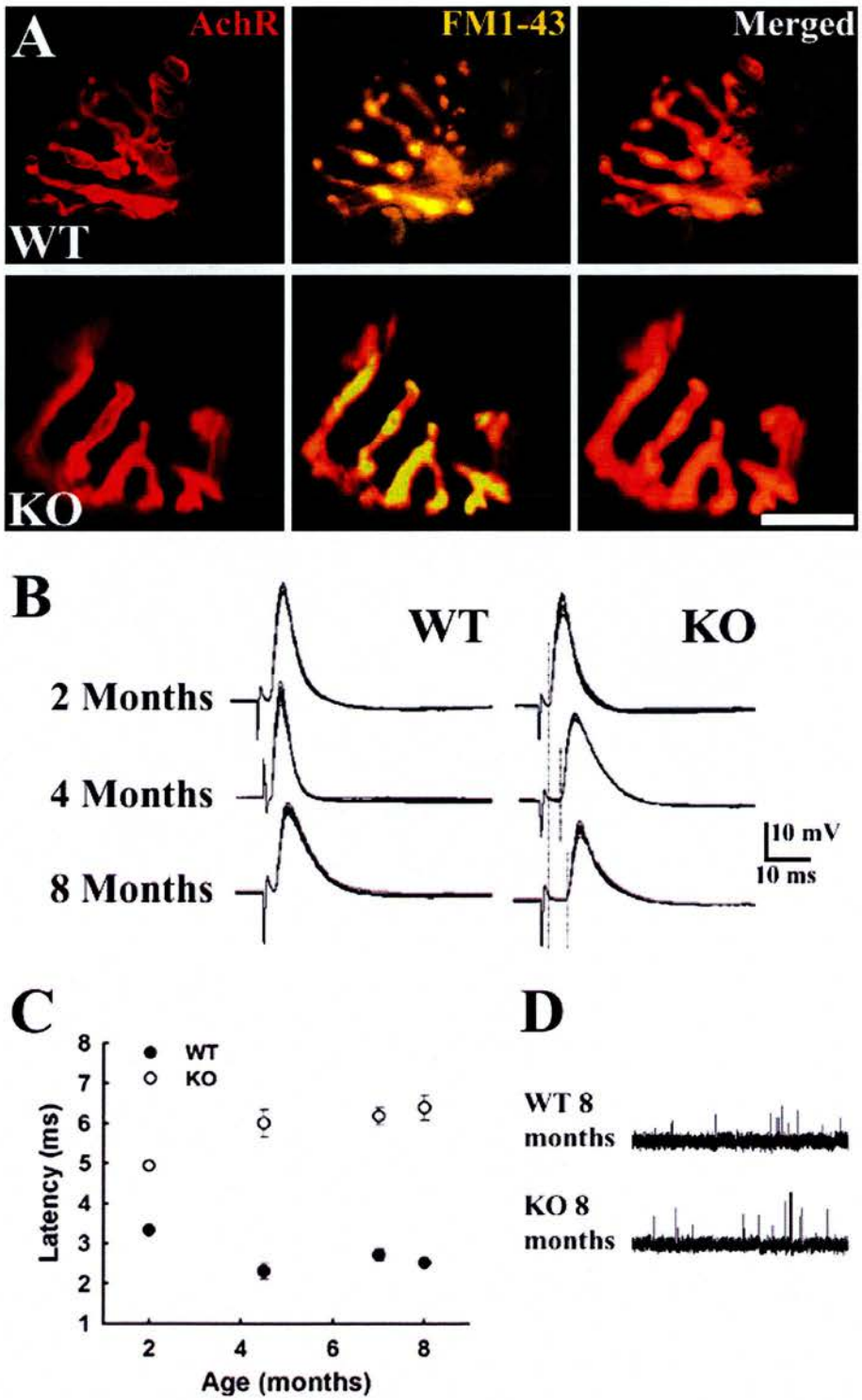
A
AchR
FM1-43
Merged
WT
KO
B
WT
KO
2 Months
4 Months
8 Months
10 mV
10 ms
C
WT
KO
Latency (ms)
Age (months)
D
WT 8 months
KO 8 months

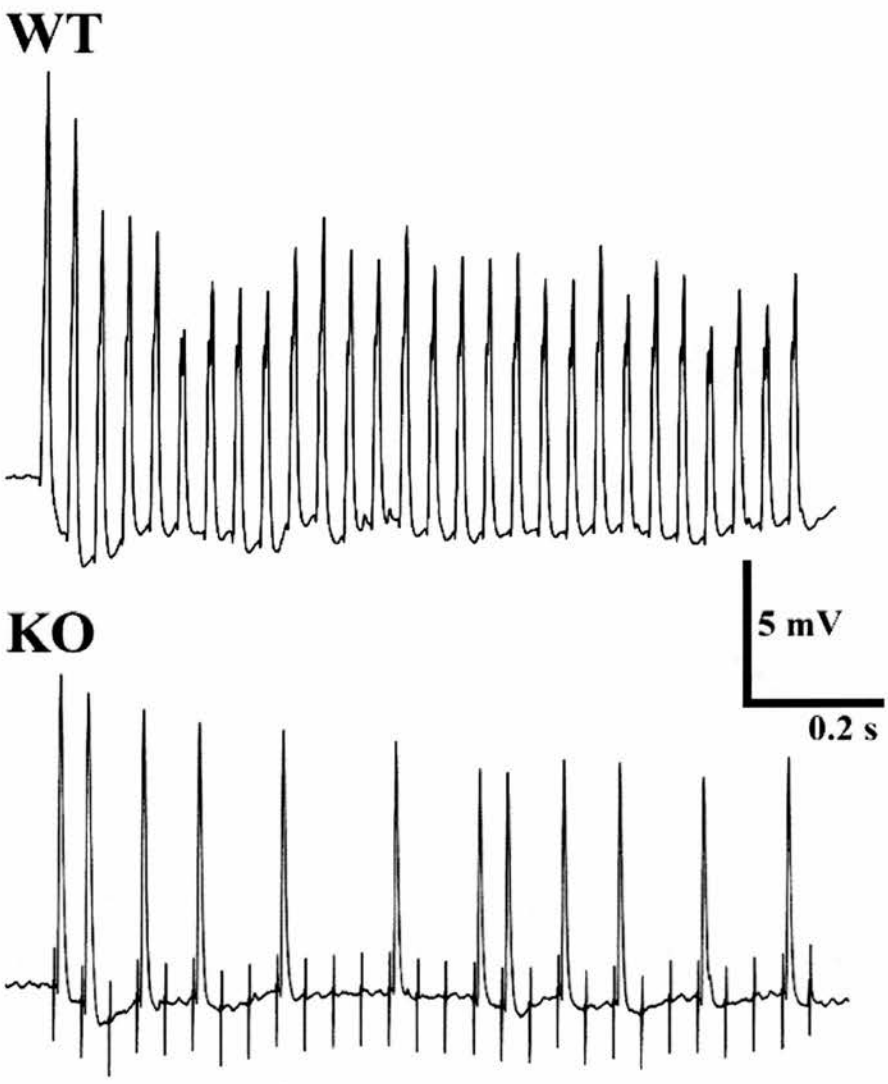

Figure 38. Periaxin null neuromuscular junctions respond intermittently to repetitive stimulation.
Following a 30 Hz stimulation for 1 second, many KO end plates responded only to some stimuli compared with a 100% response in the wild-type animals. This result may be related to a decrease in the safety factor for nerve conduction, perhaps as a result of increased pre-terminal branching and terminal axon demyelination.

2.3.4- Summary

In this chapter I have shown that peripheral nerve demyelination in the periaxin KO mice results in profound morphological changes of neuromuscular junctions and intermittent failure of neuromuscular function. Although the pattern of motor-axon connections in KO neuromuscular junction is formed normally, with age it develops a series of defects associated with pre-terminal demyelination of nerve fibres. These defects include increased pre-terminal branching with proximal nodes at far distances from the endplate, a feature never observed in WT neuromuscular junctions. In addition, abnormal accumulation of neurofilament in pre-terminal regions of KO neuromuscular junctions was detected, resulting in large axonal swellings.

At low stimulation frequencies, neuromuscular transmission of the nerve impulse appears normal in KO muscle preparation but becomes intermittent when the frequency is increased. The intermittent nature of neuromuscular transmission probably results from extensive pre-terminal axon demyelination, branch-point failure and axonal bulb formation. These electrophysiological characteristics also provide the most plausible explanation for the abnormal reflex responses and trembling, the most overt phenotypical features of periaxin null mice.

tremor in periaxin null mice. Future studies could establish directly the relationship between the morphological and physiological features of abnormally functioning neuromuscular junctions in periaxin null mice, by recording from terminals labelled with vital fluorescent dyes, or by cross breeding periaxin null mice with transgenic mice expressing fluorescent proteins in motor neurons and the neuromuscular synapses.

3- DISCUSSION

3.1- SCHWANN CELL-AXON RELATIONSHIP IN THE REGULATION OF NERVE CONDUCTION VELOCITY

The abaxonal Schwann cell cytoplasmic compartment consist of longitudinal bands running along the internode from nuclei to paranodal regions, referred to as Cajal bands (Court et al., 2004). Disruption of Cajal bands in periaxin null mice results in reduced elongation of Schwann cells, underscoring the critical role of Cajal bands in trophic support of Schwann cell distal domains and leading to the first experimental verification of the sensitivity of nerve conduction velocity to internodal length.

In this section I will discuss possible mechanisms responsible for the formation of Cajal bands and their role in Schwann cell elongation. As a coda, I will speculate how the lack of Cajal bands might be responsible for the late onset demyelinating phenotype exhibited by periaxin null mice.

3.1.1- Schwann cell appositions and their consequence: Cajal bands

During the first stages of myelination, Schwann cells enwrap axons with a few loops of cytoplasmic rich extensions. After 2-3 wraps the cytoplasm is extruded from the loops, leading to the compacted myelin sheath. It is known that myelin compaction requires the presence of proteins that maintain its apposing membrane faces together, but the mechanisms responsible for cytoplasms extrusion and cytoskeleton reorganisation have not been elucidated. Morphological analysis during early stages of myelination in WT peripheral nerves have shown that apposition formation takes place after myelin compaction, therefore the organisation of the cytoplasm in terms of exclusion from specific domains (i.e. myelin and appositions) occurs at different stages of Schwann cell growth.

The presence of cytoplasmic compartmentalisation and pseudo-apposition formation in the abaxonal surface of periaxin null Schwann cells indicates that periaxin may has a role in the stabilisation of apposition and not in their formation. Therefore, a periaxin-independent mechanism may be responsible for the convergence of membranes in regions where appositions will be formed.

One interesting possibility is that the initial formation of Cajal bands results from the segregation of cytoplasm by contraction of the cytoskeletal framework; this event

would generate regions devoid of cytoplasm, in which the plasma membrane could approach the myelin sheath, creating pseudo-appositions subsequently stabilised by a periaxin-dependent mechanisms (Fig. 39). Actin cytoskeleton contraction has been described during the formation of microvilli on endothelial cells (Murray, 1993), this event results in an orderly pattern of actin rich regions and cytoskeleton free domains. Reorganisation of the actin cytoskeleton can be achieved by proteins crosslinking actin filaments. Myosin light chain (MLC), an actin-associated protein, has the ability to crosslink actin filaments after its phosphorylation by myosin light chain kinase (Totsukawa et al., 2000). Interestingly, phosphorylation of MLC in peripheral nerves has been detected between P1 and P3 (Melendez-Vasquez et al., 2004), corresponding to the time of cytoplasm segregation in both WT and KO Schwann cells. Therefore it will be interesting to determine if the activation of MLC via phosphorylation takes place in the adaxonal Schwann cell cytoplasm in both WT and KO mice, being responsible for its initial compartmentalisation.

A second stage in the process of apposition formation may be their stabilisation by a periaxin-dependent mechanism, which results in appositions with the characteristic 14 nm separation between apposing membranes. Periaxin might stabilise apposition by acting as a bridge between proteins located in the plasma membrane and in the outermost loop of the myelin sheath. The homodimerisation of periaxin by its PDZ domains in a *trans* configuration might provide a larger "bridge" between apposing membranes, also allowing the association of equivalent periaxin domains to proteins in both membranes.

The association of periaxin with the dystroglycan (DG) complex via DRP2 (Sherman et al., 2001), suggests that the DG complex might represent the link between periaxin and the plasma membrane responsible for appositions formation. Nevertheless, in Schwann cells that lack dystroglycan, appositions are still present, and DRP2 still localises in patches but its expression level is reduced (Saito et al., 2003) indicating that the function of periaxin in the stabilisation of appositions is independent of the presence of dystroglycan in the plasma membrane. Therefore, and according to the bridge hypothesis, another protein in the plasma membrane should be associating with periaxin or DRP2, in addition to a molecule in the opposite side. The

identification of protein partners of periaxin and DRP2 will be crucial to identify the periaxin-dependent mechanisms of appositions stabilisation.

As Schwann cells grow longitudinally and radially, their trophic requirements to distal regions increases. Concomitantly, there is an increase in the amount of cytoplasm reflected by addition of new Cajal bands. This indicates that appositions are continually formed during the growth of the nerve fibre; hence the mechanisms of apposition formation can be studied during an extended period of time. The presence of microtubule bundles running continually from the perinuclear area up to the nodes through Cajal bands is a constant feature of myelinating Schwann cells. It is possible that polymerization of new bundles of microtubules in the perinuclear area is responsible for the addition of Cajal bands during postnatal development of the Schwann cell. In this respect the branched morphology of oligodendrocytes, that bears some resemblance to the Cajal band network in Schwann cells, is dependent on proteins that regulates the equilibrium between polymerization and depolymerization of microtubules (Liu et al., 2003).

3.1.2- Cajal bands and the capacity of Schwann cells to elongate

One of the paradigms used to investigate the trophic role of Cajal bands was the Schwann cell capacity for longitudinal elongation. Previous reports have shown a positive relation between the growth of the nerve and the Schwann cell internodal length, suggesting that after association with the axon, Schwann cells extend at a rate similar to axonal growth (Hiscoe, 1947). Although some works have shown that the rate of growth of axons and Schwann cells are similar, others studies reported a higher growth rate of Schwann cells compared to axons, indicating that some Schwann cells need to be eliminated during nerve lengthening (Hildebrand et al., 1996; Nilsson and Berthold, 1988). In WT quadriceps nerves, the growth of Schwann cells and the nerve have similar rates, therefore no addition or deletion of Schwann cells are required in order to populate the axon during its extension. Periaxin null Schwann cells lacking Cajal bands elongate at a lower rate than WT Schwann cells, this decreased growth capacity is not a consequence of axonal elongation defects as the growth rate of KO nerves is similar to WT nerves. Internodal lengths at P2 were similar between WT and KO Schwann cells, ruling out a defect in the initial

association of KO Schwann cells with the axon. In addition, the decreased internodal lengths of KO Schwann cells in chimeric nerves containing mixed population of WT and KO Schwann cells indicates that the growth capacity of Schwann cell is cell autonomous.

As periaxin null nerve fibres at all ages studied were completely populated by Schwann cells, the mismatch between Schwann cell growth and nerve elongation during the first 3 weeks of postnatal development requires the addition of Schwann cells to the growing axon. Myelin forming Schwann cells associated with the axons were never detected in a proliferating state, therefore the incorporated Schwann cells should derive from a population of cells present in peripheral nerves but outside the myelinated nerve fibre. It is also possible that nonmyelin forming Schwann cells proliferate in order to supply the cells required by the myelinated nerve fibres. Although Schwann cell precursors have not been described in adult peripheral nerves, it has been shown that nonmyelin forming Schwann cells proliferate and have the ability to myelinate axons in the presence of exogenously administered NGF or GDNF (Hoke et al., 2003). As in adult WT nerves no proliferation of Schwann cells takes place (Hoke et al., 2003), proliferation assays in KO nerves using BrdU incorporation together with immunostaining with specific cell type marker antibodies may be a useful protocol to identify the cellular population responsible for supplying Schwann cells to the growing nerve fibres.

In principle, it will be possible to inject into growing KO nerves Schwann cells derived from other strains (e.g. WT Schwann cells expressing a reporter protein) that might be incorporated into the nerve fibres. In addition, the possibility of partially rescuing the demyelinating phenotype of periaxin null mice by injecting WT or genetically modified Schwann cells into the nerves might have important therapeutic applications.

The precise matching between the growth rate of Schwann cells and their associated axons in normal mice raises the question about the mechanisms by which Schwann cells sense and are able to adapt to axonal elongation. Axoglial junctions located in the paranodal regions, might act as an anchor between Schwann cells and the axon, conveying the extent of axonal growth by mechanical stretching of the Schwann cell. However, in myelinated nerves fibres lacking axoglial junctions as a result of genetic

deletion of the protein contactin, internodal lengths are similar to wild-type internodal lengths (Boyle et al., 2001).

Another interesting possibility is that Schwann cells regulate their longitudinal length by mechanisms dependent on the maintenance of contact between adjacent Schwann cells in the same nerve fibre. Therefore, as the axon grows, microvilli from apposing Schwann cells separate and this event results in the activation of Schwann cell elongation. Microvilli in Schwann cells extend to the node and interdigitate with microvilli from the adjacent Schwann cell (Fig. 6C). This characteristic and their expression of several proteins directly involved in the regulation of the actin cytoskeleton make the microvilli the ideal structure for inter-Schwann cell communication. Studies in axon-Schwann cell cocultures have suggested that the local activation of proteins in the microvilli affect the length of Schwann cells (Gatto et al., 2003). It will be interesting to test if the inhibition of microvilli-associated proteins has any consequence to Schwann cell growth. These studies should be performed *in vivo*, as axonal growth cannot be reproduced in *in vitro* conditions.

A direct implication of the reduced internodal distances of KO Schwann cells is that axonal proteins destined to the nodes and paranodes should be upregulated by two-fold the normal values as reflected by immunofluorescence and immunoblot analyses. Therefore a mechanism should exist that regulates the neuronal synthesis of nodal and paranodal specific proteins in relation to the number of Schwann cells populating its axonal projection.

3.1.3- How Cajal bands aid Schwann cell longitudinal extension

Periaxin null Schwann cells lacking Cajal bands have a reduced capacity to grow longitudinally. Thus, an important question is how a continuous cytoplasmic arrangement can affect the Schwann cell's internodal elongation. A critical observation is that the microtubule network in KO Schwann cells is disrupted as it approaches the paranodal regions contrasting with the WT situation, in which the microtubule network organises in Cajal bands and extends from the perinuclear area up to the paranodes. Microtubules and their associated molecular motors are known to be responsible for the transport of organelles, proteins and mRNAs to their target locations in many cell types (Carson et al., 1998; Pokrywka and Stephenson, 1995;

Rogers and Gelfand, 2000). Therefore their disruption should affect the cell growth capacity especially in Schwann cells undergoing longitudinal extension and production of large membrane surfaces.

Paranodal localisation of MBP mRNA is not detected in 3-week old periaxin null Schwann cells, in which MBP mRNA concentrates in the perinuclear area. This configuration can be mimicked by depolymerisation of microtubules in WT Schwann cells using colchicine, indicating that a microtubule-dependent mechanism is responsible for the proper localisation of MBP mRNA. Carson and colleagues have studied the dynamics of mRNA granules in detail, consisting of all the translational machinery necessary for local protein synthesis, in distal domains of oligondrocytes (Ainger et al., 1993). Using fluorescent-conjugated MBP mRNA in order to track RNA granules movement, they have build up a model in which RNA granules move along microtubules by means of the molecular motors kinesin and dynein (Barbarese et al., 1999; Carson et al., 1997). Due to the morphological resemblance between oligodendrocyte processes that myelinate several axonal segments and Schwann cells Cajal bands, it is very likely that these two cell types share mechanisms responsible for the transport of mRNA, proteins, organelles and membranous vesicles to their sites of incorporation. Therefore, it will be important to determine how microtubule disruption affects the dynamic movement of mRNAs and other cargoes along the KO Schwann cell cytoplasms and the expression of motor-proteins under these conditions.

In addition, disruption of microtubules may also lead to a defective transport of signals related to growth regulation originated in the paranodal regions of Schwann cells. Evidence for this possibility is provided by recent studies related to kinesin-dependent transport along microtubules of preassembled signalling modules (Schnapp, 2003).

Although the microtubule network is disrupted in KO Schwann cells, nodal and paranodal compartments are correctly formed and the levels of proteins specific for these domains are similar to WT nerves, suggesting that defects in microtubules do not affect the targeting of proteins to their final destinations, and is probably related to the rate of transported molecules.

Disrupted microtubule network leading to abnormal transport of proteins and mRNA to the Schwann cell distal domains provides a satisfactory explanation for the reduced elongation capacity of KO Schwann cells. Nevertheless, the relation between lack of Cajal bands and microtubule disruption is not evident. It is possible that the increased cytoplasmic volume per unit length in KO Schwann cells lacking apposition to a double of WT values might be involved in the misregulation of the dynamics between microtubule polymerization and depolymerization. Microtubule polymerization as a bimolecular reaction, is dependent on the free tubulin concentration, whereas microtubule depolymerization is independent on tubulin concentration. Therefore, an increase in the cytoplasmic volume without a correspondent increase in free tubulin concentration can lead to a decrease in the polymerization rate. In addition, a decrease in the effective concentration of microtubule stabilizing factors (Sanchez et al., 2000), might have a role in distal disruption of the microtubule network. In this respect, it will be important to determine if KO Schwann cells with increased cytoplasmic volume do not compensate for the decreased concentration of proteins involved in microtubule formation and stabilisation by increasing their expression levels.

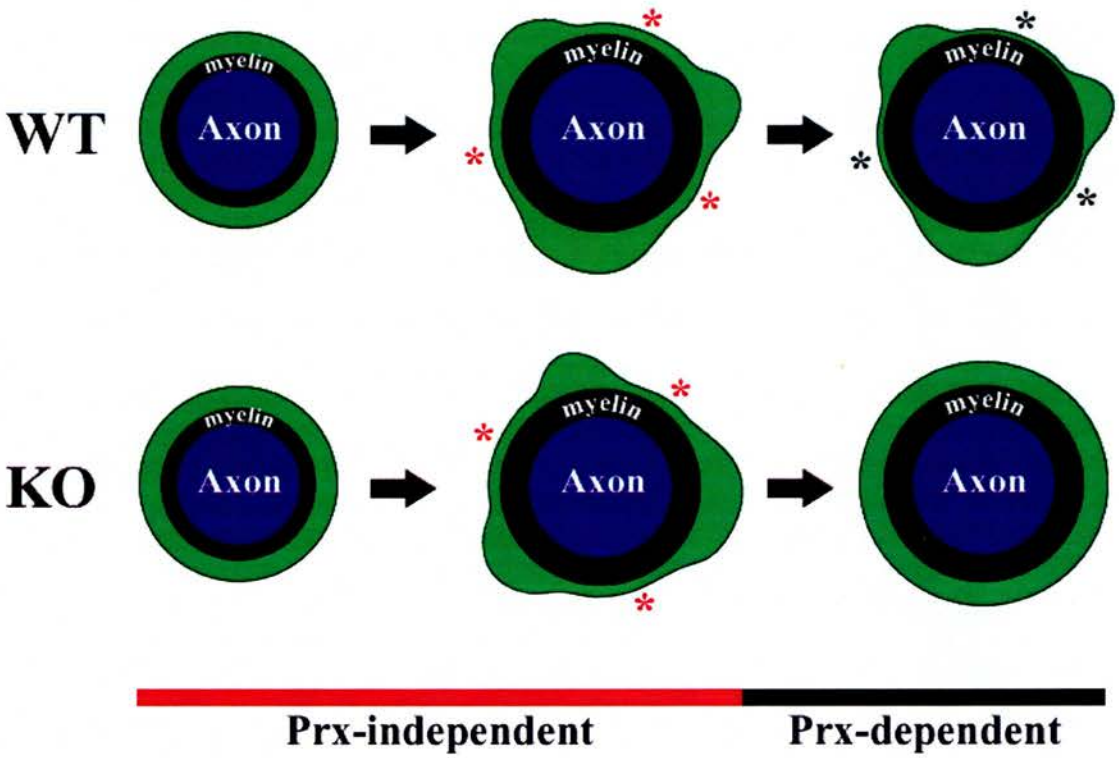

Figure 39. Formation of Cajal bands in Schwann cells
(A) Diagram representing a transversal view of a myelinated nerve fiber depicting the stages during apposition formation. In WT and KO nerve fibers, a periaxin-independent mechanism is responsible for the redistribution of cytoplasm and formation of pseudo-appositions (red asterisks). In WT Schwann cells, appositions are stabilised by a periaxin-dependent mechanisms resulting in the formation of appositions (black asterisk). In Schwann cells lacking periaxin, pseudo-appositions are not stabilised and the cytoplasm redistribute as a continuous domain (Prx, periaxin).

3.1.4- Internodal length as a critical parameter in the function of the myelinated nerve fibre

The principal parameters determining the velocity of "saltatory" conduction of the action potential in the myelinated nerve fibres has been defined and tested experimentally except for the influence of internodal length that has been proposed only on theoretical grounds. During the first experimental studies demonstrating the discontinuous nature of the action potential regeneration in myelinated nerve fibres, it was shown that the time for electrotonic spread of the action potential in the internode is negligible compared to the time required for regeneration of the action potential at the node (Huxley and Stampfli, 1949). Therefore, a decrease in the node spacing should decrease the velocity of the action potential. Mathematical models of the myelinated nerve fibre subsequently showed that nerve conduction velocity was sensitive to internodal length at smaller ranges but become less sensitive at longer internodal distances (Brill et al., 1977; Moore et al., 1978). This theoretical treatment eluded experimental verification due to the fact that both myelin sheath thickness and axonal diameter covary with internodal lengths. One exception is the study of nerve conduction velocity in regenerated nerves fibres. After regeneration, axon diameters and myelin sheath thickness recover their original sizes but internodal lengths are reduced and nerve conduction velocity is normal (Sanders and Whitteridge, 1945). Nevertheless, the comparison between normal and regenerated nerve fibres is not informative as their internodal lengths lie in the range in which mathematical models have shown not to affect nerve conduction velocity. Therefore, the decreased nerve conduction velocity in periaxin null nerve fibres with smaller internodal lengths constitutes the first experimental verification of the role of internodal lengths in nerve conduction regulation. The validity of this result relies in the constancy of all other parameter known to affect nerve conduction velocity. In KO quadriceps nerves, axonal diameter distribution, myelin thickness and the ultrastructure of the node-paranode regions were found to be normal. In addition, the localisation and levels of several proteins required for the regeneration of the action potential at the nodes and paranodes were similar to WT nerves fibres.

In order to control for any possible defect in periaxin null nerve fibres not detected by the analyses performed that could be responsible for the decreased nerve

conduction velocity, I used a model of the nerve fibre that can be adjusted for several morphological parameters of the myelinated nerve fibre (McIntyre et al., 2002). This model, adjusted with mean parameters of 3-week old nerve fibres from murine quadriceps nerves, showed results consistent with the experimental outcomes. Finally, the intermediate nerve conduction velocity of chimeric nerves containing mixed populations of WT and KO Schwann cells support the proposed relation between the internodal length and the conduction velocity of the action potential.

The significant decrease in nerve conduction velocity of KO nerves is probably responsible for defects in motor coordination of 3-week old KO mice as neuromuscular junctions at this age do not shown any morphological or electrophysiological abnormalities.

3.1.5- Cajal bands, internodal length and demyelination

A critical question is how the early defect in internodal elongation and microtubule disruption in Schwann cells lacking Cajal bands are responsible for the demyelinating phenotype.

Even with a disrupted microtubule network at the paranodal region, KO Schwann cells continue to grow longitudinally up to 6 weeks of age, almost doubling the internodal lengths exhibited at 3 weeks. It is possible that at some stage, the distance from the nuclei to the paranodal regions of KO Schwann cells exceed its capabilities for trophic support of distal regions due to disrupted microtubules, disruption that probably worsens as the internodal distance increases. According to this proposition, the first regions affected in periaxin null Schwann cells should be the paranodal domains and this is exactly what is found in 6-week old periaxin null nerve fibres (Fig. 40). The myelin disruption in these regions consists of abnormally thick myelin sheaths and whorls of myelin in the paranodal cytoplasm, whereas in more central regions of the internode the myelin sheath appears relatively normal. Therefore, the reported hypermyelination of axons in periaxin null nerve fibres (Gillespie et al., 2000) is only a local feature of distal region of the Schwann cell, and is probably indicative of defective distribution of myelin components along the internode as a consequence of a disrupted microtubule network. Abnormal organisation of the myelin structure rather than changes in the expression of myelin constituents are

consistent with the normal expression of the myelin protein P0 found in KO nerves at all ages examined (Fig. 18C-D). The normal myelin sheath and structure of the nodal-paranodal regions found in 3-week old KO mice suggests that for shorter internodal lengths, Schwann cells lacking Cajal bands are capable of maintaining their structural integrity. Therefore, it will be interesting to assess if regenerated KO nerve fibres, which possess Schwann cells with shorter internodal lengths, display a less severe demyelinating phenotype than KO nerves fibres with longer internodal lengths.

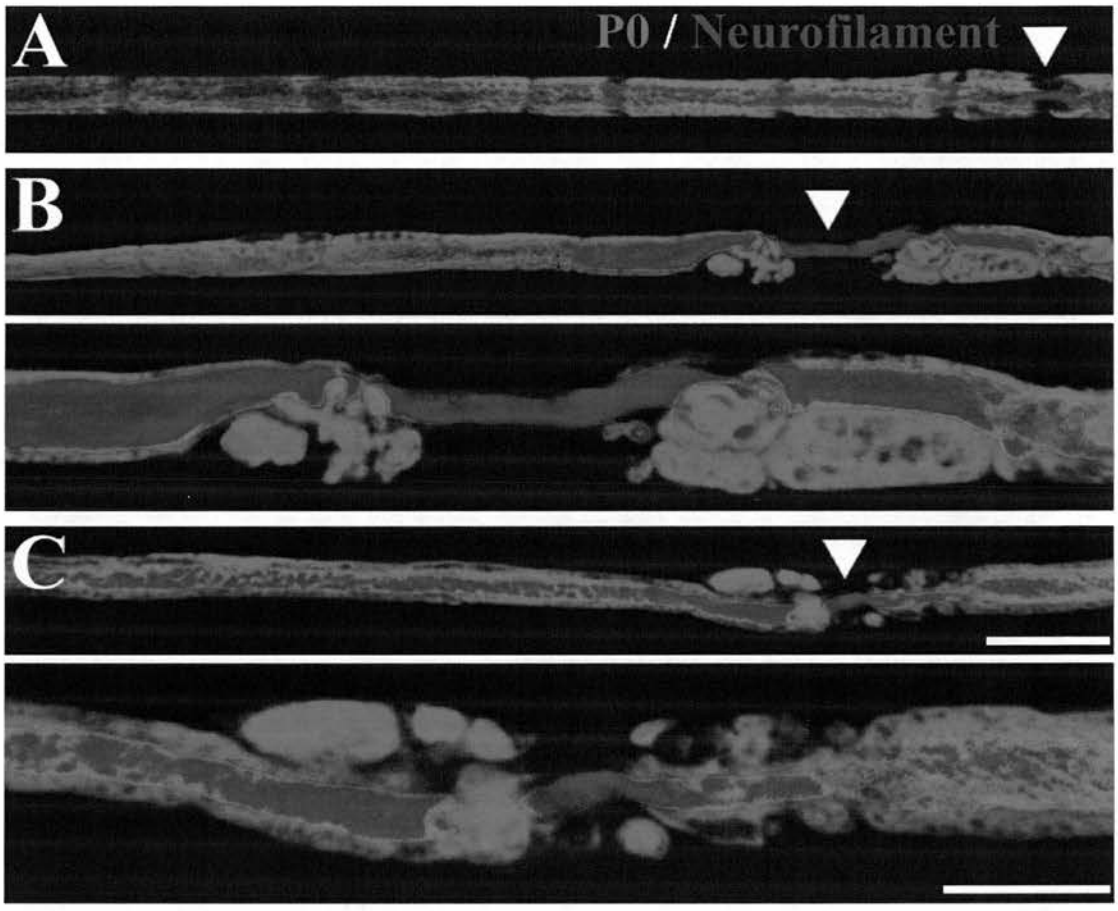

Figure 40. Abnormal organisation of the myelin sheath in paranodal regions of periaxin null mice.

Teased nerve fibers from 6-week old wild-type (WT) and periaxin null (KO) mice stained with antibodies against the myelin protein P0 (red) and neurofilament (blue). **(A)** WT nerve fiber with a myelin sheath of regular thickness up to the nodal region. In KO nerve fibers, Myelin disruption is present in paranodal regions while the internodal organisation of the myelin sheath appears relatively normal, **(B)** and **(C)**. Lower panels of **B** and **C** shown a higher magnification of the nodal-paranodal regions of the corresponding upper panels. Arrowheads indicate the nodes of Ranvier. Scale bar, 20 μm in **A** and upper panels of **B** and **C**; 10 μm lower panels of **B** and **C**.

3.2- CELL ORGANISATION AT THE NEUROMUSCULAR JUNCTION

The use of a novel antibody has led to the identification of a neuromuscular associated cell, referred to as junctional fibroblast. A critical role for junctional fibroblasts is suggested by their relation with other neuromuscular-associated cell components and their orchestrated response following muscle denervation. In the present section, I will discuss the evidence that leads to the conclusion that junctional fibroblasts represent a new neuromuscular-associated cell type, the possible mechanisms responsible for their neuromuscular localisation and the evidences suggesting their role in guiding terminal Schwann cell sprouting.

3.2.1- Tardy characterisation of 2166-positive cells restricted to the neuromuscular synapse

The fact that a cell type restricted to the neuromuscular junction has not been fully characterised calls for an explanation. Although the morphology of the neuromuscular junction has been extensively studied using both, optical and electron microscopy, the presence of junctional fibroblasts localised at the neuromuscular junction has remained unnoticed, perhaps partly due to the fact that these cells extend fine processes which could be wrongly attributed to terminal Schwann cell projections and partly because these cells lie outside the synaptic basal lamina. For example, Fischbach and colleagues (Trinidad et al., 2000) mis-interpreted their neuregulin (GGF II isoform) staining pattern at endplates as due to Schwann cells, whereas the cells they shown immunopositive for the neuregulin-1 antibody (HM-24 antibody) appear more likely to be the junctional fibroblast descibed here rather than terminal Schwann cells. In fact, I confirmed this by using the HM-24 antibody in TS muscle preparations, antibody that clearly stains 2166-positive cells at the neuromuscular junction. Nevertheless, these data were not included in the present thesis because the HM-24 antibody is not specific for neuregulin (Dr. S. Arber, personal comunication).

Cells located near the neuromuscular junction have been reported previously and termed "perijunctional fibroblasts" due to their localisation near the synapse and the

expression of Thy-1 protein, a marker for a subpopulation of fibroblasts (Gatchalian et al., 1989). An antibody against the Thy-1 protein was used in whole muscle preparations in order to confirm these results. However, Thy-1 immunosignal was not detected in any cell near the neuromuscular junction, although axons, known to express Thy-1, were stained (Reynolds and Woolf, 1992). This result suggests that the resolution used in the study by Gatchalian and colleagues was not sufficient to distinguish the Thy-1 immunosignal originating from axons or from other source.

It is also known that cells located in intersticial spaces of muscles fibres, proliferate and express several extracellular matrix proteins after muscle denervation, including tenascin-C (Sanes et al., 1986; Weis et al., 1991), but the exact localisation of these cells before and after nerve injury has not been studied in detail. One characteristic of all the previously described studies is the use of muscle tissue slices for immunohistochemical staining, which results in lost of valuable information concerning the cellular relationship at the neuromuscular junction..

The novel 2166 antibody as a specific marker for neuromuscular-associated cells used in whole mount muscle preparations, a technique that preserves the full cellular repertoire and architecture of muscle tissue, were crucial in the present characterisation of junctional fibroblasts and the study of their response following neuromuscular junction-destabilising stimuli.

3.2.2- The 2166 antigen

The identity of the protein recognised by the 2166 antibody was study by performing mass spectrometry on the 2166-positive band from electrophoresis-resolved cytoskeletal fractions of mouse cerebellum. The results from this approach indicated that this band represents the protein tubulin. Nevertheless, this result has to be taken with caution as the fractionation protocol used to obtain soluble and cytoskeletal samples is not sufficient to obtain bands that represent single proteins. Therefore it is very likely that more than one protein locates in the same region of the gel. As in protein mixtures mass spectrometry tends to resolve the most abundant protein, it might be that the identified tubulin was not the 2166 antigen but the most abundant protein in that region of the gel, masking the real protein recognised by the 2166 antibody. For mass spectrometry approaches it will be desirable to

immunoprecipitate the unknown protein with the 2166 antibody as a way to obtain single proteins bands. This was not possible as immunoprecipitation of proteins was never achieved with the 2166 antibody. A more stringent fractionation of the cytoskeletal fraction will be necessary to resolve single proteins bands using mass spectrometry or alternatively the use of two-dimesional gels.

Based on immunofluorescence, it is evident that the 2166-protein represents a cytoskeletal component of the cell. In addition, the colocalisation of the 2166 and tubulin antibody immunosignal suggests that the 2166 antibody might be recognising the protein tubulin. The 2166 antibody could be recognising a postranslational modification of tubulin restricted to cells in the muscle tissue, as the 2166 antibody did not gave a band when tested in purified tubulin from bovine brain, a tissue which probably contains the most common postranslational tubulin modifications.

3.2.3- Lineage characterisation of neuromuscular associated 2166$^+$ cells

The possibility that 2166-positive cells represent a cell type known to be present in muscle was investigated using a battery of cell type-specific antibodies.

Neuromuscular-associated 2166 cells were positive for prolyl-4-hydroxylase (rPH) and CD34. The rPH enzyme is involved in the synthesis of collagen (Pihlajaniemi et al., 1991), therefore 2166 positive cells may represent fibroblasts, as collagen synthesis is one characteristics of this cell type. Other cell types including endothelial cells and myelin forming Schwann cells, also express collagen (Singh et al., 1997), therefore the fibroblast lineage of 2166 cells cannot be definitively asserted. In this respect, fibroblasts represent a heterogeneous cell population often included in this category by their capacity to synthesise extracellular matrix components (Koumas et al., 2002; Phipps et al., 1997).

The expression of CD34 by 2166-positive cells constitutes an interesting characteristic of these cells that deserves further study. The CD34 antigen has been characterised as a hematopoietic stem cell marker (Krause et al., 1994). In muscle, CD34-positive cells locate in interstitial spaces outside the basal lamina as is the case for 2166-positive cells. Cloned cells derived from the CD34-positive population could differentiate into different lineages (Lee et al., 2000). Therefore, it will be interesting to determine if 2166-positive cells located at the neuromuscular junction

behave as stem cells under conditions of synaptic plasticity or muscle damage. Isolation and culture of 2166-positive cells associated with the neuromuscular junction will be necessary to asses the differentiation capabilities of these cells. During preliminary studies, I found that 2166-positive cells at the neuromuscular junction are more resistant to trypsin dissociation than extrasynaptic cells, this feature might be fundamental to the isolation and culture of junctional fibroblasts.

Finally, the surface expression of the CD34 antigen by junctional fibroblasts provides a way to eliminate these cells by using complement-mediated cell lysis, an approach that will provide information about the requirement of these cells for the normal function of the neuromuscular junction. This approach has been applied for ablation of terminal Schwann cell at the neuromuscular junction, providing information about the short and long term function of terminal Schwann cells (Reddy et al., 2003).

3.2.4- Restriction of 2166 cells to the neuromuscular junction

2166 positive cells become restricted to the neuromuscular junction during postnatal development. The restriction of these cells to neuromuscular synapses is possibly mediated by signals restricted to this area. Cellular components, as motor axons and terminal Schwann cells exclusively present in the neuromuscular area could signal by soluble factors to cells located in the muscle inducing their neuromuscular localisation. In addition, the molecular composition of the basal lamina at the neuromuscular junction differs from the composition in extrasynaptic areas (Patton et al., 1997; Sanes et al., 1990) and could be responsible for the differential association of 2166-positives cells to neuromuscular synapses. The requirement of the basal lamina for the control of synaptic structure has been revealed in several mutant mice that lack specific components of the synaptic basal lamina (Noakes et al., 1995; VanSaun et al., 2003). In addition, it has been shown that motor neurons and Schwann cells are able to distinguish between synaptic and extrasynaptic isoforms of laminin (Cho et al., 1998). Therefore, it will be interesting to screen for the presence of junctional fibroblasts in these mutant mice lacking basal lamina components in order to define if the unique composition of basal lamina at the synapse is responsible for the restriction of 2166-cells to these areas. It is also possible that

junctional fibroblasts concentrate on neuromuscular junctions in response to endogenous electric fields generated at the synapse (Betz et al., 1980).

3.2.5- Junctional fibroblasts as a substrate for cellular pathfinding in the neuromuscular arena

The striking association between junctional fibroblasts and the neuromuscular synapse, in particular with terminal Schwann cells, raises the question of how this cell population might respond to stimuli that produce activation of known cellular component at the neuromuscular junction.

The early response of junctional fibroblast to denervation, characterised by process extension, is followed by terminal Schwann cell activation and sprouting often associated with junctional fibroblasts. As fibroblasts located near neuromuscular junctions express several adhesive molecules after denervation of skeletal muscles (Sanes et al., 1986), it is possible that activated junctional fibroblasts are involved in connective tissue remodelling that in turn serves as a positive substrate for terminal Schwann cell growth. The expression of tenascin-C by junctional fibroblasts and its deposition in the muscle surface after denervation might be necessary for terminal Schwann extension from the neuromuscular junction. Tenascin-C has been shown to promote neurite outgrowth (Meiners et al., 1999) and antibodies against this protein delay endplate reinnervation (Langenfeld-Oster et al., 1994). In addition, abnormal reinnervation of neuromuscular junction in tenascin-C null mice has been reported (Cifuentes-Diaz et al., 2002). Therefore, a detailed analysis of Schwann cell and junctional fibroblasts reaction in denervated muscles from tenascin-C null mice will be necessary to unravel the role of this protein in the cellular responses triggered by muscle denervation.

At the moment, terminal Schwann cells have been considered as the main director of motor axons regrowth following denervation. The studies of Son *et al.* (Son and Thompson, 1995) have clearly shown that terminal Schwann cells extend processes following denervation, which eventually reach innervated endplates to guide axons back to the empty synapse. The results presented here strongly suggest that junctional fibroblasts might be an important cellular component of the neuromuscular junction, involved in the plastic responses elicited by different

destabilising stimuli as denervation and muscle paralysis (Fig. 41A). Although the requirement of 2166 cells for plastic responses is not yet resolved, the characterisation of junctional fibroblast represents a first step in the study of their role in synaptic maintenance and plasticity.

Therefore, junctional fibroblasts represent an integral cellular component of neuromuscular synapses and thus four cells, and not three, should be represented in diagrams of neuromuscular junction organisation (Fig. 41B)

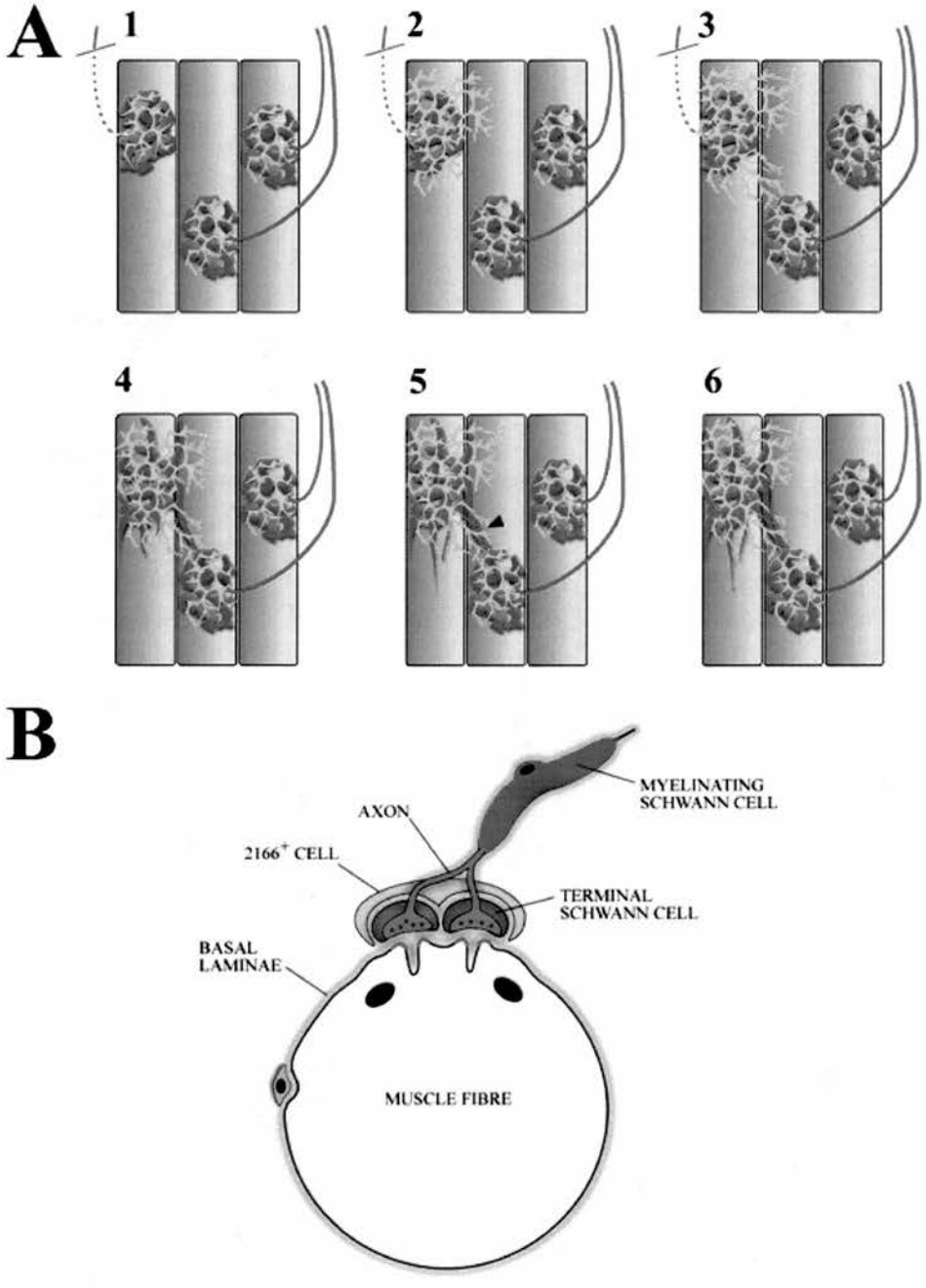

Figure 41. Proposed model for the response of neuromuscular-associated cells to partial denervation.

(A) Proposed model for the response of neuromuscular-associated cells to partial denervation (numbers indicate the order of events). Junctional fibroblast (yellow) react first to denervation, forming a cellular substrate for the Schwann cell reaction (green). **(B)** Diagram representing a transverse view of a muscle fiber and associated cells in the neuromuscular junction including junctional fibroblasts (yellow).

3.3- CONSEQUENCES OF DEMYELINATION TO THE STRUCTURE AND FUNCTION OF THE NEUROMUSCULAR JUNCTION

The study of neuromuscular junctions in periaxin null mice revealed abnormalities associated with preterminal regions of motor axons, including increased preterminal branches and axonal swellings. In addition, neuromuscular junctions respond intermittently to repetitive stimulation. In this section, the relation between demyelination and axonal defects will be discussed, together with the possible explanation of the defects in conduction of the action potential, based in the morphological abonormalities observed in periaxin null neuromuscular junctions.

3.3.1- Demyelination leads to motor axon abnormalities at the neuromuscular junction

Neuromuscular junctions in 3-week old periaxin KO mice are innervated normally as revealed by immunofluorescence and quantification of the innervation pattern. This is consistent with the lack of periaxin expression by neuromuscular junction cells and the fact that nerves fibres from 3-week old periaxin null mice are normally myelinated and only display a reduction in Schwann cell internodal lengths. In addition, the normal organisation of 3-week old periaxin null neuromuscular junctions indicate that the reduction of nerve conduction velocity as a results of decreased internodal lengths have no detectable effects on the structure of the synapse.

In older KO mice, demyelination of nerves fibres proximal to the neuromuscular junction is observed and axonal sprouts originated from demyelinated regions result in an increase of branches invading the endplate. Axonal processes are also detected in demyelinated regions of proximal nerve fibres (Fig. 11C). The increase in branching from preterminal regions suggests that axons are endowed with an active sprouting capacity that is repressed by myelin forming Schwann cells (Court and Alvarez, 2000); this inhibitory capacity of Schwann cells is not only provided by the myelin sheath as WT axons do not extend processes in nodal regions, domains that are covered by Schwann cell microvilli but are not myelinated. In agreement with

this proposition, wild-type axons approaching the neuromuscular junction branches after the last myelinated segment.

Other abnormalities detected in preterminal axons of periaxin null mice are neurofilament-rich axonal swellings; these structures were associated with segments of the axon still myelinated. Axonal swellings have been described in multiple sclerosis lesions (Trapp et al., 1998), a chronic inflammatory demyelinating disease of the CNS and in axons of mice lacking the protolipid protein (PLP) a component of the myelin formed by oligodendrocytes in the CNS (Griffiths et al., 1998). Axonal swellings in PLP null mice are characterised by the accumulation of dense bodies, organelles and membranous vesicles, suggesting that defects in axonal transport may underlie the swelling formation (Griffiths et al., 1998). Therefore, in periaxin null mice, abnormal axonal transport in the interface between myelinated and demyelinated regions might be responsible for the accumulation of neurofilaments and other transported cargoes. In addition, it is well known that myelin regulates axonal caliber by inducing neurofilament phosphorylation (de Waegh et al., 1992). Therefore, swellings in KO axons might represent an abnormal regulation of neurofilament phosphorylation in residually–myelinated regions. The study of preterminal axon ultrastructure and analysis of neurofilament phosphorylation state will be necessary to resolve the contribution of axonal transport defects and neurofilament phosphorylation in the formation of axonal swelling in their preterminal regions.

The axonal abnormalities reported in KO axons adds to the increasing evidence that myelin, in addition to its role in conduction of the action potential, is required for the integrity of the axon in the nerve fibre and neuromuscular junction. Therefore, the consequences of demyelination in the structure of the axon at the neuromuscular junction should be considered in the study and treatment of demyelinating conditions.

Removal of synaptic connection due to progressive abnormalities in terminal regions of the axon might results in loss of target-derived trophic support and degeneration of the complete axon. Although degenerating axons are not present in 9-month old periaxin null nerves (Dr. Diane L. Sherman, personal communication), remains to be determined if progression of morphological abnormalities in KO preterminal axons

eventually leads to lost of synaptic connection and axonal degeneration in older animals.

3.3.2- Electrophysiological abnormalities of periaxin null neuromuscular junctions

At low stimulation frequency, the transmission of the action potential in periaxin null neuromuscular junctions is similar to WT in terms of end-plate potential amplitude and time course. Only a decrease in conduction velocity is detected in KO neuromuscular preparations probably reflecting the extent of demyelination in the nerve fibre.

At higher stimulation frequencies, KO end-plates respond intermittently, with the propagated potentials exhibiting normal amplitudes. This frequency-related conduction defect is indicative of conduction block in some region of the preterminal nerve fibre. The block of action potential conduction at high frequency stimulation can occur in demyelinated segments of periaxin null nerve fibres or in preterminal regions of the axon, characterised by swellings and abnormal branching.

Axonal branch points represent regions with a relatively low safety factor for conduction of the action potential that can result in propagation failures at high frequency stimulation (Zhou and Chiu, 2001). The reduced internodal lengths described in myelinated nerve fibres approaching their terminal arborization (Quick et al., 1979) probably reflects a physiological mechanisms to increase the safety factor in these regions.

In order to distinguish between transmission block due to demyelination of the nerve fibre or increased branching of preterminal axons in the periaxin null mice, electrophysiological recording from identified neuromuscular junction should be performed. By using an extracellular recording electrode, it can be assessed if during high frequency stimulation action potentials are blocked in branch points or if the failures of propagation take places in the nerve fibre before branching of the axon.

Finally, the intermittent transmission of the action potential in the periaxin null mice provide a plausible explanation for their abnormal reflex responses, tremor and muscle weakness phenotype.

3.4-CONCLUSION

In this thesis I have study differents aspects of the cellular architecture in peripheral nerves and neuromuscular junctions in normal and mutant mice. My focus has been non-neuronal cells and their function, including myelinating and terminal Schwann cells and a novel form of fibroblasts with a selectively neuromuscular distribution.

In peripheral nerves, I have shown that periaxin is directly involved in the formation of the cytoplasmic compartment in Schwann cells, a domain that is crucial for the Schwann cell elongation capacity and establishment of extensive myelinated segments around the axon, the internode, which in turn regulates the conduction velocity of the action potential. This result represents the first experimental verification on the sensitivity of nerve conduction velocity to internodal lengths underscoring the influence of Schwann cell in the regulation of the myelinated nerve fibre function. At the neuromuscular junction, I have identified a novel cell type highly restricted to the peripheral synapse. From its protein expression, close contact with other neuromuscular junction cell-components, association with the developing neuromuscular synapses and reaction to neuromuscular system destabilizing stimuli, this cell type appears to be a crucial component of the neuromuscular synapse.

Finally, I have shown that primary abnormalities in Schwann cell organisation have important secondary consequences on motor nerve terminal structure and neuromuscular transmission. Taken together, these findings underscore the crucial role for "supporting" cells in peripheral nerve function. Future studies will demarcate the permissive and instructive roles of these different cell types in securing faithful nerve conduction, synaptic transmission, and the maintenance of spatial integrity required for sensory neurons, motoneurons and muscle fibre to perform their function.

4- METHODS

4.1- Animals

The following mice lines were used in the present work, C57Bl/6, peraxin null (Gillespie et al., 2000), CMTX (Anzini et al., 1997), R6/2 (Dr. A. J. Morton, Cambridge). In addition, Spraw-Dawley rats were used.

Chimeric mice (generated by Dr. Diane L. Sherman) were generated by injecting the ES cell line E14Tg2aSc4TP6.3 expressing GFP-tagged tau protein (Pratt et al., 2000) into C57Bl/6 or peraxin null blastocysts.

All animals procedures reported in this thesis were performed according to Home Office regulations under the necessary project and personal licences.

4.2- Electron Microscopy

Quadriceps and sciatic nerves were immersed *in situ* in 4% paraformaldehyde, 2.5% glutaraldehyde in 0.1 M sodium cacoldylate buffer (pH 7.3) for 15 minutes, removed and postfixed in the same solution for 2 hours. After extensive washes in sodium cacoldylate buffer (pH 7.3), the nerves were postfixed in OsO_4 for 1 hour, washed with cacodylate buffer and dehydrated with ethanol and propylene oxide. Nerves were subsequently embedded in araldite in longitudinal and transverse orientation. Ultrathin sections were stained with uranyl acetate and lead citrate and examined on a Phillips BioTwin electron microscope.

4.3- Light Microscopy

4.3.1- Teased nerve fibres immunohistochemistry

Quadriceps and sciatic nerves were dissected and immersion fixed in 4% paraformaldehyde in 0.1M phosphate buffer saline (PBS, pH 7.4) for 45 minutes. After washing in PBS, the perineurium was dissected and nerve fibre bundles were separated using a pair of acupunture needles, followed by either one of the two alternative protocols for immunohistochemistry described below.

(A) Dry fibres method. Nerve fibres were teased individually on a PBS drop in 3-aminopropyltriethoxysilane (TESPA; Sigma) coated slides. After teasing, the slide was dried at room temperature and stored at –70 celsius degrees (^{o}C) until use. Slides

stored at –70 °C were immersed into pre-chilled (-20 °C) acetone for 20 minutes. The acetone was air dryied and teased fibres were blocked/permeabilised with 0.1% Triton, 5% fish skin gelatine (Sigma) in PBS for 1 hour at room temperature. First antibodies were applied in the same blocking/permeabilising solution overnight at room temperature in a humid chamber. Subsequently, fibres were washed in PBS, 0.1% Triton. Secondary antibodies were applied in blocking/permeabilizing solution for 1.5 hours at room temperature. After washing in PBS, teased fibres were mounted in Vectashield (Vector Labs, Burlingame, California).

(B) Floating fibres method. Nerve fibre bundles were blocked/permeabilised with 0.1% Triton, 5% fish skin gelatine (Sigma) in PBS for 1 hour at room temperature. First antibodies were applied in the same blocking/permeabilising solution overnight at 4°C. Subsequently, fibre bundles were washed in PBS, 0.1% Triton. Secondary antibodies were applied in blocking/permeabilizing solution for 1.5 hours at room temperature. After washing in PBS, individual fibres were teased on a PBS drop in TESPA coated slides and mounted in Vectashield.

For phalloiding/DAPI staining, the floating method was used. Phalloidin was applied overnight at 4°C. Subsequently, fibre bundles were washed in PBS and mounted in Vectashield containing DAPI (Sigma).

4.3.2- Muscle tissue immunohistochemistry

For whole muscle preparations, muscles were dissected in 0.1 M phosphate buffer solution (PBS, pH 7.4) and fixed in 4% paraformaldehyde for 20 minutes, following by incubation in fluorescent-conjugated bungarotoxin (30 min). After washing in PBS and blocked/permeabilised for one hour in 1% BSA, 0.4% Lysine, 0.5% Triton X-100 in PBS, primary antibodies were applied overnight at 4 °C. Muscles were washed and secondary antibodies were incubated for 3.5 hours at room temperature following by extensive washes for 1 hour and mounted in Vectashield.

For muscle sections immunohistochemistry, dissected muscles were embedded in OCT (Tissue TEK) and frozen in isopentane precooled with liquid nitrogen. Cryostat sections were collected, fixed with 4% paraformaldehyde for 5 minutes and blocked/permeabilised for 1 hour with 5% fish gelatine and 0.1% Triton X-100 in PBS. Primary antibodies were applied overnight at room temperature. Sections were

washed and secondary antibodies were incubated for 1 hour at room temperature following by three 10 minutes washes in PBS and finally mounted in Vectashield.

4.3.3- Image acquisition

Immunofluorescence stainings of teased fibres and whole mount muscles were imaged using a BioRad Radiance 2000 (Nikon Eclipse E600-FN microscope) confocal system. FITC, TRITC and Alexa Fluor-647 fluorophores were excited with an Argon (488 nm), HeNe (543 nm) and Red Diode (637 nm) laser, respectively. Emission wavelengths were captured with the following filter sets: HQ515/30, HQ590/70, HQ660LP. In addition a Leica TCS SL system was used occassionally.
For projections in the Z axis of the volume obtained by confocal microscopy the post processing sofware Laservox (BioRad) was used. In addition, a Olympus BX60 microscope equiped with a Hamatsu ORCA-ER digital camera and OpenLab 3.1.7 software was used for fluorescent and bright field imaging of ISH preperations and internodal length measurements on teased fibres stained with phalloidin and DAPI. Deconvolution and rendering were performed using the software Volocity 2.6.1 (OpenLab).

4.4- Morphometry

Nerves were prepared for electron microscopy as described. For measurement of g-ratios, number of appositions per nerve fibre and cytoplasms volume, micrographs of randomly selected fields of ultrathin transverse sections of quadriceps nerves from 3 and 6 week-old WT and KO mice (n=3 for each group, 120 fibres per group) were scanned and axon area, fibre area, number of appositions and cytoplasms area in the abaxonal domain were measured using NIH image software, calibration of the images was performed by using micrographs from calibrated grids at the same magnification used for the tissue. The axonal and fibre diameters were estimated (diameter=$2\sqrt{(area/\pi)}$) and the g-ratio was calculated (axon diameter/fibre diameter).
For internodal length measurements, nerve fibres from quadriceps nerves of WT, KO and CMTX mice were stained with TRITC-phalloidin and DAPI and teased as described above. The lengths of quadriceps nerves were measured from spinal cord exit to muscle insertion point. For each animal (n=3), 100 internodes and the lengths

of two quadriceps nerves were measured by using a 10X objective. In addition, the fibre diameter for each internode was measured using a 40X objective. Chimeras with equal contribution of WT and KO Schwann cells were used and 200 internodal distances were measured for each Schwann cell type (n=3).

To estimate the cytoplasms volume of individual Schwann cells, the cytoplasms area of Schwann cells and correspondent fibre diameter was measured from ultrathin transverse sections of quadriceps nerves from 3 and 6 week-old WT and KO mice as described above. Using the fibre diameter value, the correspondent internodal length was estimated from fibre diameter/internodal lengths measured on teased fibres. This internodal length value was multiplied by the Schwann cell cytoplasm area to obtain the cytoplasmic volume.

4.5- Physiology

4.5.1- Nerve conduction velocity

Quadriceps nerves from 3 week-old WT, CMTX, periaxin null and chimeric mice, were dissected and mainteined in oxygenated Kreb's solution. Nerves were transferred for periods of no longer than 10 min to an isolated chamber containing an array of Ag-AgCl electrodes with 1 mm intervals and surrounded by liquid paraffin maintained at 37 ^{o}C. The proximal end of the nerve was excited by a square wave (0.1 ms, 0.1-1.5 V) and the conduction distance was varied from 2-7 mm by altering the stimulating electrode position. The voltage was adjusted to ensure exact duplication of the active population and the compound action potential (CAP) was viewed on a storage oscilloscope. Values were stored as digitised signals using Chart software (MacLab System). Conduction times were measured from the stimulus artefact to the peak of the CAP for all conduction distances. The conduction velocity was calculated from the slope of the regression line generated by plotting these points.

4.5.2- RotaRod

3 week-old wild-type (C57bl/6) and periaxin null mice (n=6 per group) were tested in the RotaRod to measure motor performance at two different revolutions per minute (rpm), 24 and 32. One day before the trial the animals were conditioned to the

RotaRod. The trial was terminated either when the mouse fell from the rod or at 60 seconds in the rotarod. For each rpm, 4 trials per animal were performed (24 in total for each group), each one separated from the next by at least 10 minutes to avoid exhaustation of the animals. The rod was cleaned (70% ethanol) between each animal trial to avoid animals get distracted by olfactory perception of the last animal tested.

4.5.3- Intracellular recording from muscle fibres

Periaxin null and C57Bl/6 mice aged 7 weeks to 11 months were killed by cervical dislocation and flexor digitorum brevis (FDB) muscle were dissected in mammalian physiological solution (MPS, 120 mM NaCl, 5 mM KCl, 2 mM CaCl2, 1 mM MgCl2, 23.8 mM NaHCO3, 5.6 mM D-glucose), bubbled with O2/CO2 (95%/5%). Muscle/nerve preparation was pinned in a sylgard coated recording chamber continually perfused with MBS. The nerve was placed in a suction electrode and a pulled microelectrode was used to record end-plate potentials (EPPs) after blocking muscle action potentials for 20 minutes with μ-conotoxin (2 μM).

4.5.4- Styryl dye staining of motor axon terminals

Recycling synaptic vesicles in TS motor nerve terminals from WT and periaxin null mice were stained using the vital aminostyryl dye FM1-43 (Molecular Probes). Nerve muscle preparations in MPS were incubated with 5 μM FM1-43 for 5 minutes. The nerve was stimulated by a suction electrode by pulses at 20Hz, 10V, 0.1ms bandwidth for 10 minutes. Following nerve stimulation, the nerve/muscle preparations were washed in MPS for 30 minutes. After washing, postsynaptic receptors were stained with fluorescent-conjugated alpha-bungarotoxin for 10 minutes in MPS, washed for 10 minutes and observed using fluorescent microscopy.

4.6- *In vivo* procedures

4.6.1- Topical treatment with colchicine

Depolymerization of Schwann cell microtubules in sciatic nerve *in vivo* was performed by topical colchicine treatment as described by Trapp and colleagues (Trapp et al., 1995) with some modifications. Three week-old WT mice were

anaesthetised intraperitoneally with 1mg/kg medetomidine (Domitor), 75mg/kg ketamine (Vetalar) and the sciatic nerve exposed. A 3 millimeters strip of Parafilm was placed around the nerve in order to avoid any diffusion of colchicine from the treated region to adjacent tissues. A piece of cotton wool was wraped around the nerve and 10 µl of 2.5 mM of colchicine (Sigma) was applied. The strip of parafilm was closed as a ring and a square piece of parafilm was placed above the wound to avoid any liquid evaporation. After one hour of colchicine treatment, the parafilm and cotton wool was removed and the wound closed. Anaesthetic condition were reversed at the end of the procedure with a subcutaneous injection of atipamezole (Antisedan) at 1mg/kg. Three to five days later, animals were killed by cervical dislocation. Treated and contralateral sciatic nerves were dissected, followed by ISH protocol or immunofluorescence in teased fibres as described above.

4.6.2- Denervation of TS muscle

Adult C57Bl/6 mice were anaesthetised intraperitoneally with 1mg/kg medetomidine (Domitor), 75mg/kg ketamine (Vetalar) and the ventral side of the rib cage was exposed. Transversal sterni (TS) muscle innervation, was crushed unilaterally. One to six days later, animals were killed by cervical dislocation and the TS muscles dissected, following by whole mount immunohistochemistry as described above.

4.6.3- Botulinum toxin injection

Adult C57Bl/6 mice were anaesthetised intraperitoneally with 1mg/kg medetomidine (Domitor), 75mg/kg ketamine (Vetalar) and the ventral side of the rib cage was exposed. 2.5 µl of 10 ng/ml botulinum toxin type A (Sigma) was injected into the intercostal nerves that lies above the TS muscle using a fine needle's syringe. One to six days later, animals were killed by cervical dislocation and the TS muscles dissected, following by whole mount immunohistochemistry as described above.

4.7- Model of NCV

Simulation of the sensitivity of nerve conduction velocity on internodal length was performed using the model described by McIntyre *et al.* (McIntyre et al., 2002). This model use 10 segments between sucessive nodes, representing geometrical properties

of the node, paranode, juxtaparanode and internode (Fig. 24B). The electrical parameters of the nerve fibre were used as reported in the article. Modifications were made to geometrical parameters to reflect the experimental morphology measurements of 3 week-old mice quadriceps nerves,

Axon diameter=3.0 μm

Node diameter=1.7 μm

Paranode initial diameter=1.7 μm

Juxtaparanode diameter=3.0 μm

Internode diameter=3.0 μm

Juxtaparanode length=33 μm

Number of myelin lamellae=60

Internodal length=125-1750 μm

4.8- *In situ* hybridisation analysis

Sciatic nerves from C57Bl6, periaxin null and colchichine treated nerves were fixed in 4% paraformaldehyde in 0.1 M phosphate buffer (pH 7.4) for 15-20 minutes, washed 2 times 5 minutes (min) with PBS and teased on TESPA coated slides. The slides were stored –70°C until use. The slides were rehydrated in PBS (DEPC) and treated with 20 μg/ml proteinase K (Roche Diagnostics) for 7.5 min in 50 mM Tris pH 7.5, 5 mM EDTA. Subsequently, they were washed in PBS and fixed for 5 min in 4% paraformaldehyde and prehybridized at room temperature (RT) for 5-6 h in hybridization buffer (50% formamide, 10% dextran sulphate, 1x Denhart's, 20 mM Tris-HCl pH8, 0.3 M NaCl, 5 mM EDTA, 10 mM NaH_2PO_4 pH8, 0.5 mg/ml yeast tRNA). Hybridization buffer was removed from the slides and the probe diluted in hybridization buffer was added to the fibres on the slide and covered with a glass coverslip (ethanol cleaned). The slides were placed in a sealed humidified box at 50°C overnight. Slides were washed with 2X SSC (50°C, 10 min); 50% formamide, 2X SSC (50°C, 1 h); 0.15X SSC (RT, 20 min); 0.1 M maleic acid, 0.15 M NaCl, pH 7.5 (10 min) and blocked for 1 h at RT with 10% sheep serum, 1% blocking agent (Boehringer Mannheim) in 100 mM maleic acid, 150 mM NaCl, pH 7.5. Anti-digoxigenin-AP Fab fragments (1:2000, Roche Diagnostics) were added in blocking

buffer for 1 h and 20 min. The slides were then washed 4 times, 5 minutes each with 50 mM TRIS pH 7.5, 150 mM NaCl, 5 min with NBT (100 mM Tris-HCl, 100 mM NaCl, 5 mM $MgCl_2$, pH 9.5) and 5 min with NBT containing 1 mM levamisole. Colourimetric reaction was obtained by incubating teased fibres in the dark with 5 µl NBT and 3.5 µl BCIP per ml of NTM containing 1 mM levamisole.

Bright field images of teased sciatic nerve fibres (WT, KO and colchicine treated nerves) stained for MBP mRNA by *in situ* hybridization were inverted as shown in figure 23A. Between 9-12 individual Schwann cells (from node to node) for each group (WT, KO and WT-colchicine) were cropped from the original images. The longitudinal size of individual Schwann cells were normalised by rescaling each image to 400 pixels in length. The normalised images were imported to MATLAB software as two-dimensional matrix of numbers representing pixel intensity. For each group a three dimensional array was created by concatenating the individual images in the Z dimension. From this array, the mean value of pixel intensity in the Z dimension was calculated for each pixel resulting in a two dimensional matrix of mean pixel intensity. A surface plot of the mean pixel intensity matrix of the MBP signal with the Z axis representing mean pixel intensity was created in MATLAB.

4.9- Sample preparation and Western blotting

4.9.1- Protein extraction from peripheral nerves

Sciatic nerves were dissected from 3-week old WT and periaxin null mice and protein were extracted by boiling nerves in pre-warmed 2% Sodium dodecyl sulfate (SDS) for 10 minutes followed by centrifugation (13,000 rpm) for 5 minutes at room temperature. After centrifugation the supernatant was recovered and stored at -70°C until use. For P0 protein quantification, five millimeters of quadriceps nerves were dissected from WT and periaxin null mice at different ages (P1, P5, P10, 2 weeks, 3 weeks 6 weeks and 12 weeks). Nerves were stored at -70°C until the protein extraction protocol described above was applied.

4.9.2- Soluble/cytoskeletal fraction preparation from cerebellum tissue

Cerebellum from 3 week-old mouse was dissected and homogenised in a manual glass homogenizer in homogenisation buffer containing 50 mM Tris pH 7.5, 150 mM

NaCl and protease inhibitors (0.5 mM TLCK, 1 mM Benzamidine, 10 μg/ml Leupeptine, 10 μg/ml Antipain, 0.7 μg/ml Chymostatin and 1mM PMSF). An equal volume of lysis buffer (20 mM HEPES pH 7.4, 1 mM EGTA, 0.2 M NaCl, 2% (v/v) Triton X-100, 120 mM Octylglucopyranoside, 10 μg/ml Leupeptine, 10 μg/ml Antipain, 1 mM Benzamidine and 1mM PMSF) was added and left to mix in windmill rotator for 2 hours at 4°C. Following centrifugation at 20,000 rpm for 30 minutes at 4°C, the supernatant was frozen for subsequent use and the pellet containing the cytoskeletal fraction was resuspended in lysis buffer, centrifuged as above and resuspended in homogenisation buffer. Following centrifugation, the pellet was resuspended in 2% SDS and boiled for 5 minutes. Finally, four volumes of solution A (50 mM Tris HCl pH 7.5, 1 mM EGTA, 1 mM EDTA, 150 mM NaCl, 2.5 % (v/v) Triton X-100 and protease inhibitors) were added to the supernatant fraction.

4.9.3- Western blotting

Proteins separated by size in the SDS-PAGE were transferred to a nitrocellulose membrane for 2 h at 480 mA in buffer containing 25 mM Tris HCl pH 8.3, 250 mM glycine and 20% methanol, and blocked overnight in 5% skimmed milk, 0.1% Tween 20 in PBS. The next day, the filter was rinsed with 0.2% gelatine, 0.1% Tween 20 in PBS. To detect proteins blotted on the membrane, the primary antibodies was added at the dilution specified in the table below and incubated for 1 h at room temperature, followed by 3 washes before incubation of the filter in the correspondent species HRP-labelled antibody. The excess of secondary antibody was removed by 3 washes of 10 minutes in PBS, and the peroxidase detected using the enhanced chemiluminescence (ECL) method (Amersham).

Purified tubulin (>99% liphilized; Cytoskeleton, inc.) was reconsituted in 2% SDS to obtain 1 μg of tubulin per milliliter (ml) and stored at -70 °C.

4.9.4- Mass spectrometry

The band revealed by the 2166 antibody by western blotting was identified in coomassie blue stained gels. Precasted 10% SDS gels were used to run cytoskeletal fraction of cerebellum (see above). The gel was stained with coomassie blue (0.025% in 40% methanol, 7% acetic acid) for 1 hour and destained with 40% methanol, 7%

acetic acid for 30 minutes, followed by a second destain step in 5% methanol, 7% acetic acid for 30 minutes. Subsequently, the gel was washed in sterile MilliQ water and the band was excised and sended to the proteomics facility of the University of Aberdeen.

4.10- Reagents used for immunofluorescence and Western blot

The following tables indicates information about primary and secondary antibodies together with dyes and fluorescent conjugated toxins used in the present study (IF, immunofluorescence; WB, western blot).

4.10.1- Primary antibodies

Antibody Name	Species	Source	Dilution
2166	Rabbit	P. J. Brophy	1:200 (IF)
Anti-Desmin	Mouse	DAKO	1:100 (IF)
F4/80	Rat IgG2k	Serotec	1:50 (IF)
Anti-GFAP	Mouse IgG1	Boehringer	1:100 (IF)
Anti-Laminin (a2 chain)	Rat IgG	Alexis	1:200 (IF)
Anti-M-Cadherin	Rabbit	A. Wernig	1:50 (IF)
Anti-NCAM	Rabbit	E. Bock	1:100 (IF)
Anti-Nestin	Mouse IgG1	S. Hockfield	1:200 (IF)
Anti-Neurofilament (165 kDa)	Mouse	DHSB	1:200 (IF)
Anti-Neurofilament (200 kDa)	Mouse IgG1	Sigma	1:1000 (IF)
Anti-Periaxin	Rabbit	P. J. Brophy	1:3000 (IF)
Anti-S100	Rabbit	DAKO	1:200 (IF)
Anti-S100 (SA1259)	Mouse IgG1	Affinity	1:200 (IF)
Anti-SV2	Mouse	SAPU	1:200 (IF)
Anti-Thy 1.1	Mouse IgG1	Serotec	1:100 (IF)
Anti-Tubulin (YL1/2)	Rat IgG	Serotec	1:200 (IF), 1:1000 (WB)
Anti-CD34	Rat IgG2b	BD PharMingen	1:50 (IF)
Anti-Thy1.2	Rat IgG2b	BD PharMingen	1:50 (IF)
Anti-DRP2	Rabbit	P. J. Brophy	1:200 (IF)
Anti-neurofascin	Rabbit	P. J. Brophy	1:1000 (IF), 1:10000 (WB)
Anti-pan Na+ channel	Mouse	M. Rasband	1:300 (IF)
Anti-b-dystroglycan (MANDAG 2)	Mouse IgG1	G.E. Morris	1:100 (IF)
Anti-betaIV-spectrin	Chicken	M. Komada	1:100 (IF), 1:1000 (WB)
Anti-caspr	Guinea pig	D. Colman	1:200 (IF), 1:2000 (WB)
Anti-Kv1.1 channel	Rabbit	Chemicon	1:200 (IF)
Anti-P0	Rabbit	T. Brookes	1:400 (IF)
Anti-P0	Rabbit	D. Coleman	1:5000 (WB)
Anti-MBP (clone 12)	Rat IgG	Dr. Groome	1:200 (IF)
Anti-prolyl-4-hydroxylase	Mouse IgG1	Acris Medicorp	1:100 (IF)
Anti-Tenascin	Rat IgG	Abcam	1:200 (IF)

4.10.2- Secondary antibodies

Antibody name	Species	Source	Dilution
TRITC-conjugated anti-rat IgG	Donkey	Jackson	1:200
TRITC-conjugated anti-mouse IgG	Goat	Southern Biotech	1:200
FITC-conjugated anti-rabbit IgG	Donkey	Jackson	1:200
TRITC-conjugated anti-guinea pig IgG	Donkey	Jackson	1:200
FITC-conjugated anti-chicken IgY	Donkey	Jackson	1:100
AlexaFluor-647-conjugated anti-mouse IgG1	Goat	Molecular Probes	1:100
AlexaFluor-647-conjugated anti-rabbit IgG	Goat	Molecular Probes	1:100
HRP-conjugated anti-rabbit IgG	Donkey	SAPU	1:2000
HRP-conjugated anti-rat IgG	Rabbit	Jackson	1:2000
HRP-conjugated anti-chicken IgY	Donkey	Sigma	1:5000
HRP-conjugated anti-guinea pig IgG	Goat	Jackson	1:2000
HRP-conjugated anti-mouse IgG	Sheep	SAPU	1:2000

4.10.3- Dyes and fluorescent-conjugated toxins

Name	Source	Concentration
TRITC-conjugated phalloidin	Sigma	50 ng/ml
4,6-diamidino-2-phenylindole (DAPI)	Sigma	4 µg/ml
Totpro3	Molecular Probes	1mM
Rhodamine conjugated α -bungarotoxin (BTX)	Molecular Probes	5 µg/ml
TRITC, FITC or AlexaFluor 647-conjugated BTX	Molecular Probes	5 µg/ml

4.11- 2166 antibody

The 2166 antibody was generated by Dr. Shona Melrose in Prof Peter J. Brophy's lab. A peptide (amino acid sequence CAIRNSRDVI) corresponding to the C-terminus of the Tspan-2 protein coupled to keyhole limpet hemocyanin (KLH) was used to inoculate male New Zealand white rabbits of approximately 1.5 Kg in weight. After three injections of KLH-coupled peptide, serum was collected from the rabbits at appropriate time points and subsequently affinity purified (a standard protocol performed by Dr. Shona Melrose). In western blots of cerebellum homogenate, 2166 antibody identified a single band of ~47 kDa, a size not expected for Tspan-2 protein which should be around 25 kDa (Birling et al., 1999). In addition, immunohistochemistry performed in the central nervous system (CNS) reveals that the 2166 antibody stains both $GFAP^+$ and $GFAP^-$ populations of

astrocytes in the cortex and cerebellum, but no expression was found in oligodendrocytes (which express the Tspan-2 protein).

4.12- Statistics

All statistical analyses were performed using Prism 3.03, including linear regression, curve fitting and Student t test used to compare morphological parameters between two samples (values are ± SEM). Graphics were produced using SigmaPlot.

The growth rate of internodal lengths and nerve length were fitted to different functions and the best fit (F-test, Prism 3.03) was selected. Selected curves were superimposed to the measured values in the graph (Figure 17C). The growth rate of WT internodal length (IL) follows a rectangular hyperbola (Equation: $Y=A*X/(B+X)$) with parameters (in μm) A=821.2 and B=11.51; R^2=0.9914). The growth rate of KO internodal length follows a straight line (linear regression) with a slope of 6.9 ± 0.30 μm; r^2=0.996, P=0.0019. The growth rate of WT and KO nerve length follows a rectangular hyperbola with parameters (in mm): WT, A=19.74 and B=1.405, R^2= 0.9901; KO, A= 19.53 and B= 1.396, R^2= 0.9902. The fitted nerve length curves shown no significant differences tested by F-test (testing the null hypotesis that there is no difference between curves, P=0.945).

5- REFERENCES

Ainger, K., Avossa, D., Morgan, F., Hill, S. J., Barry, C., Barbarese, E., and Carson, J. H. (1993). Transport and localization of exogenous myelin basic protein mRNA microinjected into oligodendrocytes. J Cell Biol *123*, 431-441.

Altevogt, B. M., Kleopa, K. A., Postma, F. R., Scherer, S. S., and Paul, D. L. (2002). Connexin29 is uniquely distributed within myelinating glial cells of the central and peripheral nervous systems. J Neurosci *22*, 6458-6470.

Anzini, P., Neuberg, D. H., Schachner, M., Nelles, E., Willecke, K., Zielasek, J., Toyka, K. V., Suter, U., and Martini, R. (1997). Structural abnormalities and deficient maintenance of peripheral nerve myelin in mice lacking the gap junction protein connexin 32. J Neurosci *17*, 4545-4551.

Apel, E. D., Glass, D. J., Moscoso, L. M., Yancopoulos, G. D., and Sanes, J. R. (1997). Rapsyn is required for MuSK signaling and recruits synaptic components to a MuSK-containing scaffold. Neuron *18*, 623-635.

Bailey, P., Holowacz, T., and Lassar, A. B. (2001). The origin of skeletal muscle stem cells in the embryo and the adult. Curr Opin Cell Biol *13*, 679-689.

Balice-Gordon, R. J. (1996). Dynamic roles at the neuromuscular junction. Schwann cells. Curr Biol *6*, 1054-1056.

Balice-Gordon, R. J., Bone, L. J., and Scherer, S. S. (1998). Functional gap junctions in the schwann cell myelin sheath. J Cell Biol *142*, 1095-1104.

Barbarese, E., Brumwell, C., Kwon, S., Cui, H., and Carson, J. H. (1999). RNA on the road to myelin. J Neurocytol *28*, 263-270.

Barry, J. A., and Ribchester, R. R. (1995). Persistent polyneuronal innervation in partially denervated rat muscle after reinnervation and recovery from prolonged nerve conduction block. J Neurosci *15*, 6327-6339.

Bermingham, J. R., Jr., Scherer, S. S., O'Connell, S., Arroyo, E., Kalla, K. A., Powell, F. L., and Rosenfeld, M. G. (1996). Tst-1/Oct-6/SCIP regulates a unique step in peripheral myelination and is required for normal respiration. Genes Dev *10*, 1751-1762.

Betz, W. J., Caldwell, J. H., Ribchester, R. R., Robinson, K. R., and Stump, R. F. (1980). Endogenous electric field around muscle fibres depends on the Na+-K+ pump. Nature *287*, 235-237.

Bhat, M. A., Rios, J. C., Lu, Y., Garcia-Fresco, G. P., Ching, W., St Martin, M., Li, J., Einheber, S., Chesler, M., Rosenbluth, J., *et al.* (2001). Axon-glia interactions and the domain organization of myelinated axons requires neurexin IV/Caspr/Paranodin. Neuron *30*, 369-383.

Birling, M. C., Tait, S., Hardy, R. J., and Brophy, P. J. (1999). A novel rat tetraspan protein in cells of the oligodendrocyte lineage. J Neurochem *73*, 2600-2608.

Bladt, F., Riethmacher, D., Isenmann, S., Aguzzi, A., and Birchmeier, C. (1995). Essential role for the c-met receptor in the migration of myogenic precursor cells into the limb bud. Nature *376*, 768-771.

Bouzidi, M., Tricaud, N., Giraud, P., Kordeli, E., Caillol, G., Deleuze, C., Couraud, F., and Alcaraz, G. (2002). Interaction of the Nav1.2a subunit of the voltage-dependent sodium channel with nodal ankyrinG. In vitro mapping of the interacting domains and association in synaptosomes. J Biol Chem *277*, 28996-29004.

Boyle, M. E., Berglund, E. O., Murai, K. K., Weber, L., Peles, E., and Ranscht, B. (2001). Contactin orchestrates assembly of the septate-like junctions at the paranode in myelinated peripheral nerve. Neuron *30*, 385-397.

Brand-Saberi, B., and Christ, B. (1999). Genetic and epigenetic control of muscle development in vertebrates. Cell Tissue Res *296*, 199-212.

Brigant, J. L., and Mallart, A. (1982). Presynaptic currents in mouse motor endings. J Physiol *333*, 619-636.

Brill, M. H., Waxman, S. G., Moore, J. W., and Joyner, R. W. (1977). Conduction velocity and spike configuration in myelinated fibres: computed dependence on internode distance. J Neurol Neurosurg Psychiatry *40*, 769-774.

Brittis, P. A., Lu, Q., and Flanagan, J. G. (2002). Axonal protein synthesis provides a mechanism for localized regulation at an intermediate target. Cell *110*, 223-235.

Brown, M. C., and Ironton, R. (1978). Sprouting and regression of neuromuscular synapses in partially denervated mammalian muscles. J Physiol *278*, 325-348.

Buffelli, M., Burgess, R. W., Feng, G., Lobe, C. G., Lichtman, J. W., and Sanes, J. R. (2003). Genetic evidence that relative synaptic efficacy biases the outcome of synaptic competition. Nature *424*, 430-434.

Bunge, R. P., Bunge, M. B., and Bates, M. (1989). Movements of the Schwann cell nucleus implicate progression of the inner (axon-related) Schwann cell process during myelination. J Cell Biol *109*, 273-284.

Bunge, R. P., Bunge, M. B., and Eldridge, C. F. (1986). Linkage between axonal ensheathment and basal lamina production by Schwann cells. Annu Rev Neurosci *9*, 305-328.

Burden, S. J. (1998). The formation of neuromuscular synapses. Genes Dev *12*, 133-148.

Campagna, J. A., Ruegg, M. A., and Bixby, J. L. (1995). Agrin is a differentiation-inducing "stop signal" for motoneurons in vitro. Neuron *15*, 1365-1374.

Carson, J. H., Kwon, S., and Barbarese, E. (1998). RNA trafficking in myelinating cells. Curr Opin Neurobiol *8*, 607-612.

Carson, J. H., Worboys, K., Ainger, K., and Barbarese, E. (1997). Translocation of myelin basic protein mRNA in oligodendrocytes requires microtubules and kinesin. Cell Motil Cytoskeleton *38*, 318-328.

Castonguay, A., and Robitaille, R. (2001). Differential regulation of transmitter release by presynaptic and glial Ca2+ internal stores at the neuromuscular synapse. J Neurosci *21*, 1911-1922.

Chan, J. R., Watkins, T. A., Cosgaya, J. M., Zhang, C., Chen, L., Reichardt, L. F., Shooter, E. M., and Barres, B. A. (2004). NGF controls axonal receptivity to myelination by Schwann cells or oligodendrocytes. Neuron *43*, 183-191.

Chen, L. M., Bailey, D., and Fernandez-Valle, C. (2000). Association of beta 1 integrin with focal adhesion kinase and paxillin in differentiating Schwann cells. J Neurosci *20*, 3776-3784.

Chen, Z. L., and Strickland, S. (2003). Laminin gamma1 is critical for Schwann cell differentiation, axon myelination, and regeneration in the peripheral nerve. J Cell Biol *163*, 889-899.

Cho, S. I., Ko, J., Patton, B. L., Sanes, J. R., and Chiu, A. Y. (1998). Motor neurons and Schwann cells distinguish between synaptic and extrasynaptic isoforms of laminin. J Neurobiol *37*, 339-358.

Cifuentes-Diaz, C., Faille, L., Goudou, D., Schachner, M., Rieger, F., and Angaut-Petit, D. (2002). Abnormal reinnervation of skeletal muscle in a tenascin-C-deficient mouse. J Neurosci Res *67*, 93-99.

Costanzo, E. M., Barry, J. A., and Ribchester, R. R. (2000). Competition at silent synapses in reinnervated skeletal muscle. Nat Neurosci *3*, 694-700.

Court, F., and Alvarez, J. (2000). Nerve regeneration in Wld(s) mice is normalized by actinomycin D. Brain Res *867*, 1-8.

Court, F. A., Sherman, D. L., Pratt, T., Garry, E. M., Ribchester, R. R., Cottrell, D. F., Fleetwood-Walker, S. M., and Brophy, P. J. (2004). Restricted growth of Schwann cells lacking Cajal bands slows conduction in myelinated nerves. Nature *431*, 191-195.

Crow, M. T., and Stockdale, F. E. (1986). Myosin expression and specialization among the earliest muscle fibers of the developing avian limb. Dev Biol *113*, 238-254.

Dai, Z., and Peng, H. B. (1995). Presynaptic differentiation induced in cultured neurons by local application of basic fibroblast growth factor. J Neurosci *15*, 5466-5475.

de Waegh, S. M., Lee, V. M., and Brady, S. T. (1992). Local modulation of neurofilament phosphorylation, axonal caliber, and slow axonal transport by myelinating Schwann cells. Cell *68*, 451-463.

DeBello, W. M., O'Connor, V., Dresbach, T., Whiteheart, S. W., Wang, S. S., Schweizer, F. E., Betz, H., Rothman, J. E., and Augustine, G. J. (1995). SNAP-mediated protein-protein interactions essential for neurotransmitter release. Nature *373*, 626-630.

Devaux, J. J., Kleopa, K. A., Cooper, E. C., and Scherer, S. S. (2004). KCNQ2 is a nodal K+ channel. J Neurosci *24*, 1236-1244.

Dong, Z., Brennan, A., Liu, N., Yarden, Y., Lefkowitz, G., Mirsky, R., and Jessen, K. R. (1995). Neu differentiation factor is a neuron-glia signal and regulates survival, proliferation, and maturation of rat Schwann cell precursors. Neuron *15*, 585-596.

Duclert, A., Savatier, N., Schaeffer, L., and Changeux, J. P. (1996). Identification of an element crucial for the sub-synaptic expression of the acetylcholine receptor epsilon-subunit gene. J Biol Chem *271*, 17433-17438.

D'Urso, D., Brophy, P. J., Staugaitis, S. M., Gillespie, C. S., Frey, A. B., Stempak, J. G., and Colman, D. R. (1990). Protein zero of peripheral nerve myelin: biosynthesis, membrane insertion, and evidence for homotypic interaction. Neuron *4*, 449-460.

Duxson, M. J., Usson, Y., and Harris, A. J. (1989). The origin of secondary myotubes in mammalian skeletal muscles: ultrastructural studies. Development *107*, 743-750.

Ebens, A., Brose, K., Leonardo, E. D., Hanson, M. G., Jr., Bladt, F., Birchmeier, C., Barres, B. A., and Tessier-Lavigne, M. (1996). Hepatocyte growth factor/scatter factor is an axonal chemoattractant and a neurotrophic factor for spinal motor neurons. Neuron *17*, 1157-1172.

Eldridge, C. F., Bunge, M. B., and Bunge, R. P. (1989). Differentiation of axon-related Schwann cells in vitro: II. Control of myelin formation by basal lamina. J Neurosci *9*, 625-638.

Fallon, J. R., and Gelfman, C. E. (1989). Agrin-related molecules are concentrated at acetylcholine receptor clusters in normal and aneural developing muscle. J Cell Biol *108*, 1527-1535.

Fannon, A. M., Sherman, D. L., Ilyina-Gragerova, G., Brophy, P. J., Friedrich, V. L., Jr., and Colman, D. R. (1995). Novel E-cadherin-mediated adhesion in peripheral nerve: Schwann cell architecture is stabilized by autotypic adherens junctions. J Cell Biol *129*, 189-202.

Feltri, M. L., Graus Porta, D., Previtali, S. C., Nodari, A., Migliavacca, B., Cassetti, A., Littlewood-Evans, A., Reichardt, L. F., Messing, A., Quattrini, A., *et al.* (2002). Conditional disruption of beta 1 integrin in Schwann cells impedes interactions with axons. J Cell Biol *156*, 199-209.

Feng, G., Laskowski, M. B., Feldheim, D. A., Wang, H., Lewis, R., Frisen, J., Flanagan, J. G., and Sanes, J. R. (2000). Roles for ephrins in positionally selective synaptogenesis between motor neurons and muscle fibers. Neuron *25*, 295-306.

Ferns, M., and Carbonetto, S. (2001). Challenging the neurocentric view of neuromuscular synapse formation. Neuron *30*, 311-314.

Fischbach, G. D., and Rosen, K. M. (1997). ARIA: a neuromuscular junction neuregulin. Annu Rev Neurosci *20*, 429-458.

Fraher, J., and Dockery, P. (1998). A strong myelin thickness-axon size correlation emerges in developing nerves despite independent growth of both parameters. J Anat *193 (Pt 2)*, 195-201.

Fraher, J. P. (1978). Quantitative studies on the maturation of central and peripheral parts of individual ventral motoneuron axons. I. Myelin sheath and axon calibre. J Anat *126*, 509-533.

Garbay, B., Heape, A. M., Sargueil, F., and Cassagne, C. (2000). Myelin synthesis in the peripheral nervous system. Prog Neurobiol *61*, 267-304.

Garratt, A. N., Britsch, S., and Birchmeier, C. (2000). Neuregulin, a factor with many functions in the life of a schwann cell. Bioessays *22*, 987-996.

Garver, T. D., Ren, Q., Tuvia, S., and Bennett, V. (1997). Tyrosine phosphorylation at a site highly conserved in the L1 family of cell adhesion molecules abolishes ankyrin binding and increases lateral mobility of neurofascin. J Cell Biol *137*, 703-714.

Gatchalian, C. L., Schachner, M., and Sanes, J. R. (1989). Fibroblasts that proliferate near denervated synaptic sites in skeletal muscle synthesize the adhesive molecules tenascin(J1), N-CAM, fibronectin, and a heparan sulfate proteoglycan. J Cell Biol *108*, 1873-1890.

Gates, H. J., and Ridge, R. M. (1992). The importance of competition between motoneurones in developing rat muscle; effects of partial denervation at birth. J Physiol *445*, 457-472.

Gatto, C. L., Walker, B. J., and Lambert, S. (2003). Local ERM activation and dynamic growth cones at Schwann cell tips implicated in efficient formation of nodes of Ranvier. J Cell Biol *162*, 489-498.

Gautam, M., Noakes, P. G., Moscoso, L., Rupp, F., Scheller, R. H., Merlie, J. P., and Sanes, J. R. (1996). Defective neuromuscular synaptogenesis in agrin-deficient mutant mice. Cell *85*, 525-535.

Georgiou, J., Robitaille, R., Trimble, W., and Charlton, M. (1994). Synaptic regulation of glial protein expression in vivo. Neuron *12*, 443-455.

Geren, B. B. (1954). The formation from the Schwann cell surface of myelin peripheral nerves of chick embryos. Exp Cell Res *7*, 558-562.

Gillespie, C. S., Sherman, D. L., Fleetwood-Walker, S. M., Cottrell, D. F., Tait, S., Garry, E. M., Wallace, V. C., Ure, J., Griffiths, I. R., Smith, A., and Brophy, P. J. (2000). Peripheral demyelination and neuropathic pain behavior in periaxin-deficient mice. Neuron *26*, 523-531.

Goda, Y., and Davis, G. W. (2003). Mechanisms of synapse assembly and disassembly. Neuron *40*, 243-264.

Gordon, T. R., Kocsis, J. D., and Waxman, S. G. (1990). Electrogenic pump (Na+/K(+)-ATPase) activity in rat optic nerve. Neuroscience *37*, 829-837.

Griffiths, I., Klugmann, M., Anderson, T., Yool, D., Thomson, C., Schwab, M. H., Schneider, A., Zimmermann, F., McCulloch, M., Nadon, N., and Nave, K. A. (1998). Axonal swellings and degeneration in mice lacking the major proteolipid of myelin. Science *280*, 1610-1613.

Griffiths, I. R., Mitchell, L. S., McPhilemy, K., Morrison, S., Kyriakides, E., and Barrie, J. A. (1989). Expression of myelin protein genes in Schwann cells. J Neurocytol *18*, 345-352.

Guthrie, S., and Lumsden, A. (1992). Motor neuron pathfinding following rhombomere reversals in the chick embryo hindbrain. Development *114*, 663-673.

Guthrie, S., and Pini, A. (1995). Chemorepulsion of developing motor axons by the floor plate. Neuron *14*, 1117-1130.

Hall, A. C., Lucas, F. R., and Salinas, P. C. (2000). Axonal remodeling and synaptic differentiation in the cerebellum is regulated by WNT-7a signaling. Cell *100*, 525-535.

Harris, A. J. (1981). Embryonic growth and innervation of rat skeletal muscles. III. Neural regulation of junctional and extra-junctional acetylcholine receptor clusters. Philos Trans R Soc Lond B Biol Sci *293*, 287-314.

Harris, A. J., Duxson, M. J., Fitzsimons, R. B., and Rieger, F. (1989). Myonuclear birthdates distinguish the origins of primary and secondary myotubes in embryonic mammalian skeletal muscles. Development *107*, 771-784.

Hassan, S. M., Jennekens, F. G., Veldman, H., and Oestreicher, B. A. (1994). GAP-43 and p75NGFR immunoreactivity in presynaptic cells following neuromuscular blockade by botulinum toxin in rat. J Neurocytol *23*, 354-363.

Hawke, T. J., and Garry, D. J. (2001). Myogenic satellite cells: physiology to molecular biology. J Appl Physiol *91*, 534-551.

Hildebrand, C., Loeliger, S., Bjartmar, C., and Karlsson, M. (1996). Sheath lengths of large motor axons in the ventral root L5 of neonatal and adult rats. Neurosci Lett *202*, 173-176.

Hines, M. L., and Carnevale, N. T. (1997). The NEURON simulation environment. Neural Comput *9*, 1179-1209.

Hiscoe, H. B. (1947). Distribution of nodes and incisures in normal and regenerated nerve. Anat Record *99*, 447-475.

Hoch, W. (1999). Formation of the neuromuscular junction. Agrin and its unusual receptors. Eur J Biochem *265*, 1-10.

Hoke, A., Ho, T., Crawford, T. O., LeBel, C., Hilt, D., and Griffin, J. W. (2003). Glial cell line-derived neurotrophic factor alters axon schwann cell units and promotes myelination in unmyelinated nerve fibers. J Neurosci *23*, 561-567.

Huxley, A. F., and Stampfli, R. (1949). Evidence for saltatory conduction in peripheral myelinated nerve fibres. J Physiol *108*, 315-339.

Ichimura, T., and Ellisman, M. H. (1991). Three-dimensional fine structure of cytoskeletal-membrane interactions at nodes of Ranvier. J Neurocytol *20*, 667-681.

Irintchev, A., Zeschnigk, M., Starzinski-Powitz, A., and Wernig, A. (1994). Expression pattern of M-cadherin in normal, denervated, and regenerating mouse muscles. Dev Dyn *199*, 326-337.

Jackson, K. A., Mi, T., and Goodell, M. A. (1999). Hematopoietic potential of stem cells isolated from murine skeletal muscle. Proc Natl Acad Sci U S A *96*, 14482-14486.

Jacob, J., Hacker, A., and Guthrie, S. (2001). Mechanisms and molecules in motor neuron specification and axon pathfinding. Bioessays *23*, 582-595.

Jaegle, M., Mandemakers, W., Broos, L., Zwart, R., Karis, A., Visser, P., Grosveld, F., and Meijer, D. (1996). The POU factor Oct-6 and Schwann cell differentiation. Science *273*, 507-510.

Jahromi, B. S., Robitaille, R., and Charlton, M. P. (1992). Transmitter release increases intracellular calcium in perisynaptic Schwann cells in situ. Neuron *8*, 1069-1077.

Jessen, K. R., and Mirsky, R. (1999). Schwann cells and their precursors emerge as major regulators of nerve development. Trends Neurosci *22*, 402-410.

Jo, S. A., Zhu, X., Marchionni, M. A., and Burden, S. J. (1995). Neuregulins are concentrated at nerve-muscle synapses and activate ACh-receptor gene expression. Nature *373*, 158-161.

Jockusch, B. M., Bubeck, P., Giehl, K., Kroemker, M., Moschner, J., Rothkegel, M., Rudiger, M., Schluter, K., Stanke, G., and Winkler, J. (1995). The molecular architecture of focal adhesions. Annu Rev Cell Dev Biol *11*, 379-416.

Juliano, R. L. (2002). Signal transduction by cell adhesion receptors and the cytoskeleton: functions of integrins, cadherins, selectins, and immunoglobulin-superfamily members. Annu Rev Pharmacol Toxicol *42*, 283-323.

Kang, H., Thompson, W. J., Mignone, J., and Enikolopov, G. (2001). Changes of nestin expression pattern in neonates and adults neuromuscular junction of nestin transgenic mice. In Society for Neuroscience 31st Annual Meeting (San Diego, CA, USA). Program No 694.8.

Kania, A., Johnson, R. L., and Jessell, T. M. (2000). Coordinate roles for LIM homeobox genes in directing the dorsoventral trajectory of motor axons in the vertebrate limb. Cell *102*, 161-173.

Komada, M., and Soriano, P. (2002). [Beta]IV-spectrin regulates sodium channel clustering through ankyrin-G at axon initial segments and nodes of Ranvier. J Cell Biol *156*, 337-348.

Koumas, L., Smith, T. J., and Phipps, R. P. (2002). Fibroblast subsets in the human orbit: Thy-1+ and Thy-1- subpopulations exhibit distinct phenotypes. Eur J Immunol *32*, 477-485.

Krause, D. S., Ito, T., Fackler, M. J., Smith, O. M., Collector, M. I., Sharkis, S. J., and May, W. S. (1994). Characterization of murine CD34, a marker for hematopoietic progenitor and stem cells. Blood *84*, 691-701.

Kuschel, R., Yablonka-Reuveni, Z., and Bornemann, A. (1999). Satellite cells on isolated myofibers from normal and denervated adult rat muscle. J Histochem Cytochem *47*, 1375-1384.

Landgraf, M., Baylies, M., and Bate, M. (1999). Muscle founder cells regulate defasciculation and targeting of motor axons in the Drosophila embryo. Curr Biol *9*, 589-592.

Landon, D. N. (1975). The Peripheral nerve (New York, Wiley).

Langenfeld-Oster, B., Faissner, A., Irintchev, A., and Wernig, A. (1994). Polyclonal antibodies against NCAM and tenascin delay endplate reinnervation. J Neurocytol *23*, 591-604.

Laskowski, M. B., and Sanes, J. R. (1987). Topographic mapping of motor pools onto skeletal muscles. J Neurosci *7*, 252-260.

Lee, J. Y., Qu-Petersen, Z., Cao, B., Kimura, S., Jankowski, R., Cummins, J., Usas, A., Gates, C., Robbins, P., Wernig, A., and Huard, J. (2000). Clonal isolation of muscle-derived cells capable of enhancing muscle regeneration and bone healing. J Cell Biol *150*, 1085-1100.

Lin, W., Burgess, R. W., Dominguez, B., Pfaff, S. L., Sanes, J. R., and Lee, K. F. (2001). Distinct roles of nerve and muscle in postsynaptic differentiation of the neuromuscular synapse. Nature *410*, 1057-1064.

Lin, W., Sanchez, H. B., Deerinck, T., Morris, J. K., Ellisman, M., and Lee, K. F. (2000). Aberrant development of motor axons and neuromuscular synapses in erbB2-deficient mice. Proc Natl Acad Sci U S A *97*, 1299-1304.

Liu, A., Muggironi, M., Marin-Husstege, M., and Casaccia-Bonnefil, P. (2003). Oligodendrocyte process outgrowth in vitro is modulated by epigenetic regulation of cytoskeletal severing proteins. Glia *44*, 264-274.

Mallart, A., and Brigant, J. L. (1982). Electrical activity at motor nerve terminals of the mouse. J Physiol (Paris) *78*, 407-411.

Martin, J. R., and Webster, H. D. (1973). Mitotic Schwann cells in developing nerve: their changes in shape, fine structure, and axon relationships. Dev Biol *32*, 417-431.

Martini, R., Zielasek, J., Toyka, K. V., Giese, K. P., and Schachner, M. (1995). Protein zero (P0)-deficient mice show myelin degeneration in peripheral nerves characteristic of inherited human neuropathies. Nat Genet *11*, 281-286.

Mata, M., Kupina, N., and Fink, D. J. (1992). Phosphorylation-dependent neurofilament epitopes are reduced at the node of Ranvier. J Neurocytol *21*, 199-210.

McIntyre, C. C., Richardson, A. G., and Grill, W. M. (2002). Modeling the excitability of mammalian nerve fibers: influence of afterpotentials on the recovery cycle. J Neurophysiol *87*, 995-1006.

Meier, C., Dermietzel, R., Davidson, K. G., Yasumura, T., and Rash, J. E. (2004). Connexin32-containing gap junctions in Schwann cells at the internodal zone of partial myelin compaction and in Schmidt-Lanterman incisures. J Neurosci *24*, 3186-3198.

Meier, T., and Wallace, B. G. (1998). Formation of the neuromuscular junction: molecules and mechanisms. Bioessays *20*, 819-829.

Meiners, S., Mercado, M. L., Nur-e-Kamal, M. S., and Geller, H. M. (1999). Tenascin-C contains domains that independently regulate neurite outgrowth and neurite guidance. J Neurosci *19*, 8443-8453.

Melendez-Vasquez, C. V., Einheber, S., and Salzer, J. L. (2004). Rho kinase regulates schwann cell myelination and formation of associated axonal domains. J Neurosci *24*, 3953-3963.

Mi, H., Deerinck, T. J., Jones, M., Ellisman, M. H., and Schwarz, T. L. (1996). Inwardly rectifying K+ channels that may participate in K+ buffering are localized in microvilli of Schwann cells. J Neurosci *16*, 2421-2429.

Michailov, G. V., Sereda, M. W., Brinkmann, B. G., Fischer, T. M., Haug, B., Birchmeier, C., Role, L., Lai, C., Schwab, M. H., and Nave, K. A. (2004). Axonal neuregulin-1 regulates myelin sheath thickness. Science *304*, 700-703.

Mikol, D. D., Hong, H. L., Cheng, H. L., and Feldman, E. L. (1999). Caveolin-1 expression in Schwann cells. Glia *27*, 39-52.

Mirsky, R., Parkinson, D. B., Dong, Z., Meier, C., Calle, E., Brennan, A., Topilko, P., Harris, B. S., Stewart, H. J., and Jessen, K. R. (2001). Regulation of genes involved in Schwann cell development and differentiation. Prog Brain Res *132*, 3-11.

Mochida, S. (2000). Protein-protein interactions in neurotransmitter release. Neurosci Res *36*, 175-182.

Moore, J. W., Joyner, R. W., Brill, M. H., Waxman, S. D., and Najar-Joa, M. (1978). Simulations of conduction in uniform myelinated fibers. Relative sensitivity to changes in nodal and internodal parameters. Biophys J *21*, 147-160.

Murray, J. D. (1993). Mathematical biology, 2nd, corr. edn (Berlin ; New York, Springer-Verlag).

Nakamura, F., Kalb, R. G., and Strittmatter, S. M. (2000). Molecular basis of semaphorin-mediated axon guidance. J Neurobiol *44*, 219-229.

Nilsson, I., and Berthold, C. H. (1988). Axon classes and internodal growth in the ventral spinal root L7 of adult and developing cats. J Anat *156*, 71-96.

Nitkin, R. M., Smith, M. A., Magill, C., Fallon, J. R., Yao, Y. M., Wallace, B. G., and McMahan, U. J. (1987). Identification of agrin, a synaptic organizing protein from Torpedo electric organ. J Cell Biol *105*, 2471-2478.

Noakes, P. G., Gautam, M., Mudd, J., Sanes, J. R., and Merlie, J. P. (1995). Aberrant differentiation of neuromuscular junctions in mice lacking s-laminin/laminin beta 2. Nature *374*, 258-262.

Parkinson, D. B., Bhaskaran, A., Droggiti, A., Dickinson, S., D'Antonio, M., Mirsky, R., and Jessen, K. R. (2004). Krox-20 inhibits Jun-NH2-terminal kinase/c-Jun to control Schwann cell proliferation and death. J Cell Biol *164*, 385-394.

Patton, B. L., Miner, J. H., Chiu, A. Y., and Sanes, J. R. (1997). Distribution and function of laminins in the neuromuscular system of developing, adult, and mutant mice. J Cell Biol *139*, 1507-1521.

Phipps, R. P., Borrello, M. A., and Blieden, T. M. (1997). Fibroblast heterogeneity in the periodontium and other tissues. J Periodontal Res *32*, 159-165.

Pihlajaniemi, T., Myllyla, R., and Kivirikko, K. I. (1991). Prolyl 4-hydroxylase and its role in collagen synthesis. J Hepatol *13 Suppl 3*, S2-7.

Pokrywka, N. J., and Stephenson, E. C. (1995). Microtubules are a general component of mRNA localization systems in Drosophila oocytes. Dev Biol *167*, 363-370.

Poliak, S., Matlis, S., Ullmer, C., Scherer, S. S., and Peles, E. (2002). Distinct claudins and associated PDZ proteins form different autotypic tight junctions in myelinating Schwann cells. J Cell Biol *159*, 361-372.

Poliak, S., and Peles, E. (2003). The local differentiation of myelinated axons at nodes of Ranvier. Nat Rev Neurosci *4*, 968-980.

Poliak, S., Salomon, D., Elhanany, H., Sabanay, H., Kiernan, B., Pevny, L., Stewart, C. L., Xu, X., Chiu, S. Y., Shrager, P., *et al.* (2003). Juxtaparanodal clustering of Shaker-like K+ channels in myelinated axons depends on Caspr2 and TAG-1. J Cell Biol *162*, 1149-1160.

Porter, B. E., Weis, J., and Sanes, J. R. (1995). A motoneuron-selective stop signal in the synaptic protein S-laminin. Neuron *14*, 549-559.

Pratt, T., Sharp, L., Nichols, J., Price, D. J., and Mason, J. O. (2000). Embryonic stem cells and transgenic mice ubiquitously expressing a tau-tagged green fluorescent protein. Dev Biol *228*, 19-28.

Previtali, S. C., Nodari, A., Taveggia, C., Pardini, C., Dina, G., Villa, A., Wrabetz, L., Quattrini, A., and Feltri, M. L. (2003). Expression of laminin receptors in schwann cell differentiation: evidence for distinct roles. J Neurosci *23*, 5520-5530.

Pun, S., Sigrist, M., Santos, A. F., Ruegg, M. A., Sanes, J. R., Jessell, T. M., Arber, S., and Caroni, P. (2002). An intrinsic distinction in neuromuscular junction assembly and maintenance in different skeletal muscles. Neuron *34*, 357-370.

Quick, D. C., Kennedy, W. R., and Donaldson, L. (1979). Dimensions of myelinated nerve fibers near the motor and sensory terminals in cat tenuissimus muscles. Neuroscience *4*, 1089-1096.

Qu-Petersen, Z., Deasy, B., Jankowski, R., Ikezawa, M., Cummins, J., Pruchnic, R., Mytinger, J., Cao, B., Gates, C., Wernig, A., and Huard, J. (2002). Identification of a novel population of muscle stem cells in mice: potential for muscle regeneration. J Cell Biol *157*, 851-864.

Ramón y Cajal, S. (1933). Histology (London, Bailliere, Tindall & Cox).

Reddy, L. V., Koirala, S., Sugiura, Y., Herrera, A. A., and Ko, C. P. (2003). Glial cells maintain synaptic structure and function and promote development of the neuromuscular junction in vivo. Neuron *40*, 563-580.

Reynolds, M. L., and Woolf, C. J. (1992). Terminal Schwann cells elaborate extensive processes following denervation of the motor endplate. J Neurocytol *21*, 50-66.

Ritchie, J. M., and Rogart, R. B. (1977). Density of sodium channels in mammalian myelinated nerve fibers and nature of the axonal membrane under the myelin sheath. Proc Natl Acad Sci U S A *74*, 211-215.

Rogers, S. L., and Gelfand, V. I. (2000). Membrane trafficking, organelle transport, and the cytoskeleton. Curr Opin Cell Biol *12*, 57-62.

Rosenbluth, J. (1980). Peripheral myelin in the mouse mutant Shiverer. J Comp Neurol *193*, 729-739.

Rushton, W. A. (1951). A theory of the effects of fibre size in medullated nerve. J Physiol *115*, 101-122.

Saito, F., Moore, S. A., Barresi, R., Henry, M. D., Messing, A., Ross-Barta, S. E., Cohn, R. D., Williamson, R. A., Sluka, K. A., Sherman, D. L., *et al.* (2003). Unique role of dystroglycan in peripheral nerve myelination, nodal structure, and sodium channel stabilization. Neuron *38*, 747-758.

Salzer, J. L. (2003). Polarized domains of myelinated axons. Neuron *40*, 297-318.

Sanchez, C., Diaz-Nido, J., and Avila, J. (2000). Phosphorylation of microtubule-associated protein 2 (MAP2) and its relevance for the regulation of the neuronal cytoskeleton function. Prog Neurobiol *61*, 133-168.

Sanders, F. K., and Whitteridge, D. (1945). Conduction velocity and myelin thickness in regenerating nerve fibres. J Physiol *105*, 152-174.

Sanes, J. R., Engvall, E., Butkowski, R., and Hunter, D. D. (1990). Molecular heterogeneity of basal laminae: isoforms of laminin and collagen IV at the neuromuscular junction and elsewhere. J Cell Biol *111*, 1685-1699.

Sanes, J. R., and Lichtman, J. W. (1999). Development of the vertebrate neuromuscular junction. Annu Rev Neurosci *22*, 389-442.

Sanes, J. R., and Lichtman, J. W. (2001). Induction, assembly, maturation and maintenance of a postsynaptic apparatus. Nat Rev Neurosci *2*, 791-805.

Sanes, J. R., Schachner, M., and Covault, J. (1986). Expression of several adhesive macromolecules (N-CAM, L1, J1, NILE, uvomorulin, laminin, fibronectin, and a heparan sulfate proteoglycan) in embryonic, adult, and denervated adult skeletal muscle. J Cell Biol *102*, 420-431.

Scheiffele, P., Fan, J., Choih, J., Fetter, R., and Serafini, T. (2000). Neuroligin expressed in nonneuronal cells triggers presynaptic development in contacting axons. Cell *101*, 657-669.

Scherer, S. S., and Arroyo, E. J. (2002). Recent progress on the molecular organization of myelinated axons. J Peripher Nerv Syst *7*, 1-12.

Scherer, S. S., Xu, T., Crino, P., Arroyo, E. J., and Gutmann, D. H. (2001). Ezrin, radixin, and moesin are components of Schwann cell microvilli. J Neurosci Res *65*, 150-164.

Scherer, S. S., Xu, Y. T., Bannerman, P. G., Sherman, D. L., and Brophy, P. J. (1995). Periaxin expression in myelinating Schwann cells: modulation by axon-glial interactions and polarized localization during development. Development *121*, 4265-4273.

Schnapp, B. J. (2003). Trafficking of signaling modules by kinesin motors. J Cell Sci *116*, 2125-2135.

Schwab, M. H., Michailov, G. V., Brinkmann, B. G., Humml, C., Birchmeier, C., Sereda, M. W., and Nave, K. A. (2004). A threshold level of neuregulin-1 induces myelination. Paper presented at: Society for Neuroscience (Program No. 494.11).

Seale, P., Sabourin, L. A., Girgis-Gabardo, A., Mansouri, A., Gruss, P., and Rudnicki, M. A. (2000). Pax7 is required for the specification of myogenic satellite cells. Cell *102*, 777-786.

Shah, N. M., Marchionni, M. A., Isaacs, I., Stroobant, P., and Anderson, D. J. (1994). Glial growth factor restricts mammalian neural crest stem cells to a glial fate. Cell *77*, 349-360.

Sharma, K., and Belmonte, J. C. (2001). Development of the limb neuromuscular system. Curr Opin Cell Biol *13*, 204-210.

Sherman, D. L., Fabrizi, C., Gillespie, C. S., and Brophy, P. J. (2001). Specific disruption of a schwann cell dystrophin-related protein complex in a demyelinating neuropathy. Neuron *30*, 677-687.

Singh, N., Birdi, T. J., Chandrashekar, S., and Antia, N. H. (1997). Schwann cell extracellular matrix protein production is modulated by Mycobacterium leprae and macrophage secretory products. J Neurol Sci *151*, 13-22.

Smith, D. O. (1980). Morphological aspects of the safety factor for action potential propagation at axon branch points in the crayfish. J Physiol *301*, 261-269.

Son, Y. J., and Thompson, W. J. (1995). Schwann cell processes guide regeneration of peripheral axons. Neuron *14*, 125-132.

Son, Y. J., Trachtenberg, J. T., and Thompson, W. J. (1996). Schwann cells induce and guide sprouting and reinnervation of neuromuscular junctions. Trends Neurosci *19*, 280-285.

Syroid, D. E., Maycox, P. R., Burrola, P. G., Liu, N., Wen, D., Lee, K. F., Lemke, G., and Kilpatrick, T. J. (1996). Cell death in the Schwann cell lineage and its regulation by neuregulin. Proc Natl Acad Sci U S A *93*, 9229-9234.

Takashima, H., Boerkoel, C. F., De Jonghe, P., Ceuterick, C., Martin, J. J., Voit, T., Schroder, J. M., Williams, A., Brophy, P. J., Timmerman, V., and Lupski, J. R. (2002). Periaxin mutations cause a broad spectrum of demyelinating neuropathies. Ann Neurol *51*, 709-715.

Tamaki, T., Akatsuka, A., Ando, K., Nakamura, Y., Matsuzawa, H., Hotta, T., Roy, R. R., and Edgerton, V. R. (2002). Identification of myogenic-endothelial progenitor cells in the interstitial spaces of skeletal muscle. J Cell Biol *157*, 571-577.

Tasaki, I. (1939). The electro-saltatory transmission of the nerve impulse and the effect of narcosis upon the nerve fiber. Am J Physiol *127*, 211-227.

Thaler, J. P., Koo, S. J., Kania, A., Lettieri, K., Andrews, S., Cox, C., Jessell, T. M., and Pfaff, S. L. (2004). A Postmitotic Role for Isl-Class LIM Homeodomain Proteins in the Assignment of Visceral Spinal Motor Neuron Identity. Neuron *41*, 337-350.

Thompson, W. (1983). Synapse elimination in neonatal rat muscle is sensitive to pattern of muscle use. Nature *302*, 614-616.

Topilko, P., Schneider-Maunoury, S., Levi, G., Baron-Van Evercooren, A., Chennoufi, A. B., Seitanidou, T., Babinet, C., and Charnay, P. (1994). Krox-20 controls myelination in the peripheral nervous system. Nature *371*, 796-799.

Totsukawa, G., Yamakita, Y., Yamashiro, S., Hartshorne, D. J., Sasaki, Y., and Matsumura, F. (2000). Distinct roles of ROCK (Rho-kinase) and MLCK in spatial regulation of MLC phosphorylation for assembly of stress fibers and focal adhesions in 3T3 fibroblasts. J Cell Biol *150*, 797-806.

Traka, M., Goutebroze, L., Denisenko, N., Bessa, M., Nifli, A., Havaki, S., Iwakura, Y., Fukamauchi, F., Watanabe, K., Soliven, B., *et al.* (2003). Association of TAG-1 with Caspr2 is essential for the molecular organization of juxtaparanodal regions of myelinated fibers. J Cell Biol *162*, 1161-1172.

Trapp, B. D., Kidd, G. J., Hauer, P., Mulrenin, E., Haney, C. A., and Andrews, S. B. (1995). Polarization of myelinating Schwann cell surface membranes: role of microtubules and the trans-Golgi network. J Neurosci *15*, 1797-1807.

Trapp, B. D., Peterson, J., Ransohoff, R. M., Rudick, R., Mork, S., and Bo, L. (1998). Axonal transection in the lesions of multiple sclerosis. N Engl J Med *338*, 278-285.

Trinidad, J. C., Fischbach, G. D., and Cohen, J. B. (2000). The Agrin/MuSK signaling pathway is spatially segregated from the neuregulin/ErbB receptor signaling pathway at the neuromuscular junction. J Neurosci *20*, 8762-8770.

Turner, C. E. (2000). Paxillin and focal adhesion signalling. Nat Cell Biol *2*, E231-236.

Ushiki, T., and Ide, C. (1987). Scanning electron microscopic studies of the myelinated nerve fibres of the mouse sciatic nerve with special reference to the Schwann cell cytoplasmic network external to the myelin sheath. J Neurocytol *16*, 737-747.

van Deurs, B., Roepstorff, K., Hommelgaard, A. M., and Sandvig, K. (2003). Caveolae: anchored, multifunctional platforms in the lipid ocean. Trends Cell Biol *13*, 92-100.

VanSaun, M., Herrera, A. A., and Werle, M. J. (2003). Structural alterations at the neuromuscular junctions of matrix metalloproteinase 3 null mutant mice. J Neurocytol *32*, 1129-1142.

Voyvodic, J. T. (1989). Target size regulates calibre and myelination of sympathetic axons. Nature *342*, 430-433.

Wang, H., Kunkel, D. D., Martin, T. M., Schwartzkroin, P. A., and Tempel, B. L. (1993). Heteromultimeric K+ channels in terminal and juxtaparanodal regions of neurons. Nature *365*, 75-79.

Webster, H. D. (1971). The geometry of peripheral myelin sheaths during their formation and growth in rat sciatic nerves. J Cell Biol *48*, 348-367.

Weis, J., Fine, S. M., David, C., Savarirayan, S., and Sanes, J. R. (1991). Integration site-dependent expression of a transgene reveals specialized features of cells associated with neuromuscular junctions. J Cell Biol *113*, 1385-1397.

Williams, B. A., and Ordahl, C. P. (1997). Emergence of determined myotome precursor cells in the somite. Development *124*, 4983-4997.

Winder, S. J. (2001). The complexities of dystroglycan. Trends Biochem Sci *26*, 118-124.

Woldeyesus, M. T., Britsch, S., Riethmacher, D., Xu, L., Sonnenberg-Riethmacher, E., Abou-Rebyeh, F., Harvey, R., Caroni, P., and Birchmeier, C. (1999). Peripheral nervous system defects in erbB2 mutants following genetic rescue of heart development. Genes Dev *13*, 2538-2548.

Woolf, C. J., Reynolds, M. L., Chong, M. S., Emson, P., Irwin, N., and Benowitz, L. I. (1992). Denervation of the motor endplate results in the rapid expression by terminal Schwann cells of the growth-associated protein GAP-43. J Neurosci *12*, 3999-4010.

Yablonka-Reuveni, Z., Rudnicki, M. A., Rivera, A. J., Primig, M., Anderson, J. E., and Natanson, P. (1999). The transition from proliferation to differentiation is delayed in satellite cells from mice lacking MyoD. Dev Biol *210*, 440-455.

Yang, X., Arber, S., William, C., Li, L., Tanabe, Y., Jessell, T. M., Birchmeier, C., and Burden, S. J. (2001). Patterning of muscle acetylcholine receptor gene expression in the absence of motor innervation. Neuron *30*, 399-410.

Yin, X., Kidd, G. J., Pioro, E. P., McDonough, J., Dutta, R., Feltri, M. L., Wrabetz, L., Messing, A., Wyatt, R. M., Balice-Gordon, R. J., and Trapp, B. D. (2004). Dysmyelinated lower motor neurons retract and regenerate dysfunctional synaptic terminals. J Neurosci *24*, 3890-3898.

Zhou, L., and Chiu, S. Y. (2001). Computer model for action potential propagation through branch point in myelinated nerves. J Neurophysiol *85*, 197-210.

Zhou, L., Messing, A., and Chiu, S. Y. (1999). Determinants of excitability at transition zones in Kv1.1-deficient myelinated nerves. J Neurosci *19*, 5768-5781.

September 2004

International weekly journal of science

nature

$10.00

www.nature.com/nature

Ring of life
The evolution of everything

NorthGRIP ice core
An ice age begins

Memory making
Déjà vu — in a rat

Lightning research
The X-ray factor

Schwann cell function

How Cajal bands aid nerve transmission

$10.00US $12.99CAN

37>

0 71486 03070 6

Restricted growth of Schwann cells lacking Cajal bands slows conduction in myelinated nerves

Felipe A. Court, Diane L. Sherman, Thomas Pratt, Emer M. Garry, Richard R. Ribchester, David F. Cottrell, Susan M. Fleetwood-Walker & Peter J. Brophy

Centre for Neuroscience Research, University of Edinburgh, Edinburgh EH9 1QH, UK

Nerve impulses are propagated at nodes of Ranvier in the myelinated nerves of vertebrates. Internodal distances have been proposed to affect the velocity of nerve impulse conduction[1]; however, direct evidence is lacking, and the cellular mechanisms that might regulate the length of the myelinated segments are unknown. Ramón y Cajal described longitudinal and transverse bands of cytoplasm or trabeculae in internodal Schwann cells and suggested that they had a nutritive function[2]. Here we show that internodal growth in wild-type nerves is precisely matched to nerve extension, but disruption of the cytoplasmic bands in Periaxin-null mice impairs Schwann cell elongation during nerve growth. By contrast, myelination proceeds normally. The capacity of wild-type and mutant Schwann cells to elongate is cell-autonomous, indicating that passive stretching can account for the lengthening of the internode during limb growth. As predicted on theoretical grounds, decreased internodal distances strikingly decrease conduction velocities and so affect motor function. We propose that microtubule-based transport in the longitudinal bands of Cajal permits internodal Schwann cells to lengthen in response to axonal growth, thus ensuring rapid nerve impulse transmission.

Nodes of Ranvier in peripheral nerves are flanked by Schwann

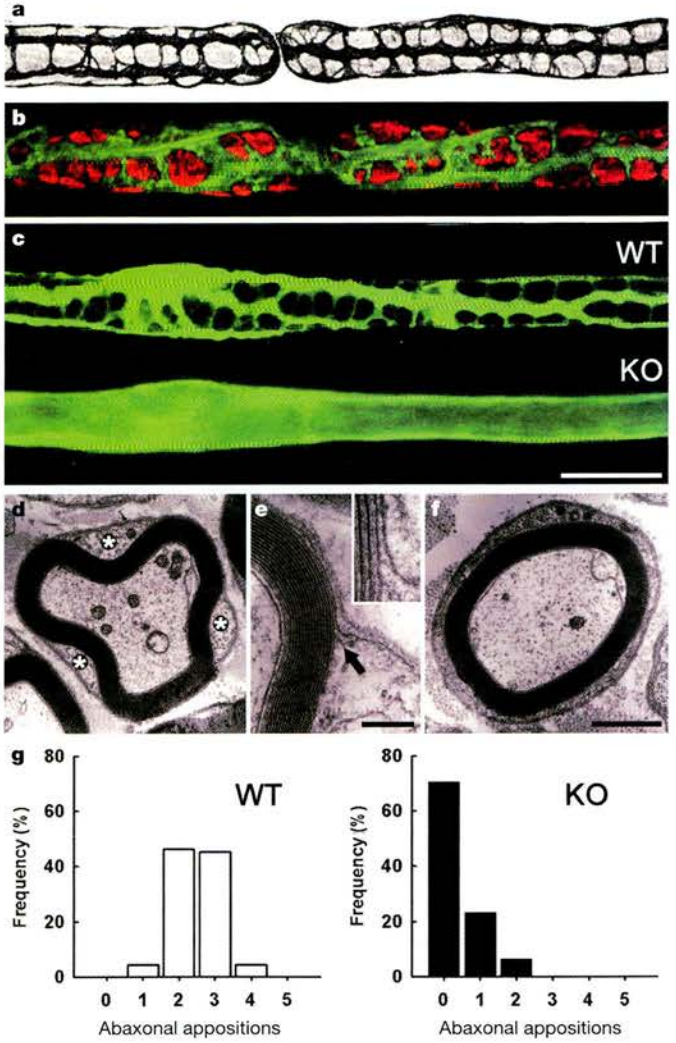

Figure 1 Longitudinal and transverse bands of Cajal in Schwann cells and their disruption in quadriceps nerve of Periaxin-null (KO) mice at 3 weeks. **a**, Longitudinal and transverse protoplasmic bands stained with silver by Ramón y Cajal (reproduced with permission)[2]. **b**, Teased fibres double-labelled with TRITC–phalloidin (green) and an antibody against DRP2 (red). Schwann cell cytoplasm is excluded from spheroidal clusters immunopositive for DRP2. **c**, Immunostaining of fibres from WT and *Prx* KO mice for the Schwann cell cytoplasmic protein S100. Scale bar, 20 μm in **b** and **c**. **d**–**f**, Electron micrographs of transverse sections of WT and KO quadriceps nerves. **d**, WT Schwann cell cytoplasm (asterisks) is restricted to regions delimited by appositions between the Schwann cell plasma membrane and the abaxonal layer of the myelin sheath. **e**, The sharp transition between the apposition and cytoplasmic zones is shown by the arrow. Scale bar, 0.2 μm. The inset shows a high-power view of the transition zone. **f**, In the absence of appositions in the KO, the Schwann cell cytoplasm forms a concentric ring around the myelin sheath. Scale bar, 1 μm (**d** and **f**). **g**, The proportion of abaxonal appositions per Schwann cell in WT and KO mice ($n = 3$ for WT and KO).

cells, and in theory the length of the internodal Schwann cell should influence the rate of impulse conduction[1]. However, this has not been experimentally verified, largely because the two other main influences on conduction velocity, namely axon diameter and myelin thickness, normally co-vary with internodal length. Further, it is not known what mechanisms set the internodal distance and allow Schwann cells to elongate so extensively during nerve growth *in vivo*. The cytoplasmic meshwork beneath the plasma membrane of myelinating Schwann cells was first described by Ramón y Cajal (Fig. 1a), who speculated that these longitudinal and transverse protoplasmic trabeculae might have a nutritive function; however, their role in cell growth and maturation has remained unclear[2].

We have previously identified spheroidal domains in the Schwann cell plasma membrane that contain the L-Periaxin-Dystrophin-related protein 2 (DRP2)–Dystroglycan (PDG) complex[3]. Double-labelling for DRP2 and cytoplasmic microfilaments by immunofluorescence showed that the PDG-rich domains are surrounded by cytoplasmic bands (Fig. 1b). To address the function of the bands, we first determined whether they were deranged in Periaxin-null ($Prx^{-/-}$) mice, because we had previously shown that the PDG complex is biochemically disrupted in these mice[3]. Immunostaining for the Schwann cell cytoplasmic marker S100 revealed that the cytoplasmic bands were absent from the Schwann cells of $Prx^{-/-}$ mice (Fig. 1c). Electron microscopy showed that there were no appositions between the abaxonal surface of the myelin sheath and the plasma membrane of the $Prx^{-/-}$ Schwann cells (Fig. 1d–g), and this was consistent with our previous ultrastructural observation that DRP2 and Periaxin localize together at these appositions[3]. Instead of being compartmentalized in bands, the Schwann cell cytoplasm now formed a continuous annulus under the plasma membrane (Fig. 1f).

What are the consequences of disrupting the longitudinal Cajal bands, in the light of Ramón y Cajal's proposal that they might serve a nutritive function? Although inactivation of the *Prx* gene causes

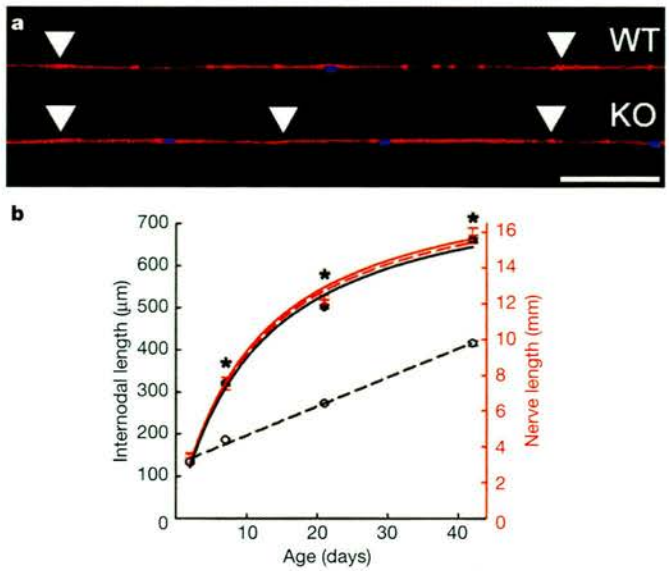

Figure 2 Internodal length is decreased in Schwann cells from $Prx^{-/-}$ mice lacking Cajal bands. **a**, Teased fibres from 3-week-old WT and KO quadriceps nerves were stained with TRITC–phalloidin (red) and DAPI (blue). Nodes of Ranvier are indicated by arrowheads. Scale bar, 100 μm. **b**, The growth rate of WT and KO internodal lengths fitted a rectangular hyperbola and a straight line respectively. The growth rates of WT and KO nerve length were similar and both fitted rectangular hyperbolas (the null hypothesis that there was no significant difference between these fitted curves was supported by *F*-test; $P = 0.945$). Internodal lengths of WT (continuous black line) and KO (dashed black line) are comparable at 2 days. Thereafter, internodal growth of WT Schwann cells matches the increase in length of the quadriceps nerve (continuous red line) exactly. In contrast, the rate of internodal growth in the KO is decreased, even though the nerve grows at a normal rate (dashed red line). Values are means ± s.e.m. for three animals (asterisks, $P < 0.0001$; Student's *t*-test for internodal lengths).

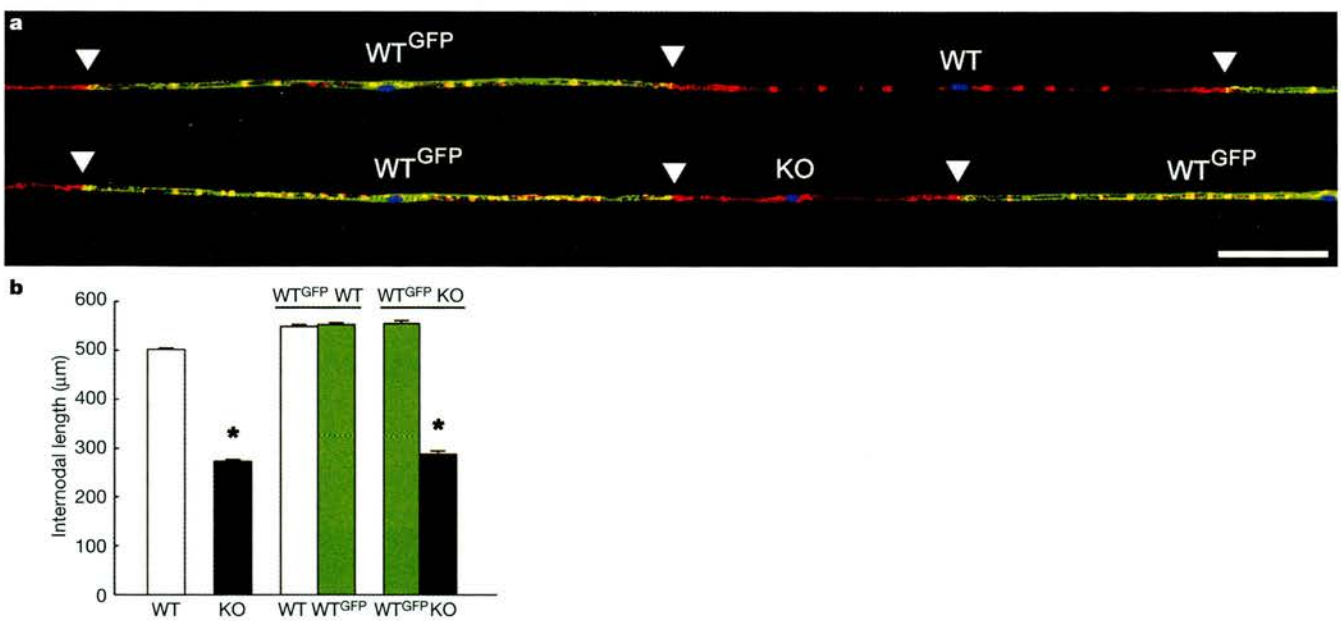

Figure 3 The capacity of Schwann cells to specify internodal length is cell-autonomous. Teased fibres in quadriceps nerves from 3-week-old mice were stained with TRITC-phalloidin and DAPI. **a**, Nerves were from chimaeric mice containing GFP-tagged Schwann cells (S129 background) and either WT Schwann cells or *Prx* KO Schwann cells (both C57BL/6 background). The green signal is from GFP. Nodes of Ranvier are indicated by arrowheads. Scale bar, 100 μm. **b**, The first two bars show that internodal lengths from non-chimaeric KO mice are decreased (*$P < 0.0001$ by Student's *t*-test; $n = 3$). In WT^{GFP}–WT chimaeras, both types of Schwann cells had similar internodal lengths. In WT^{GFP}–KO chimaeras, WT^{GFP} Schwann cells had similar internodal lengths to those in WT^{GFP}–WT chimaeras, whereas KO Schwann cells had decreased internodal lengths (asterisks, $P < 0.0001$ by Student's *t*-test; $n = 3$). The internodes of Schwann cells in WT^{GFP}–WT chimaeras were significantly larger than those of C57BL/6 WT ($P < 0.0001$ by Student's *t*-test), but the internodal lengths of KO Schwann cells were decreased similarly in a chimaeric environment and in a C57BL/6 environment ($P = 0.07$ by Student's *t*-test). All values are means + s.e.m.

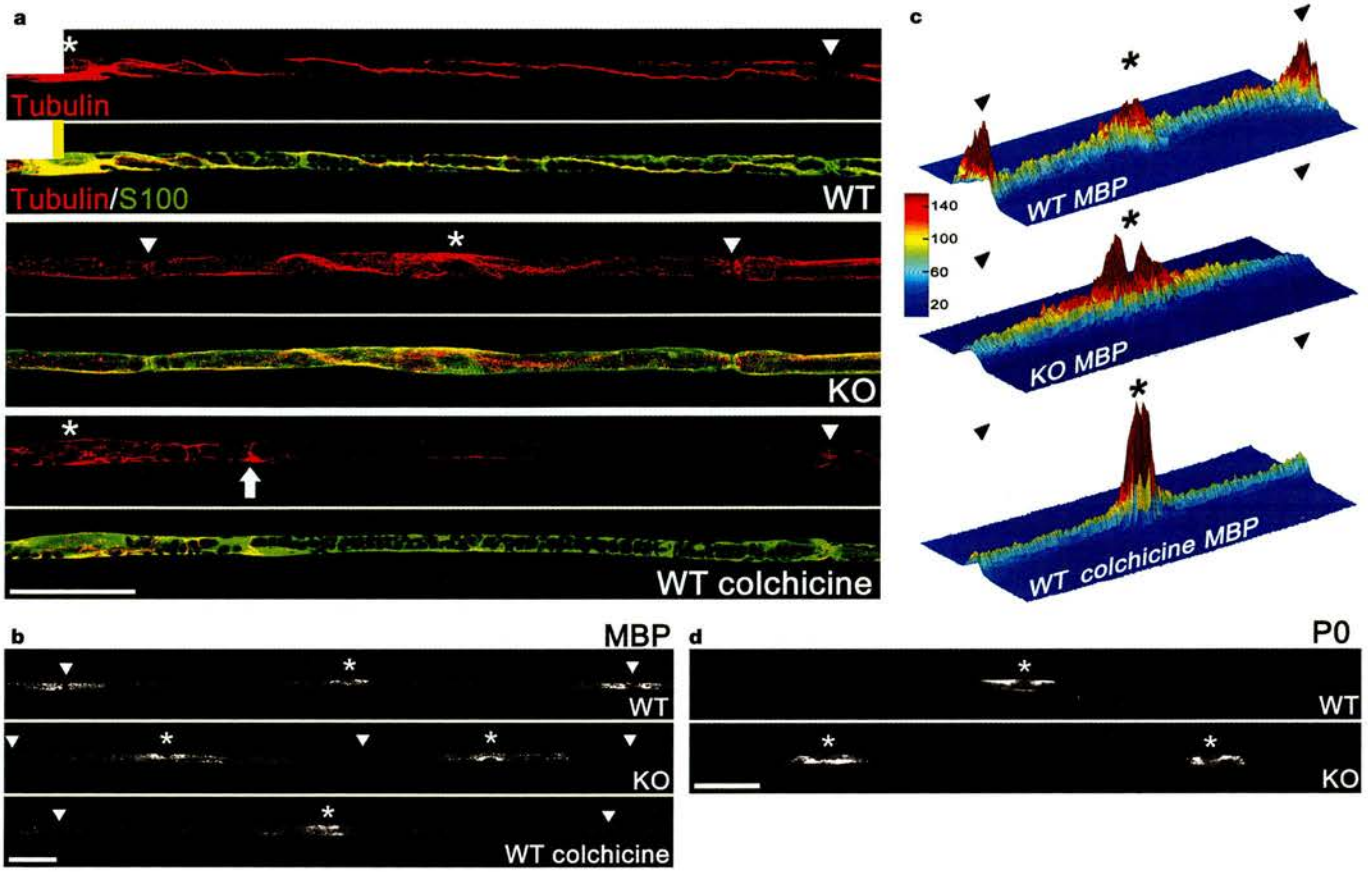

Figure 4 Intact Cajal bands and microtubules are required for MBP mRNA localization at the paranodes. Tubulin (red) and the Cajal band marker S100 (green) were visualized by immunofluorescence, and MBP and P0 mRNA were detected by *in situ* hybridization (images photographically inverted for clarity) in teased sciatic nerve fibres from 3-week-old WT and KO nerves with digoxigenin-labelled probes. **a**, In WT Schwann cells tubulin localizes with S100 in the Cajal bands, whereas in the absence of the bands tubulin staining becomes punctate as the microtubules approach the paranodes. Complete depolymerization of WT Schwann cell microtubules with colchicine *in vivo* followed by recovery for 3 days allows the microtubules to reform and partly extend (arrow indicates extent of growth). Note that Cajal bands are unaffected. **b**, MBP mRNA in WT Schwann cells accumulates in the perinuclear and paranodal domains, whereas in KO Schwann cells lacking Cajal bands the strong MBP mRNA signal declines from the perinuclear region towards the paranodes. Depolymerization of microtubules in WT cells prevents the concentration of MBP mRNA at the paranodes. Scale bar, 50 μm. **c**, Pseudocolour surface plot of the mean internodal signal intensity (scale, 0–255) for MBP mRNA in WT ($n = 9$), KO ($n = 12$) and colchicine-treated WT Schwann cells ($n = 10$). **d**, P0 mRNA is localized to the perinuclear region in both WT and KO Schwann cells. Nuclei and nodes of Ranvier are indicated by asterisks and arrowheads respectively. Scale bar, 50 μm.

demyelination in mature mice[4], the myelin sheath of murine quadriceps nerve fibres was of normal thickness at 3 weeks as measured by the *g*-ratio (axon diameter/fibre diameter) (wild type (WT), 0.62 ± 0.01; $Prx^{-/-}$, 0.63 ± 0.01), and the mean fibre diameter was unchanged (WT, 6.73 ± 0.06 μm; $Prx^{-/-}$, 6.67 ± 0.07 μm). Furthermore, there seemed to be no derangements to the protein content, protein localization or ultrastructural organization of the nodal or paranodal apparatus at 3 weeks (Supplementary Fig. 1).

In spite of the apparently normal assembly of myelin by Schwann cells, but consistent with Ramón y Cajal's proposal, there was a striking decrease in their longitudinal growth (Fig. 2a). At postnatal-day 2 (P2), when myelinating Schwann cells have established a 1:1 relationship with segments of quadriceps nerve axons, WT and knockout (KO) Schwann cells were the same length (Fig. 2b). WT Schwann cells then elongated at the same rate as the growing nerve, whereas Periaxin-null Schwann cells had lower growth rates; this deficit persisted into adulthood in spite of the fact that WT and KO quadriceps nerves grew to the same length (Fig. 2b). Consistent with the absence of spontaneous firing in their quadriceps nerves, we never observed naked axonal segments in KO mice. Hence, during the early rapid growth phase of the nerve, extra Schwann cells must be needed to ensheath nerves in the mutant, although their origin remains to be determined. At later phases after P21 it seems that KO Schwann cells can match the slower rates of nerve growth.

These results prompted us to use chimaeric mice to test whether the ability of Schwann cells to elongate in response to axonal growth was cell-autonomous. Strain S129-derived embryonic stem (ES) cells tagged with tau–green fluorescent protein (GFP)[5] were injected into blastocysts to track the fate of ES cells carrying WT *Prx* alleles. We had previously shown that the GFP fusion transgene is robustly expressed in myelinating Schwann cells. To confirm that these ES cells developed into Schwann cells with normal internodal lengths, we injected them into C57BL/6 WT as well as KO blastocysts. In each case, peripheral nerves contained Schwann cells derived from both endogenous and injected stem cells (Fig. 3a). In contrast to the normal elongation of Schwann cells tagged with GFP in a WT or KO environment, KO Schwann cells were unable to elongate normally whether alone or flanked by GFP-tagged Schwann cells with normal longitudinal bands and WT internodal lengths (Fig. 3b). This indicated that the capacity to elongate was a cell-autonomous property of Schwann cells. Internodal lengths in chimaeric nerves containing both GFP-tagged Schwann cells (derived from strain S129 mice) and WT Schwann cells (from C57BL/6 mice) were greater than in WT C57BL/6 mice because these chimaeric mice were larger and had longer quadriceps nerves (compare Figs 2b and 3b). In contrast, the internodal lengths of Periaxin-null Schwann

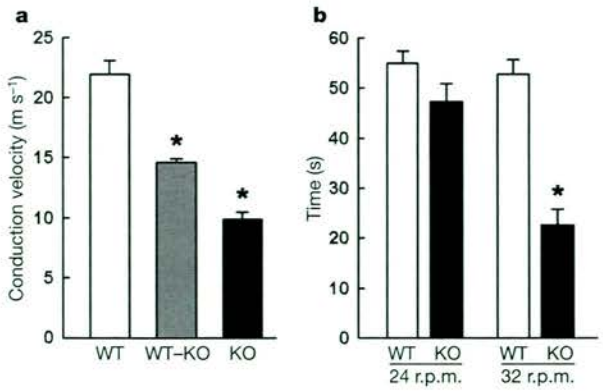

c

Response	WT	KO
Withdrawal latency from noxious heat (s)	8.5 ± 0.6	8.4 ± 0.5
Mechanical withdrawal threshold (mN mm^{-2})	281.7 ± 15.5	290.8 ± 14.3

Figure 5 Peripheral nerve function is compromised in *Prx*$^{-/-}$ animals. **a**, Nerve conduction velocities in 3-week-old quadriceps nerves were decreased in KO compared with WT mice, and chimaeras had intermediate values (57.1 ± 3.1% KO Schwann cells, $n = 3$; mean ± s.e.m.). Error bars indicate standard error of the regression coefficient (asterisks, $P < 0.0001$ for comparisons with WT, Student's *t*-test; $n = 4$ for WT and KO, $n = 3$ for chimaeras). **b**, A significant decrease in KO motor coordination compared with WT at 3 weeks was observed on the RotaRod at 32 r.p.m. but not at 24 r.p.m. Values are means ± s.e.m. (asterisk, $P < 0.0001$, Student's *t*-test; $n = 6$ for WT and KO). **c**, 3-week-old WT and KO mice showed no significant differences in a cutaneous reflex test of hindpaw withdrawal threshold to mechanical stimulation or in their withdrawal latency to thermal nociceptive sensitivity. Values are means ± s.e.m. ($n = 6$ for WT and KO).

cells in a chimaeric or pure C57BL/6 environment were indistinguishable (Fig. 3b). This further indicated that there was an upper limit to the ability of the mutant Schwann cells to elongate, irrespective of the extent of axon growth.

Microtubule-based messenger RNA translocation is believed to permit the incorporation of newly synthesized myelin basic protein (MBP) at the growing extremities of myelin-forming glia[6–9]. To test whether impaired transport of mRNA and proteins from the perinuclear to the peripheral regions of myelin-forming glia as a result of microtubule disruption might contribute to the decreased rate of elongation of Schwann cells lacking Cajal bands, we analysed the distribution of microtubules and MBP mRNA in single teased fibres from WT and KO mice. WT Schwann cells had an organized microtubule network that extended from the nucleus to the paranodes along the Cajal bands, whereas the tubulin staining in cells lacking Cajal bands frequently became punctate as the microtubules approached the paranodes (Fig. 4a). Importantly, the mutant Schwann cells could no longer accumulate MBP mRNA in the paranodal regions (Fig. 4b, c). Furthermore, the distal accumulation of MBP mRNA in WT Schwann cells was prevented when microtubules were reversibly disrupted, as found previously for oligodendrocytes[7] (Fig. 4a–c). Hence, deficits in microtubule-based transport might underlie the decreased capacity of Periaxin-null Schwann cells to elongate. In contrast to MBP mRNA, no discernible differences between WT and KO mice were observed in the distribution of the mRNA encoding the integral membrane protein P0 (Fig. 4d).

The decreased internodal length in KO mice, taken together with their normal axon diameter and myelin thickness, provided a unique opportunity to determine whether nerve conduction velocities are modulated by the internodal distance, as predicted from theory[1]. We measured the conduction time of compound action potentials in quadriceps nerves from 3-week-old WT, mutant and chimaeric mice. Nerve conduction velocities were decreased by more than 50% in KO compared with WT animals, and nerves that contained a mixture of WT and mutant Schwann cells had intermediate values, which was consistent with the effect of internodal length on conduction velocity (Fig. 5a). The substantial decrease in motor nerve conduction velocity in nerves lacking Cajal bands was accompanied by poorer performance on the RotaRod, a robust behavioural test for motor dysfunction (Fig. 5b). In sensory reflex behavioural tests, 3-week-old mice did not display the neuropathic pain behaviour that results from demyelination in mature *Prx*$^{-/-}$ mice[4]. They had normal withdrawal latencies in tests for both thermal hyperalgesia and mechanical allodynia, confirming the functional intactness of the myelin sheath (Fig. 5c). The relationship between the absence of longitudinal bands, decreased internodal length and impaired conduction in Periaxin-null mice was underlined by an analysis of *CMTX* mice, which also display late-onset demyelination. The quadriceps nerves from 3-week-old *CMTX* mice have normal bands and their Schwann cell lengths and conduction velocities are not decreased in comparison with WT animals (ref. 10 and Supplementary Fig. 2).

The physiological relationships between fibre diameter, myelin thickness and conduction velocity are well established[11]. However, our understanding of how internodal length influences conduction velocity has been largely theoretical[1,12]. We have used a recent model of mammalian motor nerve fibres that includes detailed morphological and electrical parameters[13]. As found in earlier theoretical treatments[1], we found a substantial decrease in the rate of conduction when changes in the internodal distance were modelled within our experimental range from 500 μm down to 250 μm (Supplementary Fig. 3). Nerve conduction velocities therefore become much more sensitive to changes in internodal lengths in the shorter ranges.

Ranvier speculated that internodal length and nerve elongation are related during body growth because internodes are longer in larger animals[14]. From our studies, the ability of myelinating Schwann cells to elongate during the postnatal development of peripheral nerves was cell-autonomous but matched the growth rate of axons precisely, thus supporting the proposal that passive stretching could account for the establishment of internodal lengths during nerve growth[15,16]. Schwann cells lacking longitudinal bands were unable to keep pace with axon growth, and the consequence of this decreased capacity for elongation was that the internodal distances were shorter and conduction velocities were slowed in mutant nerves. We conclude that Schwann cell elongation is an essential feature of the functional development of the vertebrate nervous system. Finally, we propose that the longitudinal cytoplasmic structures in Schwann cells be named Cajal bands to acknowledge both Ramón y Cajal's discovery and our growing understanding of their function. □

Methods

Materials and antibodies

Primary antibodies and dyes for microscopy were used at the following dilutions and concentrations; rabbit anti-DRP2 (ref. 3), 1:200; rabbit anti-S100 (Sigma), 1:200; rabbit anti-neurofascin[17], 1:1000; guinea pig anti-Caspr[17], 1:200; mouse anti-dystroglycan[3], 1:100; mouse anti-pan-Na^+ channel (gift from M. Rasband), 1:300; rat anti-tubulin

(YL1/2; Serotec), 1:200; chicken anti-betaIV-spectrin[18] (gift from M. Komada), 1:100; 4,6-diamidino-2-phenylindole (DAPI; Sigma), 4 μg ml^{-1}; tetramethylrhodamine β-isothiocyanate (TRITC)–phalloidin (Sigma), 50 ng ml^{-1}. The secondary antibodies were fluorescein isothiocyanate (FITC)-conjugated anti-rabbit IgG, 1:200; TRITC–donkey anti-guinea-pig IgG, 1:200; FITC–donkey anti-chicken IgY, 1:100 (all from Jackson ImmunoResearch); FITC–goat anti-mouse IgG1, 1:200 (Southern Biotech); Alexa Fluor-goat anti-rabbit IgG, 1:100 (Molecular Probes). For western blotting[19], primary antibodies were used at tenfold greater dilutions.

Microscopy and morphometry

Depolymerization of Schwann cell microtubules in sciatic nerve *in vivo* was performed by topical treatment with colchicine as described[20], and microtubules were allowed to reform for 3 days. By 5 days after colchicine treatment the microtubules had reached the paranodes showing that microtubule disruption is completely reversible (data not shown). Teased fibres were prepared from nerves fixed for 1 h in 4% paraformaldehyde, 0.1 M sodium phosphate buffer pH 7.3, and washed in several changes of phosphate buffer. The lengths of quadriceps nerves were measured from spinal cord exit to muscle insertion point. Teased fibres from quadriceps nerves of WT and KO mice were stained with TRITC–phalloidin and DAPI, and 100 internodes and the lengths of two quadriceps nerves were measured for each animal ($n = 3$). For chimaeras, 200 internodal distances were measured for each Schwann cell type ($n = 3$). Nerves were prepared for electron microscopy as described previously[4]. For measurement of *g*-ratios, micrographs of randomly selected fields of ultrathin transverse sections of quadriceps nerves from 3-week-old WT and KO mice ($n = 3$ for each group, 120 fibres per group) were scanned and analysed using NIH Image. The *g*-ratio was calculated and all results are shown as means ± s.e.m. The best fit for the growth rates of internodal and nerve length was found (*F*-test; Prism 3.03) and superimposed on the measured values shown in Fig. 2b. The growth rate of WT internodal length fitted a rectangular hyperbola, whereas the growth rate of KO internodal length fitted a straight line (linear regression). The growth rates of WT and KO nerve length both fitted a rectangular hyperbola. Bright-field images of teased sciatic nerve fibres stained for P0 and MBP mRNA by *in situ* hybridization with digoxigenin-labelled probes[21] were photographically inverted to compare the signal intensity between WT, KO and colchicine-treated WT Schwann cells. Sense probes gave negligible background staining. Images of internodes were normalized by rescaling to a length of 400 pixels and imported into MATLAB software as a two-dimensional matrix representing pixel intensity. A three-dimensional array was created by concatenating individual images in the *Z* dimension. From this array, the mean value of pixel intensity in the *Z* dimension was calculated for each pixel, resulting in a two-dimensional matrix.

Electrophysiology

Quadriceps nerves from 3-week-old KO and WT mice were transferred from oxygenated Krebs solution to an isolated chamber containing an array of Ag/AgCl electrodes with 1-mm intervals and surrounded by liquid paraffin maintained at 37 °C for periods no longer than 10 min. The proximal end of the nerve was excited by a square wave (0.1 ms, 0.1–1.5 V) and the conduction distance was varied from 2 mm to 7 mm by altering the stimulating electrode position. The voltage was adjusted to ensure exact duplication of the active population, and the compound action potential was viewed on a storage oscilloscope. Values were stored as digitized signals with the use of Chart software (MacLab System). Conduction times were measured as described[4].

Behavioural testing

Mice were conditioned to the RotaRod 1 day before the trial, and the RotaRod test was terminated either when the mouse fell from the rod or at 60 s. Four trials per mouse were performed, separated by at least 10 min to avoid exhaustion of the animal. The thresholds and times for hindpaw withdrawal in response to graded mechanical stimulation and thermal stimulus were performed as described[4].

Chimaeras

Chimaeras were obtained by injecting the ES cell line E14Tg2aSc4TP6.3 expressing GFP-tagged tau protein into WT or KO blastocysts[5]. For internodal length measurements in quadriceps nerves, chimaeras were selected with an approximately equal contribution from each Schwann cell type.

Received 9 May; accepted 13 July 2004; doi:10.1038/nature02841.

1. Brill, M. H., Waxman, S. G., Moore, J. W. & Joyner, R. W. Conduction velocity and spike configuration in myelinated fibres: computed dependence on internode distance. *J. Neurol. Neurosurg. Psychiatry* **40,** 769–774 (1977).
2. Ramón y Cajal, S. *Histology* (Bailliere, Tindall & Cox, London, 1933).
3. Sherman, D. L., Fabrizi, C., Gillespie, C. S. & Brophy, P. J. Specific disruption of a Schwann cell dystrophin-related protein complex in a demyelinating neuropathy. *Neuron* **30,** 677–687 (2001).
4. Gillespie, C. S. *et al.* Peripheral demyelination and neuropathic pain behavior in periaxin-deficient mice. *Neuron* **26,** 523–531 (2000).
5. Pratt, T., Sharp, L., Nichols, J., Price, D. J. & Mason, J. O. Embryonic stem cells and transgenic mice ubiquitously expressing a tau-tagged green fluorescent protein. *Dev. Biol.* **228,** 19–28 (2000).
6. Ainger, K. *et al.* Transport and localization elements in myelin basic protein mRNA. *J. Cell Biol.* **138,** 1077–1087 (1997).
7. Carson, J. H., Worboys, K., Ainger, K. & Barbarese, E. Translocation of myelin basic protein mRNA in oligodendrocytes requires microtubules and kinesin. *Cell Motil. Cytoskeleton* **38,** 318–328 (1997).
8. Colman, D. R., Kreibich, G., Frey, A. B. & Sabatini, D. D. Synthesis and incorporation of myelin polypeptides into CNS myelin. *J. Cell Biol.* **95,** 598–608 (1982).
9. Griffiths, I. R. *et al.* Expression of myelin protein genes in Schwann cells. *J. Neurocytol.* **18,** 345–352 (1989).
10. Anzini, P. *et al.* Structural abnormalities and deficient maintenance of peripheral nerve myelin in mice lacking the gap junction protein connexin 32. *J. Neurosci.* **17,** 4545–4551 (1997).
11. Hursh, J. B. Conduction velocity and diameter of nerve fibers. *Am. J. Physiol.* **127,** 131–139 (1939).
12. Huxley, A. F. & Stampfli, R. Evidence for saltatory conduction in peripheral myelinated nerve fibres. *J. Physiol. (Lond.)* **108,** 315–339 (1949).
13. McIntyre, C. C., Richardson, A. G. & Grill, W. M. Modeling the excitability of mammalian nerve fibers: influence of afterpotentials on the recovery cycle. *J. Neurophysiol.* **87,** 995–1006 (2002).
14. Ranvier, L. Des étranglements annulaires et des segments interannulaires chez les Raies et les Torpilles. *C. R. Acad. Sci.* **75,** 1129–1132 (1872).
15. Hiscoe, H. B. Distribution of nodes and incisures in normal and regenerated nerve. *Anat. Rec.* **99,** 447–475 (1947).
16. Schlaepfer, W. W. & Myers, F. K. Relationship of myelin internode elongation and growth in the rat sural nerve. *J. Comp. Neurol.* **147,** 255–266 (1973).
17. Tait, S. *et al.* An oligodendrocyte cell adhesion molecule at the site of assembly of the paranodal axo-glial junction. *J. Cell Biol.* **150,** 657–666 (2000).
18. Komada, M. & Soriano, P. βIV-spectrin regulates sodium channel clustering through ankyrin-G at axon initial segments and nodes of Ranvier. *J. Cell Biol.* **156,** 337–348 (2002).
19. Gillespie, C. S., Sherman, D. L., Blair, G. E. & Brophy, P. J. Periaxin, a novel protein of myelinating Schwann cells with a possible role in axonal ensheathment. *Neuron* **12,** 497–508 (1994).
20. Trapp, B. D. *et al.* Polarization of myelinating Schwann cell surface membranes: role of microtubules and the trans-Golgi network. *J. Neurosci.* **15,** 1797–1807 (1995).
21. Collinson, J. M., Marshall, D., Gillespie, C. S. & Brophy, P. J. Transient expression of neurofascin by oligodendrocytes at the onset of myelinogenesis: implications for mechanisms of axon-glial interaction. *Glia* **23,** 11–23 (1998).

Supplementary Information accompanies the paper on www.nature.com/nature.

Acknowledgements We thank H. Anderson and L. Ferguson for assistance, B. Smith for technical support, S. Scherer for comments, and K. Willeke and T. Ott of Bonn University for the *CMTX* mice. Figure 1a is reproduced with the permission of the Cajal Institute, CSIC, Madrid, Spain, copyright inheritors of Santiago Ramón y Cajal. This work was supported by the Wellcome Trust.

Competing interests statement The authors declare that they have no competing financial interests.

Correspondence and requests for materials should be addressed to P.J.B. (peter.brophy@ed.ac.uk).